DOCTOR OF PHILOSOPHY

An Investigation into the Finite Element Modelling of an Aircraft Tyre and Wheel Assembly

Guo, Hua

Award date:
2014

Awarding institution:
Coventry University

An Investigation into the Finite Element Modelling of an Aircraft Tyre and Wheel Assembly

By

Hua Guo

February 2014

The work contained within this document has been submitted by the student in partial fulfilment of the requirement of their course and award

An Investigation into the Finite Element Modelling of an Aircraft Tyre and Wheel Assembly

By

Hua Guo

February 2014

A thesis submitted in partial fulfilment of the University's requirements for the Degree of Doctor of Philosophy

Department of Automotive and Mechanical Engineering
Faculty of Engineering and Computing
Coventry University

Abstract

This thesis reports the investigation into the modelling and simulation of an aircraft tyre and wheel assembly in finite element environment. The finite element simulations basing on aircraft tyre test and operational scenarios could predict the loads transferred from tyre and the stresses distributed to the wheel rim. The virtual analysis could assess the safety criteria of different tyre structures, which would lead to the cost and time circle reduction in tyre R&D process.

An H41x16.0R20 radial ply aircraft test tyre and its corresponding test wheel, provided by Dunlop Aircraft Tyres Limited, are adopted as the subject of this research. The material properties, especially the rubber and fabric materials, have been investigated. The finite element hyperelastic models have been utilized to represent rubbers and been correlated to experimental data.

The 2D and 3D finite element tyre models, along with the finite element wheel models are created in the commercial finite element code, LS-Dyna.

The finite element models have been validated with either industrial standardised simulation results or experimental data. Basing on the validated models, simulations that duplicating static test and dynamic operational scenarios have been developed. The researches have provided knowledge in comparing single and double bead tyre designs with respect to wheel loading mechanisms. The computational model also allowed manufacturers to assess the performance and safety criteria of a particular tyre at its design stage. The development of such models would add to the general drive towards the use of more virtual prototypes in an area traditionally reliant on experimental testing.

Acknowledgement

I would like to express my sincere appreciation to my Director of studies, Prof. Mike Blundell for his encouragement, guidance, support and help during my PhD study. It is his solicitude, enthusiasm and professional experience that inspired me to get to the end of my PhD with confidence.

I would also like to give my special thanks to my supervisor, Mr. Christophe Bastien for his support and help on tyre modelling, finite element simulation and methodology. His previous experiences in industry and academia have extraordinary value for this PhD project. Thanks are also extended to Dr. Gary Wood, Mr. Jesper Christensen and Mr. Bill Dunn for their academic support during the PhD study.

Appreciation is also given to Dr. Wei Ding who was the head of the R&D department in the cooperating company, Dunlop Aircraft Tyres Limited (DATL), for his technical support and academic advises. The gratitude is also extended to Mr. Martin Pye and all the other colleagues in DATL giving help and encouragement to me during my PhD study.

Finally, I would like to give my appreciation to my parents, Dr. Si Guo, Dr. Ping Zeng, my cousin Mr. Guopeng Xu, the entire family and my fiancée Miss Shuang Xiao and her parents, Mr. Jianguo Xiao and Mrs. Ciqi Liao for their support, encouragement, understanding and love as always.

Table of Contents

List of Figures

List of Tables

List of Symbols

W: Also written as U, the strain energy potential (density) or stored energy function defined per unit volume.

I_1, I_2, I_3: The three invariants of the green deformation tensor

λ_1, λ_2 and λ_3: Principle extension ratios

U: Same as W, the strain energy potential (density), strain per unit of reference volume.

J_{e1}: The elastic volume ratio

$\overline{I_2}$ and $\overline{I_2}$: The first and second invariants of the deviatoric strain

C_{ij} and D_i: Material constant

N: A positive determining number of terms in the strain energy function (N = 1, 2 or 3)

J: $\lambda_1, \lambda_2, \lambda_3$

λ_i : The principal stretches

J: The Jacobean determinant

N: Number of network chains per unit volume

K: Boltzmann's constant

T: The absolute temperature

μ: The initial shear modulus

λ_m: The locking stretch, at which the upturn of the stress-strain curve would rise significantly

D: Double the inverse bulk modulus at small strain

E: Elastic modulus

G: Shear modulus

NU: Poisson's ratio

RHO: Density

δ: Stress

F: Force

A: Area

1. Introduction

Aircraft tyres play an important role in a landing gear system. They are critical for aircraft safety and performance upon landing and taxiing on the ground. The compatibility between the tyre and the wheel is a vital requirement for aircraft certification. To access the certification process, either experimental or virtual analysis can be utilized to investigate and assess the performance of the tyres.

The aim of this project is to develop a credible and efficient finite element model for a particular set of aircraft test tyre and wheel and to study the interaction between them under specified loading conditions and operational scenarios.

Specific objectives include:

1. Review the importance of tyre technology in aircraft and landing gear system
2. Review existing automotive and aircraft finite element tyre models
3. Develop a predictive FE model based on the specified Dunlop aircraft test tyre and wheel.
4. Validate and improve the FE tyre/wheel model by comparing simulation results with experimental data.

Tyre modelling, in both automotive and aerospace industries, continues to present analysts and researchers with significant challenges. Therefore, the reviews of existing researches have been processed first. For the work described here the model may be considered physical, and the complex structural form of the tyre carcass, the combination of materials requiring non-linear characterization and the complex manner in which the tyre can be loaded are areas where the development of finite element approaches is ongoing.

By developing a particular tyre finite element model, this study has demonstrated an effective use of a finite element model for predictive engineering. The models investigated in the study can be used by aircraft tyre and wheel designers to study the loading transferred from the tyre to the wheel rim for load cases corresponding with aircraft testing scenarios. Through analysing certain tyre/wheel performance criteria, tyre safety assessment has also been achieved. The modelling approach is not only suitable for a certain type of tyre, but can also be utilized for various tyre structure designs. Furthermore, the simulations designed for this particular tyre model can also be improved to duplicate more complex and realistic actual tyre operational scenarios.

The initial part of this thesis outlines a review of the literature with a general treatment of tyre modelling across a range of applications followed by a more detailed treatment of tyre models using finite element methods. For the work presented here a finite element model of an aircraft wheel has been developed for use in the study where two tyre design variants are considered, one with a single bead and one with a dual bead. All modelling work presented here has been carried out with the LS-Dyna finite element software. The 2-dimensional model was used to model a cross section of the tyre. A 3-dimensinonal model was then generated to analyse the inflation and static vertical load cases. Comparisons were then made between the computational data and the experimental data for the same tyre and wheel combinations and load conditions in order to validate the reliability and the efficiency of the finite element model.

The dynamic simulations that aim to duplicate tyre load upon aircraft landing scenarios have also been analyzed. Following the comments and guidelines from aircraft industrial data, the dynamic simulations have covered the tyre loading scenarios from normal (soft) landing, hard landing to crash landing under different aircraft landing weights and vertical speeds. Criteria such as tyre deflection rate, rated load, stress distribution at contact area and bead cords have been analyzed to achieve a safety assessment for the particular set of aircraft tyre and wheel.

The outcome of this project is to demonstrate the effective use of the finite element methodology to generate this particular model for predictive engineering. The proposed modelling approach can be used by aircraft tyre and wheel designers to study the loading transferred from the tyre to the wheel rim for load cases corresponding with aircraft test and operational scenarios. Various models generated through this methodology will allow the tyre manufactures to check that new tyre designs do not load wheels in a manner that will exceed limit failure stresses. The safety assessments can also be achieved at an early design stage.

As a summary, the unique contributions of this work include the development of a predictive finite element aircraft tyre and wheel interaction model. The research provides knowledge in comparing single and double bead tyre designs with respect to wheel loading mechanisms. The computational model will allow manufacturers to assess the performance and safety criteria of a particular tyre at its design stage. The development of such models also adds to the general drive towards the use of more virtual prototypes in an area traditionally reliant on experimental testing.

1.1 The history of the pneumatic tyre

The word ‘Tyre’ is derived from the word ‘Tie’, which refers to the outer steel ring parts of a wooden wheel that ties the wood segments together. They were considered to be the earliest version of tyres, as these kinds of durable metal bands placed on the wheels of carts and wagons served to tie the wheel segments together, and provided the wheel with a wear-resistant surface that could sustain heavy pressure. (Fleming 2010)

The invention of rubber vulcanization by Charles Goodyear in 1844 greatly promoted the development of the tyre. The vulcanization made rubber a durable and elastic engineering material for various applications, especially for tyres. In the mid 1800’s the

first tyres made of solid rubber appeared, using the rubber to carry the load entirely. It was in 1845 that the pneumatic tyre was invented and patented by Robert William Thomson, who used a number of thin inflated rubber-coated tubes inside a leather cover to build up a tyre that would only deflate after more than one puncture.

Figure-1.1 Robert William Thomson (1822-1873) and his pneumatic tyre model (Tompkins 1981)

In 1888, John Boyd Dunlop, a British veterinary surgeon managed to improve his son's bicycle by taping air-filled rubber tyres on its wheels. With the help from this first practical pneumatic tyre, another rider won a bicycle race in Belfast. With that victory, people began to take notice of the pneumatic tyre and put it into practice on carts and wagons. (Tompkins 1981)

Figure-1.2 John Boyd Dunlop (Tompkins 1981)

When automobiles came along, the pneumatic tyres were first introduced into automotive industry by Andre and Edouard Michelin in 1895. It was also the same time that cord-reinforced tyres became in use, tyre treads began thickening and being patterned for better traction and legislation discouraged the use of solid rubber tyres. Experiments with adding reinforcing materials into rubber, aiming to improve tyre durability took place in early 1900's. A successful attempt was achieved by Silvertown Rubber Company (London), 1910, by adding carbon black to white rubber. Carbon black helped conduct heat away from the tread and belt area of the tyre, reducing thermal damage hence increasing the durability. It is still universal now.

The fundamental structure of the tyre remained unchanged through the 1920's and 1930's, until Michelin revealed steel-belted radial tyres in 1948. The concept of radial tyres had been introduced in 1914 by Gray and Sloper of the Palmer Tyre Company using crossed cables around the perimeter of the tyre (straight out from the rim) to stiffen the sidewall. However, the concept was never put into practice in the Palmer Tyre Company due to the design flaws and the limitation of the existing technology then.

Figure-1.3 Michelin steel-belted radial tyres (Tompkins 1981)

Michelin applied and finally acquired a patent based on this invention, and introduced its 'X' tyre afterwards. It was considered a revolutionary achievement for the tyre industry at that time. The key advantage of radial tyres was that the constraint of the steel belts, which would neither elongate nor compress, preventing the tread from distorting. The radial cording also made the sidewalls more flexible, increasing the tread's capacity to conform to the road. The advantage of radial tyres has significantly increased tyre durability. With less rolling resistance, it also has increased the fuel economy of the vehicle.

Radial tyres were successful outside of the US, with worldwide companies producing them in large numbers. However, it wasn't until 1970's, radial tyres were finally fitted in the US. Based on the fact that the radial tyre required an independent suspension system on the vehicle, the American automotive manufacturers had to consider the cost to redesign their cars in order to adopt radial tyres. When the fuel crisis occurred in 1970's, that the American public demanded more economical cars due to the rising cost of petrol. The public demand has eventually pushed the development and the introduction of vehicles with independent suspension systems that could fit radial tyres. (Pacejka 2005)

Although the radial tyre was so slowly adopted, it was the tyre along with Dunlop's invention, which gives us the tyre we have today.

Back in 1906, 3 years after the invention of aircraft, pneumatic aircraft tyres were first put into use. Now, aircraft tyres are designed to withstand extremely heavy loads for short durations. Remarkable differences compared with automotive tyres include the advanced tread pattern design to avoid hydroplaning, inert gas for inflation to eliminate tyre explosion, and additional parts such as a heat fuse to control the failure mode.

1.2 Tyre classification and construction

Based on their construction and design variations, tyres are classified into five different construction types as listed below:

i. Cross-Ply

Cross-ply (or Bias ply tyre) are older in design. The construction utilizes body ply cords that extend diagonally from bead to bead, usually at angles in the range of 30 to 40 degrees, with successive plies laid at opposing angles forming a crisscross pattern to which the tread is applied. A Bias aircraft tyre features a casing which is constructed of alternate layers of rubber coated ply cords which extend around the beads and are at alternate angles substantially less than 90 degrees to the centre line of the tread.

The construction of a cross-ply tyre is shown in Fig-1.4. (The Goodyear Tyre & Rubber Company April 2010)

Figure-1.4 Cross-Ply aircraft tyre construction

(The Goodyear Tyre & Rubber Company April 2010)

In cross-ply tyres, without breaker belts, the position of the cords allows the entire tyre body to flex easily. When not loaded, the cross-ply tyre presents a rounded profile with a small contact area to the ground. As load is applied, the tyre flattens. The flexibility of the plies and the tread improves the cushioning action, which provides the main advantage of this construction, a smooth ride on rough road surfaces.

This cushioning characteristic also causes the major disadvantages of a cross-ply tyre: increased rolling resistance and less control and traction at higher speeds. It also significantly accelerates the tread wear and increases the fuel consumption.

ii. Belted bias

A belted bias tyre is a cross-ply tyre with two or more breaker belts added directly under the tread to increase stiffness. The belts may be cord or steel, they only lie under the tread area, without running around to the sidewalls. This construction provides smoother ride that is similar to the bias tyre, while lessening rolling resistance because the belts increase tread stiffness. The plies and belts are at different angles, which improve performance compared to non-belted bias tyres. It is considered as a transitional tyre construction type between Cross-ply and Radial-ply tyres.

iii. Radial-Ply

Radial tyre construction uses rubber coated body ply cords extending from the beads and across the tread so that the cords are laid at approximately right angles to the centreline of the tread, and parallel to each other. And the casing is stabilized by an essentially in-extensible circumferential belt.

(The Goodyear Tyre & Rubber Company April 2010)

The tread part of a radial-ply tyre stays flat with wide contact even without load. The contact area grows longer without significant width change while under load. The tread remains flat against the ground surface hence ensuring a maximum grip. With a flexible sidewall, the radial tyre can absorb bumps while rolling. The sidewall stretches in proportion to the increasing load, allowing the tread to remain flat against the road, ensuring a constant tyre patch even when lateral loads occur.

The advantage of this construction includes longer tread life, better steering control, and lower rolling resistance. Disadvantages of the radial tyre include a harder ride at low speeds on rough roads and in the context of off-roading, decreased "self-cleaning" ability and lower grip ability at low speeds.

iv. Solid

Although pneumatic tyres are commonly used in both the automotive and aircraft industries, some tyres for specific industrial and commercial applications are non-pneumatic. Those tyres are manufactured from solid rubber and plastic compounds through molding operations. Solid tyres have been used on skateboards, golf carts, scooters, lawn mowers and some light industrial vehicles and trailers where they operate under low speed or the driving and passenger comfort are not of concern.

v. Semi-pneumatic

Semi-pneumatic tyres have a hollow centre, but they are not pressurized. They are light-weight, low-cost, puncture proof, and provide cushioning. These tyres often come as a complete assembly with the wheel and even integral ball bearings. They are used on lawn mowers, wheelchairs, and wheelbarrows. They can also be rugged, typically used in industrial applications, and are designed to not separate from the wheel rim under extreme conditions.

Tyres that are hollow but are not pressurized have also been designed for automotive use, such as the Tweel (a combination of tyre and wheel). This is an experimental tyre design developed at Michelin. The outer casing is rubber as in ordinary radial tyres, but the interior has special compressible polyurethane springs to contribute to a comfortable ride. Besides the impossibility of going flat, the tyres are intended to combine the comfort offered by higher-profile tyres (with tall sidewalls) with the resistance to cornering forces offered by low profile tyres. They have not yet been delivered for market use. (Mayersohn 3 January 2005)

As mentioned above, although the tyres have been classified as five different construction types, only cross-ply and radial-ply tyres are commonly used in the automotive and aircraft industries. Belted bias tyres have not been used except in the United States. Both solid and semi-pneumatic tyres have only been applied under limited circumstances.

1.3 Tyre designation / Aircraft tyre designation

For automotive tyres, the sidewall gives information about the tyre construction, dimensions, load capacity, speed rating and manufacturer production codes. An example of ISO Metric tyre designation is shown in Figure-1.6

Figure-1.6 International Standards Organisation Metric Tyre Designation

Each symbol means:

195: Section Width, the nominal section width of the tyre in millimetres. It may be prefixed by a letter which indicates the tyre's intended usage, P for passenger tyre, LT for light truck tyre, T for temporary (spare) tyre.

65: Aspect Ratio, the cross-section height as a percentage of the section width. For this one, cross-section height will be 195 x 0.65 = 126.75mm

R: Construction Code, R means radial-ply tyre.

15: Rim size, the wheel diameter in inches to which the tyre fits.

91: Load Rating, Load capacity of the tyre which is the maximum weight the tyre can carry. A load index table can be referred for certain values. For this case, 91 means a capacity of 615kg or 1356 pounds

T: Speed Rating, Maximum speed at full load which can be referred from speed index table. In this case, T means 190 km/h or 118 mph.

The major design philosophy of an aircraft tyre, compared with other types such as passenger and truck tyres, is that they are designed for intermittent operation. (The Goodyear Tyre & Rubber Company April 2010) Because of this design feature and the operational scenarios of actual aircraft tyres, the loads and deflections for them are much higher than other tyres.

The designation of an aircraft tyre has been established to provide the information of aircraft tyre dimensions and industrial parameters such as load and pressure ratings, so that different manufacturers' tyres and wheels would be interchangeable. The nomenclature has changed throughout the years with the increasing technology, which can be seen in Table-1.1.

Tyre Name Type	Tyre size example	Nominal Diameter	Section Width	Wheel/Rim Diameter
Type III	8.50-10		8.5 inch	10 inch
Type VII	44x16	44 inch	16 inch	
Three Part	H44.5x16.5-21 28R	44.5 inch	16.5 inch	21 inch
Metric	670x210-12	670 mm	210 mm	12 inch
Radial	32x8.8 R16	32 inch	8.8 inch	16 inch

Table-1.1 Labelling of Aircraft tyres (Boeing Commercial Airplanes July 2004)

Type III was one of the earliest size designations for piston-prop type aircraft, with a low pressure for cushioning and flotation.

Type VII covers most of the older sizes and was designed for jet aircraft with its higher load capacity. The 44x16 tyre listed in Table-1.1, Type VII was used on the main gear for McDonnell Douglas DC-8-55.

All new sizes of aircraft tyres being developed are in a classification called 'Three Part Type', which was developed to meet the higher loads and operation speeds of today's aircrafts. For example, H44.5x16.5-21 28PR tyres, which are used on the Boeing 737-800 main landing gear, its designation are listed as follow:

'H' identifies that this tyre is designed for a higher percent deflection; '44.5' is the tyre diameter in inches; '16.5' is the tyre cross-section width in inches; '-' the dash line means it is a cross-ply tyre; '21' is the rim diameter in inches and '28PR' represents the ply rating of the tyre.

The tyre designation in Metric type is similar with Three Part Type, differences are the diameter and section width are in millimetres, but the rim diameter is still in inches.

Radial size nomenclature is the same as Three Part, except 'R' replaces '-' before the rim diameter, which means the construction type of the tyre is radial-ply.

A comparison has been made between a passenger tyre and an aircraft tyre (The Goodyear Tyre & Rubber Company April 2010). Both of the tyres are similar in size, but none of the other industrial parameters match. The magnitude of the parameters can be seen in Table-1.2.

Parameter	Aircraft	Passenger Car
Size	27 x 7.75 – 15	P205/75R15
Diameter	27.0 inch	27.1 inch
Section Width	7.75 inch	7.99 inch
Ply Rating	12	--
Load Rating	9650 lbs	1598 lbs
Pressure	200 psi	35 psi
Deflection	32%	11%
Max speed	225 mph	112 mph
Load/Tyre Weight	244 pound	78 pound

Table-1.2 Comparison of aircraft and passenger tyres

(The Goodyear Tyre & Rubber Company April 2010)

Comparing the load of those two tyres, the one for the aircraft can carry 9650 lbs, nearly 6 times the 1598 lbs load for the passenger car tyre. A remarkable difference can also be found for the operating pressure, 200 psi to 35 psi. The speed of the aircraft tyre is also over twice as fast as the passenger car tyre.

The heavy load coupled with high operational speed of aircraft tyres makes for extremely severe operating conditions. Compared with tyres for passenger cars, trucks, race cars, farm vehicles, and off-road applications, aircraft tyres have extreme load and speed operating ranges. This means the design, operating and maintenance practise and engineering techniques for aircraft tyres are at a higher level than other tyre applications.

1.4 Effects of aircraft operating conditions

Centrifugal force

Both heavy loads and high speeds contribute to the strong centrifugal forces acting on an aircraft tyre. When contacting the road surface, the tyre deflects as it is pneumatic. As the aircraft takes off, the tyre leaves the runway and begins to return to its un-deformed shape. Due to centrifugal force and inertia, the tread surface doesn't stop at its normal periphery but overshoots, hence causing the tyre to distort from its natural shape. A traction wave in the tread surface is set up by this. Combining this with the high speed rotation cycles, the traction wave can cause tread problems such as groove cracking and rib undercutting, resulting in tread loss.

Heat Generation

Heat has an even more detrimental effect than centrifugal forces. Heavy load and high speeds cause significant heat generation in aircraft tyres compared with other tyre applications. High internal temperatures deteriorate both fabric and rubber compound, resulting in tread and casing separations and bead face damage. An example can be seen in Figure-1.7: the tyre is designed to be operated at 32% deflection as the vertical dotted line indicates. With a constant speed and travel distance, the more a tyre deflects, the hotter it becomes. It can also be noticed: the highest rate of temperature rise versus deflection occurs in the shoulder area due to increased flexing, and the hottest part is the bead area.

Figure-1.7 Tyre temperature change vs. deflection

(The Goodyear Tyre & Rubber Company April 2010)

In this study, the thermal affect has been considered as negligible, as in the designed simulation scenarios, temperature would not significantly change. However, for further researches which would involve more complex scenarios such as tyre rolling combined with falling, the thermal affect will be put into consideration.

Tensile, Compression and Shear forces

The heavy load and high speed will also cause extremely high tensile, compression and shear forces within an aircraft tyre. If not properly maintained, these forces rise even higher until the fabric and rubber compound starts to deteriorate rapidly, causing problems such as shoulder separation, sidewall compression break, sidewall crack, liner crack, massive separation and even sidewall blow-out.

The aircraft tyres are carrying heavy loads under high speeds today, and in fact, the load and speed will probably increase in future. This will cause an increase in centrifugal force, heat generation, tensile, compression and shear forces. Aircraft tyres will function properly only when they have the correct inflation pressure. And a relatively small amount of tolerance in the amount of deflection also exists in which the tyre can operate effectively. (The Goodyear Tyre & Rubber Company April 2010)

1.5 Dunlop Aircraft Tyres Limited

The cooperating company, Dunlop Aircraft Tyres Limited (DATL), is a global supplier of new and retreaded tyres for the aerospace market. From its headquarters in Birmingham UK, new and retread tyres are designed, tested, manufactured, marketed and despatched.

Dunlop Aircraft Tyres works closely with aircraft manufacturers, MROs (Maintenance, Repair & Operation) and airlines to support a wide range of aircraft across the world. It also operates globally in the aircraft tyre market. Its products have been widely used on regional jet and turboprop, narrow bodied and wide bodied jets and also military aircraft. Regional jets (Figure-1.8) and turboprop aircraft allow airlines the opportunity to efficiently connect the spokes with the hub to provide frequent services and facilitate excellent market coverage. The regional jet and turboprop aircraft provide an essential supporting role to international air travel markets. The turboprop market has been resurgent in recent years due to the attractive economics of operating smaller more fuel efficient aircraft on short cycle time routes.

Figure-1.8 Regional jet (Dunlop Aircraft Tyres Limited)

Dunlop Aircraft Tyres is well positioned to lead the market in the Regional Jet and Turboprop segment. It has certification in place or certification pending on the most popular aircraft within the segment including the Sukhoi Superjet and Antonov 148.

Narrow and wide body jets form the bedrock of the world aircraft fleet. Narrow body jets are amongst the most flexible of aircraft and are favoured by the low cost carriers for their economy, ease of maintenance, short turnaround time and attractive economics for high frequency and high demand routes.

Dunlop Aircraft Tyres is certified on the most popular narrow body aircraft such as the Boeing 737, (Classic and Next Generation) and certain versions of the Airbus A320. The class, dominated by the A320 and the 737, is the worlds' most popular class of airplane. Over 6,500 are in active service and many of these could be fitted with Dunlop bias or Dunlop radial tyres.

Wide body Aircraft are deployed on the longest and often most profitable routes. The market is smaller in numbers and cycles than the narrow body market and is an important airliner market for Dunlop. Dunlop Aircraft Tyres have tyres certified for the 767, 757 and 747 and is developing tyres for other wide body aircraft.

Figure-1.9 Wide Body aircraft (Dunlop Aircraft Tyres Limited)

The military operations place great demands on aircraft tyres. Loads can be substantial and speeds might be upwards of 225Mph.

Dunlop Aircraft Tyres have been used in an impressive range of military airplanes from the legendary Spitfire and Vulcan to the most modern F-35 Joint Strike Fighter, the Tornado and the Hawk. Heavy military aircraft such as C-130 are often fitted with Dunlop Tyres for their excellent service record and retreadability; a factor that no doubt helped Dunlop Aircraft Tyres to win approval and selection for the A400M.

Today, Dunlop Aircraft Tyres serve Air Forces, Naval Forces and Marine Corps around the world with tyres designed to offer optimal operational characteristics in the harshest environments.

Figure-1.10 Military aircraft (Dunlop Aircraft Tyres Limited)

Apart from the applications mentioned above, Dunlop Aircraft Tyres is also certified on many Business Jets, General Aviation Aircraft and civil and military Rotorcraft.

New products are introduced into service regularly such as a new bias tyre for the A400M military transport plane and a new radial tyre for the Boeing 737 NG. The range of new tyres cope admirably with the industry's requirements for increased take off and landing speeds, lower weights, higher loads, improved landing life and improved retread characteristics. (Dunlop Aircraft Tyres Limited)

1.6 The significance, purpose and scope of the study

The tyre plays an important role for an aircraft and it is critical for aircraft safety and performance on the ground. The compatibility between the tyre and the wheel is an important requirement for aircraft certification.

The aircraft is a heavier than air machine and making it land and take off from a surface is of paramount importance. This is facilitated by what is termed a Landing Gear mechanism. The word gear can sometimes be a misnomer, but it refers to the Landing apparatus in its entirety and involves no gears. (Singh 28 November 2011)

The landing gear of a modern aircraft is a complex piece of engineering and is part of the aircraft design. It is something worked out on the design table itself and integrated with the other systems of the aircraft. It is peculiar to each class and model of aircraft. The landing gear in most aircraft consists of a tricycle configuration. This has a landing wheel that retracts into the nose (forward fuselage) of the aircraft and a set of two wheels that normally retract into the wings of the aircraft. All landing gears have a brake assembly and anti skid mechanism, which are centred on rubberized tyres or wheels. The retraction into the body is basically to cut down on air resistance and the drag coefficient. The National advisory Committee for Aeronautics (NACA) by testing in a wind tunnel in 1927 came to the conclusion that the aircraft landing gear made a significant contribution to the drag of an airplane. Retractable landing gears thus became a priority.

Modern aircraft design incorporates the Landing gear system with the aircraft. This is an entire process of engineering and parameters such as weight, runway design, structures and economics come into play. This is referred to as Multi Disciplinary Optimization (MDO). Landing gear is a part of MDO and incorporates flight mechanics, stability, control and performance.

For an aircraft approaching an airfield for landing at about 240km /hour, interactions between the tyre body and the wheel flange will generate great deformation, stress and heat when the tyre and wheel assembly come into contact with the runway surface. Modern aircraft wheels are among the most highly stressed parts of an aircraft. High tyre pressures, cyclic loadings, corrosion, and physical damage contribute to failure of aircraft wheels. Complete failure of an aircraft wheel can be catastrophic.

Figure-1.11 and 1.12 show a couple of damaged aircraft tyres and the wheel used for an A380 for an incident that occurred on 30th March 2010: a Qantas A380 burst its tyres upon landing in Sydney. As shown in the figures, not only were the tyres shredded, there was also substantial damage to the landing gear with the part of the wheel completely chipped off. (Horton 11 April 2010)

Figure-1.11 Burst A380 tyres (Horton 11 April 2010)

Figure-1.12 Damaged A380 wheel (Horton 11 April 2010)

Figure-1.13 and 1.14 show another incident that happened on 21st Sep 2005.

An Airbus A320 made an emergency landing at Los Angeles International Airport with its nose wheels rotated 90 degrees.

Figure-1.13 JetBlue A320 with its nose landing gear jammed (Al 7 Dec 2008)

Figure-1.14 A320 during its emergency landing (Al 7 Dec 2008)

A fault in the computer steering system caused the plane wheel to repeatedly steer left and right and couldn't be reset by the plane's crew while in the air. The emergency landing was successful as no one was hurt in the incident. However, upon touchdown, the nose landing gear tyres rapidly deflated and tore apart, and both wheels were worn into the axle as shown in Figure-1.15.

Figure-1.15 Damaged tyres and wheels removed from A320 (Al 7 Dec 2008)

The incidents mentioned above were under extreme situations and were fortunate enough to cause no injuries and deaths. However they still revealed how seriously the aircraft tyre and wheel could be damaged by external force and their interaction under certain conditions. It is also a fact that after each aircraft hard landing case, no matter if there's any damage, injury or not, a comprehensive safety inspection on the aircraft landing gear and tyres has to be processed. The aircraft will not be able to serve until it passes the inspection or after corresponding maintenance.

Although protection systems have been applied to minimize negative effects, it is still important for the aircraft tyre and wheel manufacturers to assess the performance and failure criteria of a tyre/wheel assembly under certain conditions in the product design and development stage. Additionally, the study of tyre properties and the interaction between the tyre and the wheel will significantly help in improving the performance of an aircraft tyre and landing dynamics. A reliable virtual model of an aircraft tyre/wheel assembly is considered to be of significant value for aircraft tyre manufacturers.

Comparing tyre modelling within the automotive industry, aircraft tyre modelling is more technically challenging because most of the available tyre models are developed for automotive applications. Due to the complexity of the inner tyre structure and various material characteristics, it is a great challenge to investigate the interaction between the tyre and the wheel using a finite element methodology.

1.7 Summary of the chapters

Abstract and Chapter 1: Introduction

Chapter 2: Literature review

Chapter 2 focuses on the review of the applications of finite element methodologies for pneumatic tyres and wheels used in both the automotive and aircraft industries. Existing tyre and wheel finite element models, along with their analysis methodology, modelling techniques and results will be reviewed in detail. The review will also include the aircraft tyre construction, aircraft tyre loading cases in operational and testing scenarios, finite element method for tyre modelling, material models, characterizations and correlation for tyre finite element analysis.

Chapter 3: Material models, theories and equation

Rubber and fabric composite materials are the major components of an aircraft tyre. Chapter 3 discusses the fundamental material models and the mathematic theories for rubber-like material subject to large elastic deformation. These models are frequently used in commercial finite element software for rubber components. The modelling of various rubber-like materials often starts with a strain energy function. To define the nonlinear hyperelastic behaviour of a rubber-like material, a stress-strain relation is also required to determine parameters in the strain energy potential. The proper selection of a rubber elastic material model is always the first and foremost concern.

Chapter 4: Finite element model building

Chapter 4 introduces the development steps of the tyre and wheel finite element model. Parts of the wheel and the tyre, finite element meshing process, meshing size chosen, simulation time steps and mass scaling set up, rubber and fabric material properties are introduced in detail. The crucial material characterization and correlation (rubber and fabric) in Ls-Dyna have also been introduced.

Chapter 5: Simulations and results discussion for different scenarios

Chapter 5 introduces several Ls-Dyna simulations duplicating aircraft tyre testing and operational scenarios. The static load simulation results and comparison with Dunlop actual test data will also be discussed. The scenarios include both dual bead and single bead model under inflation, static load and dynamic impact with various touchdown vertical speeds.

Several criteria have been chosen to assess the tyre performance and safety certification, including tyre deflection rate, rated load, and stress and load distribution on contact area and bead cord.

The results have been analyzed and compared, demonstrating how the tyre structure design change would affect its interaction with the wheel assembly.

Chapter 6: Conclusions

Chapter 6 describes the uniqueness of the study, the speciality of the finite element model, the limitations of the current study and the recommended further studies.

2. Literature review

The tyre plays an important role in aircraft landing gear and it is critical for aircraft safety and performance on the ground. The compatibility between the tyre and the wheel is an important requirement for aircraft certification. The study of tyre properties and the interaction between the tyre and wheel will significantly help in improving the performance of an aircraft tyre and landing dynamics. Comparing tyre modelling in the automotive industry, aircraft tyre modelling is more technically challenging because most of the available tyre models are developed for automotive applications. Due to the complexity of the inner tyre structure and various material characteristics, it is a great challenge to investigate the interaction between the tyre and the wheel using a finite element methodology.

Through the survey, a significant number of different tyre models have been found in the literature. The models can be classified according to the methodology used, the aim of the study and the tyre parameters studied.

The commonly used methodologies for tyre behaviour investigation include: analytical models, semi-analytical models and the finite element method.

The dynamic models for tyres can be categorized according to the aim of the analysis.

The models concerning the lateral forces generated in the contact patch are relevant in handling analysis and runway manoeuvres. The models concentrating on vertical and longitudinal forces generated in the tyre are used for ride performance analysis. Also, there are models for tyre noise, vibration and harshness analysis. All the tyre models have been analyzed under either steady state or transient dynamic response, and have been shown to predict stress and deformations in these previous studies

In this chapter, the literature review will focus on the application of the finite element methodologies for pneumatic tyres and wheels used in both automotive and aircraft industries. Existing tyre and wheel finite element models, along with their analysis

methodology, modelling techniques and results will be reviewed in detail. The review will also include the aircraft tyre construction, aircraft tyre loading cases in operational and testing scenarios, finite element method for tyre modelling and material models for tyre finite element analysis.

Although the aim of this project is to analyse the interaction between the aircraft tyre and the wheel rim while under certain load conditions, some studies using similar modelling strategies but with different scopes are presented in the literature review, therefore, the review of finite element tyre models is not limited to the tyre and wheel interaction investigation.

2.1 Finite element wheel and tyre models

The method of finite element analysis is a creditable approach in evaluating different performance effects on the components of tyres. It is able to predict different tyre behaviours in certain conditions. In industry, the design and production process of a new tyre is extremely expensive, so to apply the approach of tyre finite element analysis is of significant importance for the manufacturers to save time and cost.

Because of the application of high-performance computers and the enhancement in the capabilities of existing proprietary finite element software, recently, the use the predictive finite element models in tyre design and analysis has become more popular. The efficient use of such tyre models in solving the complex problem of pneumatic tyre behaviour has been considered as an alternative approach to the costly experimental tests routinely carried out on tyre prototypes.

The finite element model for a full scaled aircraft tyre can be described as two major parts: the model for the wheel and the model for the tyre including rubber and fabric material.

Wheel model

The development of wheels, especially aircraft wheels is driven by the requirements for reducing weight and cost and improving performance. Its process has relied on various products testing in history. The wheels tend to be fatigue limited so that the testing could be time consuming. Effective stress and fatigue analysis is required to reduce the reliance on testing.

The finite element methods of stress and fatigue analysis for aircraft wheels have significantly advanced during the last 3 decades. In the 1970s, finite element analysis was first employed in the development of aircraft wheels. In these first few years, the cost and complexity limited the extent of this numerical method. The analysis was limited to 2D and linear applications. A common approach of the time involved modelling wheels as being axisymmetric with non-axisymmetric loading via harmonic elements. (Fish, Pajot and Patterson 2002) By the mid 1980s, with the help from advanced computing power and the improvement in FEA software, 3D analysis became possible but only practical for linear analysis. But the model size and extent were still limited then.

Only until the early 1990s, with the application of low cost UNIX workstations, did a 3D finite element model of a complete aircraft wheel become feasible. Consequently, finite element models of wheels started to include non-axisymmetric features such as spokes and wheel half tie bolts.

A creditable and detailed approach of building a finite element model for an aircraft tyre was introduced by Fish, Pajot and Patterson in their work. (Fish, Pajot and Patterson 2002)

Basically, the development of wheel analysis should be able to produce analysis results which compare well with real test. The data extracted from a strain roll test provides a stress history at discrete points on the wheel and can be considered as the foundation of fatigue analysis. A completed finite element wheel analysis would have to contain the wheel assembly, axle, and tyre with the same load history. But, it is not practical to achieve that level of complexity at the moment.

Hence, two simplifying assumptions are applied in finite element wheel analysis. The first one is that the effect of the tyre can be represented with an appropriate set of tractions applied to the wheel rim. The other one is that the rolling wheel with its loads applied at the ground can alternatively be considered as a stationary wheel with loads moving around it.

The external loads, including inflation and ground loads, acting on the wheel are complicated by the nonlinear nature of the tyre. Experimental work has provided the foundation for an empirical method to describe tyre-to-wheel loads for finite element analysis. This method is continuously refined by both additional experimental measurements and detailed tyre/wheel modelling.

The load on the rim due to inflation is axisymmetric, but the distributions of rim load due to ground loads are localized and potentially have no symmetric behaviour. In practice, within the approximate nature of the empirical tyre-to-wheel loading method, there is symmetry about the vertical axis through the centre of the tyre and wheel.

Describing a typical wheel as largely axisymmetric, but interrupted with significant non-axisymmetric features geometry, Fish and his colleagues also provided a typical aircraft wheel finite element model as shown in Figure-2.1. The non-axisymmetric features, including spokes, wheel half tie bolts and drive bosses for the brake rotor discs are repeating in nature so as to fit a pattern of cyclic symmetry. Hence, this wheel model can be represented as a series of repeating pie slices where each slice encloses a window as shown in Figure-2.1.

Each of the pie slices is a plane of symmetry, which means a half slice can be reflected to generate the pie slice. This feature also allows the entire wheel geometry to be generated simply by mirroring and replicating the pie slice.

Figure-2.1 Finite element wheel model (Fish, Pajot and Patterson 2002)

The symmetries representation in both the wheel geometry and the tyre-to-wheel loading gave an opportunity to exploit these symmetrical features in order to reduce the overall cost of the finite element analysis of wheel.

Tyre model

The tyre primarily owes its ability to withstand different loading conditions, such as inflation pressure and vehicle load, to the network of fabrics sandwiched between its rubber components (Gough 1981). Long ago, the importance of employing reinforcement material in pneumatic tyres had been recognized by J. B. Dunlop, who made the first pneumatic tyre using an Irish flax fabric. However, the requirements have increased over the years because of the severity of tyre operational condition. The manufactures seek cheap but still high-quality cords such as reinforcement materials made of cotton, rayon, polyester, steel, Kevlar and fibreglass etc. As a result, those materials are increasingly being introduced into the tyre cords market.

The different characteristic properties such as adhesion to rubber, heat ageing resistance, thermal stability, and fatigue resistance of these cords are considered during the tyre

manufacturing stage to achieve the ideal tyre behaviour. Typically, nylon's high strength is required to provide adequate carcass strength, while polyester's high elastic modulus and low elongation reduce tyre deformation under service conditions, leading to a better high-speed performance and tread wear, reduce tread cracking and better steering characteristics or manoeuvrability (Bol and Reese 2003). However, in most cases, steel wire cords are employed for the belt cords of radial tyres in order to provide directional stability for the tread during steering. Since none of the single commercial cord can achieve the entire reinforcement material requirement in a tyre, various types of combined cords are used in industry depending on the different tyre properties.

2.2 Tyre (Aircraft tyre) construction

Bias-ply and Radial-ply tyres are the most used tyre types for automotive and aircraft application. Since application of radial tyres in aircraft industry is recent but increasing. It will become dominant in the future. Also considering the cooperating company, DATL's recommendation, this study has concentrated on radial-ply tyres.

Referring to the BOSCH automotive handbook (Robert Bosch GmbH 2007) the structure of a typical radial pneumatic tyre on mount contents 1-Hump, 2-Rim bead seat, 3-Rim flange, 4-Casing, 5-Airight inner liner, 6-Belt, 7-Tread, 8-Sidewall, 9-Bead, 10-Bead core. Figure-2.2 shows the tyre-construction (tubeless version)

Figure-2.2 Tyre-Construction (Tubeless version) (Robert Bosch GmbH 2007)

A detailed radial aircraft tyre contains even more complex constructions.

John A. Tanner (Tanner and Daugherty 2005) has exhibited a radial-ply aircraft tyre construction (shown in Figure-2.3) in his paper, concerning the mechanical properties of 27x7.75R15 tyres which is used as nose-gear tyre on the Boeing 737-300 through 900 aircraft. The project presented the tyre footprint characteristics, tyre vertical load-deflection characteristics, cornering characteristics and other tyre information.

Figure-2.3 Radial-ply aircraft tyre construction (Tanner and Daugherty 2005)

Attention should also be paid to the structural difference, especially in the bead area between various types of radial aircraft tyres.

For this project, a specific aircraft test tyre provided by DATL has been chosen, which contains the list of constructions below:

Cable bead: Bead Code, Wrapping

Fabric: Chafer, 1st to 4th Plies, Bias Breakers, 0 Deg Belts, Inner Tread Fabric

Compound: Chafer, Inner Liner, Apex, Clinch, Insulations, Sidewall, Breakers Cushion and Strips, Sub Tread, Tread

Figure-2.4 shows the structure definition of this specific test tyre. It can be seen that the construction of Bead area and under-tread plies differed compared with the tyre structure in Figure-2.3. Table-2.1 has listed details of the tyre structure, including bead diameter, fabric angle and compound details.

Figure-2.4 H41x16.0R20 tyre cross-section (Dunlop Aircraft Tyres Limited 2010)

Table-2.1 Tyre Structure Details (Dunlop Aircraft Tyres Limited 2010)

2.3 Aircraft tyre loading case

Operational scenario

Typical aircraft operational scenarios include aircraft take-off, landing and runway taxiing.

Patrick Berry in Linkoping University has summarised the procedure of loading case modelling for aircraft landing gear and tyre design. His focus was put on the aircraft take-off loading case. In his paper (Berry 1999), the definition of MTOW (Max Take off Weight) has been mentioned as the most important factor in main landing gear wheel tyres selection for aircraft landing gears. On the other hand, nose wheel tyre selection has been summarised as based on a quasistatic load which is about 75% of the dynamic load.

Lee S. Mayer of the Cessna Aircraft Company has summarised the approaches of simulation for aircraft landing gear dynamics using CATIA, CATDADS, DADS and NASTRAN as well. The steps for aircraft loading case analysis have been defined in his paper (Mayer 2000) as follow:

1. Aircraft modal models
2. Load coefficients
3. Non-linear landing gear models

4. Aircraft air load models
5. Flexible landing model with gears
6. Calculation and summary of aircraft loads.

The tyre loads in Mayer's study have been modelled using DADS simple-full tyre element formulation discussed in the DADS manual. The formulation accounts for vertical loads, drag forces, rotational inertia of a spinning tyre, and lateral forces as applied to the tyre/road contact patch.

On the other hand, Phillip Wang and Anita Teo have published their research on aircraft runaway and drive taxiing behaviour, respectively aiming the aircraft level steering runaway failure analysis (Wang and Dacko 2009) and the aircraft electronic wheel and tyre drive taxiing examination (Teo et al. 2008).

Anita Teo (Teo et al. 2008) has defined that the aircraft taxiing operation consisted of two main phases namely the taxi-in and taxi-out phases. The procedure for outbound flights involved three main stages: pushback, taxi-out and take off while for inbound flights, it involved five main stages: application of reverse thrust, braking, and removal of reverse thrust, retraction of nacelle cowls and other flight surfaces, and taxi-in. The loading cases in the taxiing system have covered reverse, forward and turning mode manoeuvres.
Detailed loading parameters for the runaway simulation case have also been mentioned by Phillip Wang (Wang and Dacko 2009), including steering angle, aircraft taxi speed, maximum ramp weight and hydraulic temperature.

Although all the previous works mentioned above had more focus on the modelling of landing gear structures or the aircraft itself rather than the tyre, the loading cases for the finite element modelling which have been discussed for aircraft take-off, landing, runaway and taxiing were still valuable references for this project.

Testing scenario

For this project, aircraft tyre/wheel interaction modelling, more concentration should be put onto the loading cases in the aircraft tyre and wheel testing scenario. This is because the finite element models and simulations are planned to be compared with the target industrial tests in DATL.

The series of industrial tests include:

1. Tyre inflation test, only internal pressure loaded in the test tyre mounted on the wheel rim, to establish the inflated dimensions without any external load. In an extreme case such as the bursting test, tyre burst pressure will be applied.
2. Static test, so-called deflection test, internal pressure loaded and an external radial load as well with the tyre mounted on the wheel rim and in contact with a platform, representing the road surface.
3. Dynamic test, internal pressure load, radial road, double overload and rolling speed may be applied as the input conditions.
4. Real road surface test, tyre/wheel assembly will be tested on real road surfaces, but this approach was not applied in this project.

Referring to Dennis S. Kelliher's paper (Kelliher 1999), the tyre loading cases in these test scenarios consist of:

1. Mounting of the tyre onto the rim
2. Application of internal pressure to the tyre
3. Vertical force applied via road surface to lug elements on the outside of the tyre.

The loading history of the finite element tyre model coincided closely with actual tyre:

Step 1, Mounting of the un-inflated tyre to the rim

Step 2, Application of inflation pressure to the inside of the liner

Step 3, Application of either a vertical deflection or a desired vertical force to the road surface.

Detailed finite element modelling approaches and techniques in Kelliher's work will be discussed in the next part of this review.

Jani K. Ojala has also discussed the application of Abaqus/Standard and Abaqus/Explicit in Nokian Tyres. The finite element model has been developed to simulate a studded winter tyre on ice. Loading case of the specific tyre included axisymmetric 2D model inflation, footprint analysis and steady-state rolling with camber (Ojala 2005). The steady state rolling simulation has been processed using the *STEADY STATE TRANSFORT function in Abaqus. The critical shear stress has been calculated, applying a typical finite element modelling strategy which will also be reviewed later. The case has shown the capacity of Abaqus to be rapidly implemented into company's research and development environment.

Figure-2.5 Footprint (left) and Steady state rolling with camber (right)

(Ojala 2005)

The review of aircraft tyre loading cases has confirmed the strategy of this tyre/wheel interaction modelling processes and simulation scenarios set up. The scenarios will include: inflation, static vertical load, dynamic impact and furthermore, rolling with camber, corner or slide as the case maybe. Detailed finite element modelling strategy, methods and specific techniques referring from the previous research and projects summarised here, will be discussed in the following chapter.

2.4 Finite element methods for tyre modelling

The finite element method has been introduced into tyre design and development process in order to reduce both cost and development time. The advantage of using finite element simulation methods is that the resulting data can be relatively easily acquired and also the time-cycle of research and development can be shortened. However, the finite element modelling strategies and simulations require validation and the user's competence in each individual specific field. Thus, the reviewing of the finite element methods which would be applied for this project has become essential.

Generally speaking, the tyre design and simulation process covers the cycle of design iterations, including the finite element modelling, analysis and improvements.

Figure-2.6 Tyre design and simulation process (3DS SIMULIA 2009)

The applications of Abaqus include quasi-static loading, rolling and etc.

SIMULIA (3DS SIMULIA 2009) has introduced the key features for each individual application.

For example, the rim mounting, inflation and footprint analysis have involved tyre lift equation* for mapping reinforcement geometry and Symmetric Model Generation (SMG) Revolve and Reflect features for generating Partial and Full 3-D tyre model. Treaded tyres in quasi-static loading cases can be applied by attaching the tread pattern to the carcass and the tread meshing in Abaqus/CAE.

Figure-2.7 Symmetric Model generation process and Geometry for uncured and cured tyres (3DS SIMULIA 2009)

* Structural tyre analysis is often performed using the cured tyre geometry as the reference configuration for the finite element model. However, the reinforcement geometry is more conveniently specified with respect to the 'green', or uncured, tyre configuration. The tyre lift equation provides mapping from the uncured geometry to the cured geometry as displayed in Figure-2.7. (3DS SIMULIA 2007)

The Rolling simulation contained steady state rolling and tyre dynamic rolling, within which mixed Eulerian-Lagrangian scheme, rolling resistance and torque computation, braking, cornering can be applied.

Figure-2.8 Lagrangian scheme (left) and Eulerian scheme (right)

Abaqus steady state rolling simulation (3DS SIMULIA 2009)

SIMULIA has also claimed the availability of General Contact in Abaqus/Standard, including surface-to-surface formulation and penalty method, identical user interface to Abaqus/Explicit and the comprehensive support in Abaqus/CAE.

Although further applications such as tyre hydroplaning and Noise & Vibration analysis have also been introduced and may be discussed, they are beyond the scheme of this project.

Specific modelling methods and techniques for different applications have been reviewed from Abaqus users' conference published by The Goodyear Tyre & Rubber Company (Kelliher 1999), Hankook Tyre Co. (Kennedy 2003), FIAT Auto Spa (Marco and Antonio 2003), and published papers from SAE database by Cessna Aircraft Company (Mayer 2000) and The Boeing Company (Tanner and Daugherty 2005)
Referring to Koishi's work (Koishi and Kabe 1998) the steady state rolling contact problems between a rolling deformable body and a rigid surface could be conducted using Abaqus/Standard. Detailed approaches after have been presented as follow:

1. Rim mounting, 200KPa pressure of inflation
2. 3D FE model generation based on inflated results

Figure-2.9 2D cross-section and 3D FE model (Koishi and Kabe 1998)

3. Braking and driving simulation; considered with slip angle of 0 deg in order to determine the free rolling radius of the tyre. Free rolling was defined as the state without longitudinal force other than rolling resistance. The steady state rolling simulation was based on moving reference frame technique with a vertical load of 4kN applied to axle of the tyre, a travel velocity 10km/h of the tyre and angular velocity 8 rad/s to 10 rad/s. The result has shown the driving force versus different angular velocity and indicated the free rolling occurred at an angular velocity of 8.87 rad/s. Therefore the free rolling radius of 313.28mm has been estimated.
4. Cornering simulation, conducted at several different slip angles, predicted cornering force and self-aligning torque at different slip angels (Figure-2.10, 2.11). The results have been compared with experimental data obtained using MTS Flat-Trac Tyre Test systems. Contact patch and contact pressure distribution during cornering at different slip angles have also been shown.

Figure-2.10 Driving force at different Angular velocity (Koishi and Kabe 1998)

Figure-2.11 Cornering force and self-aligning torque (Koishi and Kabe 1998)

Koishi has concluded the effectiveness and capability of using the steady state rolling contact function in Abaqus/Standard from the points of view of both accuracy and CPU cost. It has also been mentioned that some results, which were difficult to observe from actual road experiment, could be obtained through these approaches. Although Koishi has only used a simple tyre model and the research was in an early stage when Abaqus was applied into the Yokohama Rubber Co., Ltd., the methodology was still of value.

Aiming at temperature prediction in an off-road tyre analysis, Dennis S. Kelliher has developed a three part analysis procedure (Kelliher 1999), including:

1. The finite element stress analysis to determine the strain distribution within the tyre, using Hyperelastic materials, non-linear geometry, ‘glue’ contact surfaces between tread/carcass and standard contact surfaces between tyre/road and tyre/rim.

2. Energy dissipation analysis to predict heat generated by the strains predicted in part 1.
3. The finite element heat transfer analysis, using the heat generation from part 2 to determine steady state temperature.

The model has been built based on one of the largest vehicle tyres in the world, 40.00R57 for haulage trucks operating at very high temperature. The methodology is given as follows, which has been employed in numerous previous studies.

The finite element model has been divided into two parts. The rim and road were both modelled as rigid surfaces. The loading of the tyre consists of: mounting the tyre onto rim, application of internal pressure to the tyre and vertical forces applied via the road surface. The simulations were applied to five different load cases, none involved tyre rotating. The rim surface was restrained in all directions to prevent any rigid body motion. Comparing the heat transferred from rim and ambient with the high operating temperature, the heat generated from the friction between tyre/road and tyre/rim has been considered as negligible. Therefore, the tyre/rim and tyre/road contact have been assumed to be frictionless in Abaqus/Standard. The simulation results based on this assumption have shown good correlation as displayed in Figure-2.13.

The finite element tyre model has been defined as two distinct regions, tyre carcass and the tread. Two regions were meshed independently and were not congruent. For most of part, the rubber compounds and steel bead were modelled with first order hex elements supplemented with a small number of wedge elements where necessary. Hybrid elements were used for the rubber since incompressibility was assumed. The ply and belts were modelled with first order membrane elements with Rebar elements used to define the reinforcements.

*Contact Pair option has been used to attach the carcass and tread with tied contact.

*EQUATIONS function in Abaqus/Standard has also been used to prevent any rigid body motion.

Figure-2.12 Abaqus heat transfer model (Kelliher 1999)

As the result, Kelliher provided a quantitative comparison of the temperatures recorded during testing to those determined in the analysis.

Figure-2.13 Comparison of test date and FEA results (Kelliher 1999)

Although two shortcomings of the method existed, which were the requirements of prior knowledge of the cavity and rim temperatures, and the calculation of limited heat transfer coefficient (two of five load cases), the finite element based temperature prediction analysis has still been shown to be useful as a design tool for use in off-road tyre program.

Marco has published FIAT's work on numerical simulation of full vehicle tyre dynamic behaviour on the interaction between Abaqus/Standard and Explicit codes (Marco and Antonio 2003). According to his research, the critical point in facing problems such as non-linear dynamic transient behaviour of full finite element models was related to the choice of the best way to combine the simulation of quasi-static and dynamic phenomena. The ideal numerical solution was to perform the quasi-static analysis, equilibrium prior to the dynamic simulation, using an implicit code and then use the implicit results as initial condition of the dynamic analysis performed with an explicit code. The Abaqus code has both implicit and explicit solvers, with the possibility to transfer the information between them by *IMPORT capability, applied in both directions.

The advantage of using explicit was the facility to define and manage the contact problems. For example, two different contact algorithms were available: the kinematic and the penalty. In case of kinematic enforcement of contact conditions, solver would first advance the kinematic state of the model into a predicted configuration without considering the contact conditions, and then determines which slave nodes in the predicted configuration penetrate the master surfaces.

The penalty algorithm resulted in less stringent enforcement of contact constraints than kinematic. It would search for slave node penetrations in the current configuration, and then apply the contact force as a function of the penetration distance to the slave nodes to oppose the penetration, while equal and opposite forces act on the nodes of master faces being penetrated.

The negative issue related to explicit method was that the simulation of static phenomena could not be applied. On the other hand, implicit method could be used for solving both, static and dynamic problems, whereas the explicit solution could not be used if mass and damping effect were neglected.

Facing the numerical dynamic problems regarding the issue of full vehicle model passing over an obstacle using finite element approach, Marco has summarised the processes of modelling and validating, which included:

1. Tyre seating on rim, performed moving the nodes interfaced to the rim to the mounted position
2. Inflating, performed applying a distributed load to the internal surface of the plies
3. Loading, composed of an initial enforcement of the contact interaction at ground and afterward the effective loading of the wheel at test conditions.

Two different model simulations have been carried out: a semi-flexible model created by importing only tyre and wheel as deformable elements from process 4 of implicit analysis, and a complete model where all components were imported from previous implicit analysis as deformable.

Comfort Obstacle (Bumping) and Pothole Obstacle conditions have been applied respectively, which can be seen as follow.

Figure-2.14 Comfort Obstacle (top) and Pothole Obstacle (bottom)

(Marco and Antonio 2003)

As his conclusion, Marco has claimed the integrated CAE methodology, based on integration of Abaqus Implicit and Explicit codes, to be able to evaluate the transient dynamic response of full vehicle rolling on the road in the presence of obstacle. Further applications could still be carried on.

In Ojala's published paper, some detailed finite element approaches have been presented. (Ojala 2005)

In the development process of a studded winter tyre by Nokian Tyres Plc, Abaqus/CAE and Abaqus/Standard & Explicit code have been utilized.

The development focused on the stress distribution around the belt edge area. A specific tyre of size 225/70R15C was chosen as an example and the axisymmetric finite element model was first created for rim mounting and tyre inflation purpose.

Figure-2.15 Axisymmetric finite element model of 225/70R15C after inflation (Ojala 2005)

The meshing around the area of interest, which was the belt edge area, has been refined to be quite dense in order to obtain accurate results. Wheel rim was modelled as an analytical rigid surface.

According to Ojala, the technique of using rebar elements was useful for quite many tyre analyses but not in Nokian's case since with rebar element, the stress distribution accuracy couldn't be ensured. Membrane elements were used instead, sharing the nodes with elements of matrix material.

After inflation, Ojala has created a 3D finite element model for footprint analysis, using *SYMMETRIC MODEL GENERATION option in Abaqus. Ojala has recommended this to be a very efficient and user friendly tool, since all sections, material assignments and surfaces are maintained. Pictures of the 3D model and footprint can been seen as follow.

The rolling simulation with a camber has been processed as the last step in Ojala's research. The analysis has been done by using *STEADY STATE TRANSPORT option in Abaqus. Although the temperature was important factor in fatigue analysis, the analysis didn't involve the temperature related factors. The object of the research was to compare two different constructions and how the risk of belt separation could be reduced.

Results has presented the shear stresses in rubber around belt edge area, showing the mainly cause of belt separation was shear stress component, caused by the deformation of the steel cords. A comparison between old and improved design can be seen in Figure-2.16 with a remarkable reduction of the critical shear stress, indicating the positive progress of new design.

Figure-2.16 Critical Shear Stress Comparison (Ojala 2005)

Ojala's case has shown a successful example how Abaqus can be rapidly implemented into company's research and development environment, regarding the advantages and benefits of using Abaqus in Nokian Tyres.

Further researches on specific finite element modelling methods have also been processed. For example, an advanced experience with application of cylindrical elements in Abaqus has been introduced by Kennedy. The purpose of using cylindrical element was to overcome the limitations using 8-node brick elements and 4 node membrane elements when representing the cylindrical geometry around the tyre circumference (Kennedy 2003).

In the study, a P235/75R17 tyre was modelled by the Hankook Tyre Co.. Half the tyre cross-section was used to create axisymmetric model. Brick elements were used for the rubber components, with rebar in membrane elements for the ply and belt layers. Linear elastic material properties were used for each component. Analytical rigid surfaces were used to model the wheel rim and the road surface. This half cross-section, axisymmetric model was used to inflate the tyre first, and then served as the starting point for each of the 3D models used in subsequent parts of the study.

After inflation, symmetric model generation is used to revolve the half-section model to create 3D models. It's worth to mention that Kennedy has used more refined mesh in the region that will potentially come into contact with the road. Outside of the region, a progressively coarser mesh was used since the road contact region was of primary interest.

Four different 3D models were used, differing in element type and mesh refinement.
The first one consisted all of general 3D elements, as a typical model used in normal tyre analyses for design purposes, and gave reasonable results compared to experimental measurements.

Three additional models were made using cylindrical elements for comparison to the all-general element model. The first of these three was made up of all cylindrical elements, containing the same number of node segments around the tyre circumference

as the all-general model. It contained half the number of elements as the general element model since the cylindrical element used mid-side nodes on its edges around the circumference. The second cylindrical model was made up of all cylindrical elements but reduced number of elements outside the potential road contact region. The angle spans of the elements were 20, 50 and 90 degrees, while the road contact region still contained the same number of elements as the previous one. The third cylindrical model is a mixture of cylindrical and general 3D elements. The meshing refinement used outside the potential road contact region was still in use. General element mesh was used for the region where potential contact existed. All the four different 3D finite element models were shown in Figure-2.17. (Kennedy 2003)

Figure-2.17 Four different 3D models (Kennedy 2003)

The four models were used to conduct the study of element behaviour in both static and steady state rolling conditions. The CPU time, vertical spring rate, and contact footprint shape and pressure distribution were used to compare the performance of the revolved half-section models in static loading conditions. The lateral force generated by tyre ply steer was added as another model comparator in steady state rolling conditions.

In both static and steady state rolling models, results have shown a remarkable reduction of total run time and per-iteration run time while cylindrical elements in use. Evaluations of contact footprints between the tyre and road surface predicted by the four different models found only small differences in shape and pressure values.

Regarding the comparison of results, Kennedy has pointed out that a model incorporating a reduced number of cylindrical elements outside the potential ground contact region would produce roughly equivalent results at a significant reduction in model run time. Reducing mesh density of cylindrical elements outside the contact region provided a more efficient solution with nearly identical results.

It has been concluded that cylindrical elements have proven to be a useful addition to the elements available in Abaqus. Two significant improvements of using cylindrical elements included: the model run time is reduced without sacrificing significant accuracy, model failure much less likely due to improved convergence behaviour.

The cylindrical elements have been included in tyre modelling procedures of tyre industry and would be also utilized in this project of tyre/wheel interaction modelling.

2.5 Material models used for tyre finite element analysis

Considering the nature of tyre constructions, especially the complexity of rubber and so-called Fabric layers, material models in the finite element tyre application have also been studied.

Referring to the papers published by University of Birmingham (Yang and Olatunbosun 2010) and the Boeing Company (Tanner and Daugherty 2005), axisymmetric hybrid continuum elements, surface elements embedded in continuum rubber elements have been utilized and validated through the comparison of the finite element simulations and tyre experimental test.

Yang has published his research that focused on the materials testing for finite element tyre model (Yang and Olatunbosun 2010).

As he described, the hyperelastic and viscoelastic material characteristics of rubber and the elastic material characteristics of reinforcement were vital for an accurate finite element tyre model. The hyperelastic property of rubber provided a general strain energy potential function to describe its highly non-linear and nearly incompressible material behaviour. The combination of uni-axial, biaxial tension and pure shear has been suggested for best practice in determination of rubber hyperelastic behaviour (Impact Engineering Solutions Inc. 2005). For only uni-axial tension test, Neo Hookean and Yeoh material constitutive models were suggested and supported by Abaqus (3DS SIMULIA 2009). The Yeoh strain energy function in hyperelastic material model has the advantage of covering a much wider range of deformation than other models, predicting stress-strain behaviour in different deformation modes and predicting shear modulus variation with increasing deformation. Considering the material model accuracy and computational cost, the Yeoh model has been chosen by Yang for the property of rubber.

The finite element model in Yang's study has been generated by scanning the tyre cross-section image to provide accurate description of the perimeter and the locations of ply lines and cord-ends, and then imported into CAD software as displayed in Figure-2.18. Yang has mentioned some detailed Abaqus code in his paper such as: rubber components meshed with 2D axisymmetric hybrid continuum elements (CGAX4H and CGAX3H), reinforcement components modelled with rebars in surface elements (SFMGAX1) embedded in continuum rubber elements. (Danielson 1996, Yang 2009)

Figure-2.18 The finite element model for tyre cross-section

(Yang and Olatunbosun 2010)

With the results validated by comparing with experimental tests, Yang has concluded that a feasible procedure for determine tyre material property without supporting information from tyre manufacturer was developed. The material property model constants were established using Abaqus. The prediction of static vertical deformation and footprint showed good correlation with experimental results as displayed in Figure-2.19. (Yang and Olatunbosun 2010)

Figure-2.19 Footprint shape comparison between test and simulation

(Yang and Olatunbosun 2010)

Other researchers' work have also been reviewed such as Tanner's published research in the Boeing Company, concerning the tyre mechanical property data using NASA aircraft landing dynamics test facility. (Tanner and Daugherty 2005)

More detailed material models and equations will be discussed in Chapter 3, and the process of characterization and correlation for chosen material models for this study will also be introduced in Chapter 4.

2.6 Summary on the finite element models in literature

The review of these previous works has shown the successful application and further potential of using finite element analysis in tyre R&D process.

Several comments from reviewing the previous researches have been listed below:

1. Most of the models in literature used Mooney-Rivlin or Yeoh material model for the rubber matrix.
2. There are several methods of modelling rubber and composite materials. As reviewed in this chapter, the tyre models were constructed depending on the aim of the researches. Rebar elements, layered shell or membrane element, beam element in solid element have been used in different researches.

   For example, the use of rebar elements for breaker plies, which do not have bending capability, will neglect the bending stiffness of fabric cords. The use of shell elements with orthotropic material properties, it is possible to introduce bending stiffness for the fabrics.

   As displayed in Figure-2.20, the use of Rebar model has been supported by Abaqus Rebar layer function. This function can define the rebar orientation, spacing, thickness, location and material properties which are independent of rubber material properties definition.

Figure-2.20 Cord rubber Composite model by Rebar element

(Guan, Zhao and Cheng 2006)

For body plies, the reinforcement fabrics do not carry compression and bending. Rebar elements, if elastic modulus can be set different for tension and compression, will model the behaviour of fabric cords as it is reality. Shell elements, which have additional rotational degrees of freedom, will introduce slight but acceptable error; this is because the orthotropic material properties reduce bending stiffness of the element to a value close to rubber. (Ersahin 2003)

In LS-Dyna, beam element is another option to model body plies fabrics. Using beam element allows the different materials to behave independently on sidewalls, which contributes to the vertical compressive strength of the tyre. However, since the beams are only tied together in the radial direction by the sidewall rubber, this method still allows the tyre to get lateral stability from beams. (Reid, Boesch and Bielenberg 2006)

3. Tyre geometry has been simplified in those previous studies. Tread pattern has also been ignored, as some researchers concluded that tread pattern has minor effect on general stiffness of the tyre. Those tyre models still showed good agreement with the experimental results.

4. Most of the finite element modelling on tyres has been applied in the automotive industry. The methodology and some specific techniques can be learnt from previous research and experiences can be from automotive field then applied to aircraft field. However, it is still worth to mention that the finite element modelling requirements for aircraft tyre are in a higher level because of the complex nature of aircraft tyre operating and testing scenarios. Furthermore, the tyre/road interaction modelling has been studied and developed to a certain level while the research for tyre/wheel interaction has stood still.

As a conclusion, the purpose of this study, to investigate an efficient way to achieve reliable finite element modelling for aircraft tyre/wheel interaction analysis, has become a unique point of this PhD project. Based on the particular tyre finite element model, the author will propose an approach to assess aircraft tyre/wheel interaction and its safety criteria upon landing. It is recognized that LS-Dyna has its speciality in impact and crashworthiness analysis. Therefore LS-Dyna is used as the main tool of this PhD project.

The research will demonstrate the effectiveness and flexibility of the finite element model. Although most of the previous researches were applied in Abaqus environment, but the methodologies and techniques can be utilized and transferred into LS-Dyna, which is the main tool for this project, or indeed any other commercial finite element software.

3. Material models and theories

Rubber and fabric composite materials are the major components of an aircraft tyre. The review of rubber material models and the mathematic theories for the finite element analysis are of significant importance for this project. This chapter will discuss the fundamental material models and the mathematic theories for rubber-like material subject to large elastic deformation. These models are frequently used in commercial FEA software for rubber components. It is notable that the modelling of various rubber-like materials often starts with a strain energy function. To define the nonlinear hyperelastic behaviour of a rubber-like material, a stress-strain relation is also required to determine parameters in the strain energy potential. The proper selection of a rubber elastic material model is always the first and foremost concern.

Rubber material usually has long chain molecules recognized as polymers. The term elastomer is the combination of elastic and polymer and is often used interchangeably with rubber (Smith 1993). Rubber material presents a very complicated mechanical behaviour that exceeds the linear elastic theory and contains large deformations, plastic and viscoelastic properties and stress softening, which is also known as the Mullins effect. In general, rubber can be defined by a stored energy function as hyperelastic material. The coefficients in these functions should be determined by uniaxial, biaxial and shear test data. The essential problem is to determine the strain energy function for providing good fit with a number of sets of experimental data. (Ali, Hosseini and Sahari 2010)

Yang (Yang and Olatunbosun 2010) also emphasised the complexity when determining rubber materials' hyperelastic and viscoelastic characteristics. The researches regarding fitting and comparison of such models with experimental test data can also be seen in Markmann (Markmann and Verron 2006), Sharma (Sharma 2003) and Ogden's (Ogden, Saccomandi and Sgura 2004) work. Other examples in the tyre finite element

application using hyperelastic models have been published by a number of researchers, such as Shiraishi (Shiraishi et al. 2009), Zhang (Zhang, Tamini and Palmer 2004) and Ojala (Ojala 2005). It can be concluded from the previous researches that the selection of an appropriate strain energy model is of significant importance to ensure that the finite element simulation is able to replicate the response of the tyre accurately.

The next part of this chapter will introduce various popular rubber material models which are offered in the literature and are available in commercial finite element software.

3.1 Elasticity

Rubber has flexible and long molecular structures, which enables it to elongate to several times its original size. For some simple cases, the assumption of a linear stress-strain relationship can be used to represent the rubber material property. As with other solid materials, rubber can be considered as a linearly elastic material at small strains. This assumption can cover some common rubber design problems, however, for analyzing rubber behaviour under large deformation, large elastic deformation theory should be considered. (Gent 1992)

Based on Rivlin's phenomenological theory, rubber is assumed isotropic in elastic behaviour and very nearly incompressible. A strain energy function based on the strain invariants I_1, I_2 and I_3 can be used to explain the elastic properties of a rubber.

A mathematical framework has also been offered to describe rubber material behaviour, based on continuum mechanics. Stress and strain analysis problems can be solved independently in the microscopic system and molecular concepts. This theory is the starting point of the models in various published research. (Achenbach and Duarte 2003, Boyce and Arruda July 2000, Chang, Saleeb and Li 1991, Pucci and Saccomandi 2002)

The strain energy functions are represented as follow:

$W = f(I_1, I_2, I_3)$ Equation 1

Where:

W = Also written as U, the strain energy potential (density) or stored energy function defined per unit volume.

I_1, I_2, I_3 = the three invariants of the green deformation tensor given in terms of the principal extension ratios λ_1, λ_2 and λ_3, by:

$$I_1 = \lambda_1^2 + \lambda_2^2 + \lambda_3^2$$

$$I_2 = \lambda_1^2\lambda_2^2 + \lambda_2^2\lambda_3^2 + \lambda_3^2\lambda_1^2$$

$$I_3 = \lambda_1^2\lambda_2^2\lambda_3^2$$ Equation 2

Equation 1 can also be represented as:

$$W = \sum_{i+j+k=1}^{\infty} C_{ijk} (I_1 - 3)^i \cdot (I_2 - 3)^j \cdot (I_3 - 1)^k$$ Equation 3

Considering rubber as an incompressible material, $I_3 = 1$ and Equation 3 decreases to:

$$W = \sum_{i+j=1}^{\infty} C_{ij} (I_1 - 3)^i \cdot (I_2 - 3)^j$$ Equation 4

3.2 Hyperelastic models

Through the literature survey, a remarkable amount of published literature can be found on the modelling of rubber materials. It's noticeable that the model selection for rubber-like material depends on its application, corresponding variables and the available data to determine material parameters. Generally, various possible models should be studied and compared, and the optimum one is always that with higher accuracy and less material parameters (Lemaitre 2001).

The selection of a proper strain energy function W (or U) is the core in the modelling process of a hyperelastic rubber material. Determining accurate material constants for the selected function is also of great importance.

Reviewing the published literature, various forms of strain energy potentials for the modelling of isotropic and incompressible rubber-like materials have been found, however, only a few of them described the complete behaviour of the materials, especially the experimental data from different loading conditions. (Guo and Sluys 2006, Mars and Fatemi 2004, Ogden 1972)

Six different models were compared to describe the deformation behaviour with experimental data by Boyce and Arruda (Boyce and Arruda July 2000). Markmann and Verron compared twenty hyperelastic models for rubber-like materials and classified them with respect to their ability to fit experimental data in another study (Markmann and Verron 2006).

And three major categories of hyperelastic models have been classified, including phenomenological, empirical and physical-based models.

As a summary from Chagnon (Chagnon, Markmann and Verron 2004), an efficient and reliable hyperelastic model has four main qualities:

1. It should be able to exactly reproduce the whole responses of rubbers in an expected 'S' shape.
2. The change of deformation modes must be reasonable. For instance, if the model operates sufficiently in uniaxial tension, it must also be exact in simple shear or in equibiaxial tension without an obvious problem.
3. The number of fitting material parameters should not be large, so the number of experimental tests for their determination can be reduced.
4. The mathematical formulation of the strain energy potential should also be simple and practicable for the numerical performance of the model.

3.3 Polynomial model

The polynomial model for the compressible form is based on the 1st and the 2nd invariant $\overline{I_2}$ and $\overline{I_2}$ of the deviatoric Cauchy-Green tensor.

This model of strain energy function is usually used in modelling the stress-strain behaviour of a filled elastomer, with four to five terms. (Forni, Martelli and Dusi 1999)

The formulation is shown as:

$$U = \sum_{i+j=1}^{N} C_{ij} (\overline{I_1} - 3)^i (\overline{I_2} - 3)^j + \sum_{i+j=1}^{N} \frac{1}{D_i} (J_{e1} - 1)^{2i} \qquad \text{Equation 5}$$

Where:

U = Same as W in Equation 1, the strain energy potential (density), strain per unit of reference volume.

J_{e1} = The elastic volume ratio

$\overline{I_2}$ and $\overline{I_2}$ = The first and second invariants of the deviatoric strain

C_{ij} and D_i = Material constant, C_{ij} describes the shear behaviour of the material and D_i introduces compressibility and is set equal to zero for fully incompressible

N = A positive determining number of terms in the strain energy function (N = 1, 2 or 3)

3.4 Reduced polynomial model

The reduced polynomial model follows a simple form of polynomial model. The only difference is that the second invariant of the left Cauchy-Green tensor has been ignored (Peeters and Kussner 1999). In this case, the strain energy function has become:

$$U = \sum_{i=1}^{N} C_{i0} (\overline{I_1} - 3)^i + \sum_{i=1}^{N} \frac{1}{D_i} (J_{e1} - 1)^{2i} \qquad \text{Equation 6}$$

Where, j is always equal to zero.

3.5 Ogden model

The Ogden model proposes the strain energy function with the principal stretches (λ_1, λ_2, λ_3) for incompressible material, in which λ_1, λ_2 and λ_3 are assumed to be 1. The principal stretches are directly measurable quantities and using them is one obvious advantage (Chang, Saleeb and Li 1991).

The formulation of the Ogden strain energy potential is shown as follow:

$$U = \sum_{i=1}^{N} \frac{2\mu_i}{\alpha_i^2}\left(\overline{\lambda_1}^{\alpha_i} + \overline{\lambda_2}^{\alpha_i} + \overline{\lambda_1}^{\alpha_i} - 3\right) + \sum_{i=1}^{N} \frac{1}{D_i}(J_{e1} - 1)^{2i} \qquad \text{Equation 7}$$

Where:

$$\overline{\lambda_i} = J^{\frac{-1}{3}}\lambda_i$$

$J = \lambda_1, \lambda_2, \lambda_3$

λ_i = The principal stretches

J = The Jacobean determinant

J_{el} = The elastic volume ratio

In the Ogden model, the constants μ_1 and α_1 describe the shear behaviour of the material and D_i describes the compressibility.

Comparing the Ogden model with the polynomial model, the calculation of the invariant derivatives in Ogden's energy function is more computationally intensive, which means the Ogden model can be more accurate in fitting experimental data available from multiple tests (Korochkina, Claypole and Gethin 2005).

3.6 Mooney-Rivlin Model

The strain energy potential for the Mooney-Rivlin model is proposed as follow:

$$U = \sum_{i,j=0}^{N} C_{ij}\,(\overline{I_1} - 3)^i(\overline{I_2} - 3)^j + \sum_{i=1}^{N} \frac{1}{D_i}(J_{e1} - 1)^{2i} \qquad \text{Equation 8}$$

Where:

U = The strain energy potential (density), strain per unit of reference volume

J_{el} = The elastic volume ratio

$\overline{I_1}$ and $\overline{I_2}$= The first and second invariants of the deviatoric strain

C_{ij} and D_i = Material constant

N = A positive determining the number of terms in the strain energy function

C_{ij} are the material parameters to be defined either by an experimental test data, or the calculation from a curve fitting programme, and $C_{00} = 0$. (Markmann and Verron 2006)

The first order for incompressible materials is presented as:

$$U = C_{10}(\overline{I_1} - 3) + C_{01}(\overline{I_2} - 3) \qquad \text{Equation 9}$$

By setting N = 0, $\alpha_1 = 0$ and $\alpha_2 = -2$ in Ogden model, the Mooney-Rivlin model is obtained as: (Sasso et al. 2008, Toth, Faffai and Bojtar 2005)

$$U = \frac{\mu_1}{2}\left(\overline{\lambda_1}^2 + \overline{\lambda_2}^2 + \overline{\lambda_3}^2 - 3\right) - \frac{\mu_2}{2}\left(\overline{\lambda_1}^{-2} + \overline{\lambda_2}^{-2} + \overline{\lambda_3}^{-2} - 3\right) \qquad \text{Equation 10}$$

Where:

$$C_{10} = \frac{\mu_1}{2} \text{ and } C_{01} = -\frac{\mu_2}{2}$$

The Mooney-Rivlin and Ogden models are considered the most preferred constitutive models. However, there is one obvious disadvantage, which is that the material parameters for those models must be obtained from experiments and they are not physically-based parameters. The fitting programme for the Mooney-Rivlin or Ogden model can be complicated if the number of parameters is large (Bol and Reese 2003).

3.7 Neo-Hookean model

The Neo-Hookean model is pre-programmed into the Abaqus finite element package.

The strain energy function for Neo-Hookean model is the same as the reduced polynomial model when N = 1.

$$W = C_{10}(\overline{I_1} - 3) + \frac{1}{D_1}(J_{e1} - 1)^2 \qquad \text{Equation 11}$$

The Neo-Hookean model can be offered in terms of the first deviatoric invariant. (Timbrell 2003) It can also be offered by setting N = 1 and $\alpha_1 = 2$ in the Ogden model with the constant $C_{10} = \frac{\mu_1}{2}$. (Bol and Reese 2003):

$$U = \frac{\mu_1}{2}\left(\overline{\lambda_1}^2 + \overline{\lambda_2}^2 + \overline{\lambda_3}^2 - 3\right) = C_{10}(I_1 - 3) \qquad \text{Equation 12}$$

The Neo-Hookean model is the simplest hyperelastic model for rubber-like materials. When material experimental data is insufficient, this model can still be reliable. The significance of the Neo-Hookean model is that the statistical theory of rubber elasticity appears in the strain energy function:

$$W = \frac{1}{2} NKT (I_1 - 3)$$ Equation 13

Where:

N = Number of network chains per unit volume

K = Boltzmann's constant

T = The absolute temperature

Although the statistical and phenomenological function begin from quite various premises, equation 13 is still of the same form as equation 11 according to Achenbach and Duarte's research (Achenbach and Duarte 2003).

3.8 Yeoh model

The strain energy function for the Yeoh model is shown below and is the same as the reduced polynomial model when N = 3 (Peeters and Kussner 1999).

$$U = \sum_{i=1}^{3} C_{i0}\left(\overline{I_1} - 3\right)^{i} + \sum_{i=1}^{3} \frac{1}{D_i} (J_{e1} - 1)^{2i}$$ Equation 14

The initial shear modulus and bulk modulus are given by

$$\mu_0 = 2C_{10} \text{ , } K_0 = \frac{2}{D_1}$$ Equation 15

The Yeoh model has been chosen to describe the hyperelastic properties of rubber compounds for the following reasons: (Ghosh, Saha and Mukhopadhyay 2003)

1. The Yeoh model is applicable for a much wider range of deformation.
2. The Yeoh model is able to predict the stress-strain behaviour in different deformation modes from data gained in one simple deformation mode like uniaxial extension.

3.9 Arruda and Boyce model

Physical models such as the Arruda and Boyce model are based on an explanation of a molecular chains network. It is assumed that the strain energy is equal to the sum of the strain energies of the individual chains oriented randomly in space (Raoult, Stolz and Bourgeois 2005). The strain energy function is shown below:

$$U = \mu \sum_{i=1}^{5} \frac{C_i}{\lambda_m^{2i-2}} \left(\overline{I_1}^{i} - 3^i \right) + \frac{1}{D} \left[\frac{{J_{e1}}^2 - 1}{2} - \mathrm{Ln}(J_{e1}) \right] \quad \text{Equation 16}$$

With:

$$C_1 = \frac{1}{2}, C_2 = \frac{1}{20}, C_3 = \frac{11}{1050}, C_4 = \frac{19}{7000}, C_5 = \frac{519}{673750} \quad \text{Equation 17}$$

μ = The initial shear modulus

λ_m = The locking stretch, at which the upturn of the stress-strain curve would rise significantly

D = Double the inverse bulk modulus at small strain, i.e. D = 2 / K

The Arruda and Boyce model helps to make accurate solutions neglecting the second invariant of the left Cauchy-Green tensor in the range of smaller strains. With an increasing locking stretch parameter, sufficient accuracy in both small and large strain can be obtained (Seibert and Schoche 2000).

It is noticeable that the strain energy function is independent of the second stretch invariant for several hyperelastic constitutive models, such as the Neo-Hookean model, the Yeoh model and the Arruda and Boyce model (Sharma 2003). Each of these models has a mathematical formulation with different parameters that are established by using an algorithm based curve fitting of experimental data. A single experimental test, such as a uniaxial tension test is needed to determinate the material response, if the strain energy density is supposed to be independent of the second invariant. Although, these hyperelastic constitutive models can not represent very close behaviour in other modes as multi-parameter models, but still, reasonable approximation can be achieved and they are much easier to use (Marlow 2003).

3.10 Van der Waals model

The Van der Waals model is also known as the Kilian model. The strain energy function is shown as follow: (Seibert and Schoche 2000)

$$U = \mu \left\{ -\left(\lambda_m{}^2 - 3\right)[\mathrm{Ln}(1-\eta)+\eta] - \frac{2}{3}a\left(\frac{\tilde{I}-3}{2}\right)^{\frac{3}{2}} \right\} + \frac{1}{D}\left(\frac{J^2-1}{2} - \mathrm{Ln}(J)\right) \quad \text{Equation 19}$$

With β represents the linear mixture parameter in:

$$\tilde{I} = (1-\beta)\, I_1 + \beta \tilde{I_2} \text{ and } \eta = \sqrt{\frac{\tilde{I}-3}{\lambda_m{}^2 - 3}} \quad \text{Equation 20}$$

Differing from the hyperelastic constitutive models, the Van der Waals model uses two invariants of the left deviatoric Cauchy-Green tensor in $\tilde{I}$. If $\beta = 0$, only the first invariant is considered and if there is only one type of experimental test data available, the parameter is recommended to be set to zero. The disadvantage of the Van der Waals model is that the interaction parameter α is difficult to measure and is usually set to a value between 0.1 and 0.3. Also, when the deformation of the material is larger than the locking stretch, this model formula cannot be used (Peeters and Kussner 1999).

3.11 H41 Tyre Material model chosen and correlation

Hyperelastic models are applied in different commercial finite element analysis software. Generally, the nonlinear relationship between stress and strain is required for the rubber material properties in the finite element process. The material parameters in the strain energy formulations can be determined by the fitting of the strain energy function to the stress-strain experimental data based on a nonlinear least square optimization method.

The optimization process is used in software to minimize the error with respect to the model's parameters, with various algebraic forms.

The strain energy function parameters have been fitted on experimental data from either tensile, compression or pure shear. Then, the coefficients for hyperelastic models should be determined to provide a good fit between the predictions from the model and the experimental stress-strain data. The uniaxial test data have been commonly employed to obtain the coefficients.

However, great effort is required to use curve fitting with good accuracy. The parameters for the material properties can be assessed by checking and matching stress-strain data over a large range of deformations. And the fitting results should always be checked in a curve fitting approach with the proper strategies, i.e. using different models and providing more data points (Ali, Hosseini and Sahari 2010).
It is also noticeable that models with fewer material parameters are usually preferred in order to improve computational efficiency.

For this H41 tyre finite element model, the materials have been characterised and correlated individually. Considering that rubber and fabric materials are the major component of this model, their hyperelastic properties are of priory concern. Although previous research (Behroozi, Olatunbosun and Ding 2012) has pointed out that a non-linear viscoelastic property is a more accurate representation of real world behaviour of rubbers, viscous effects are considered as negligible in this H41 tyre finite element model.

Viscous effects in this H41 model can be disregarded for two main reasons. First one is the designed static analyses for inflation and static load scenarios are free of viscous effects. Second one is that, although it has been investigated that the viscoelastic property of rubber has a significant influence on the traction, steering response and rolling resistance property of a tyre (Ghosh, Saha and Mukhopadhyay 2003), none of the situations are involved in the dynamic scenarios designed for this H41 tyre model.

It is also worth mentioning that the rubber material aging effects have been disregarded in this study. Although it is recognized that a large number of aircraft tyres serves for a long time within which period, rubber aging effect could have made significant influences on material properties changes. However, to put this effect into consideration requires abundant experimental data, which are not available at the current research stage. Therefore, the research will not investigate this particular aspect unless further agreement or experimental data availability can be arranged.

Material experimental tests

To obtain the hyperelastic (stress-strain) properties of the rubber materials, a series of uniaxial tension tests have been processed in DATL. The experimental tests use samples with gauge length 25mm, width 4mm and thickness 2mm, applied with uniaxial extensions up to 250mm. The forces applied on the test sample, along with the gauge deformations are recorded, thus the force vs. displacement curves are given to represent materials' stress-strain properties.

For the fabrics, similar uniaxial tension tests have also been processed. The samples are in 250mm length, various diameters. The force vs. displacement relationships are recorded from extension tests up to 200mm.

Rubber, Mat_77

For the LS-Dyna finite element tyre model, material properties are represented by material models. With its database, Ls-Dyna has plenty of material cards to represent rubber in the finite element models, including Mooney-Rivlin rubber, Frazer-Nash rubber, General Viscoelastic (Maxwell Model), Hyperelastic and Ogden Rubber (Yeoh model), Arruda Boyce Rubber and etc. It is noticed that each material cards in Ls-Dyna requires the setting of orders, coefficients, or relative experimental data of each individual energy function.

Take Mooney-Rivlin model for example, the strain energy potential is proposed: (Markmann and Verron 2006)

$$U = \sum_{i,j=0}^{N} C_{ij} (\overline{I_1} - 3)^i (\overline{I_2} - 3)^j + \sum_{i=1}^{N} \frac{1}{D_i} (J_{e1} - 1)^{2i} \qquad \text{Equation 8}$$

U = the strain energy potential (density), strain per unit of reference volume

J_{el} = the elastic volume ratio

$\overline{I}_1$ and $\overline{I}_2$ = the first and second invariants of the deviatoric strain

C_{ij} and D_i = material constant

N = a positive determining the number of terms in the strain energy function

Where, C_{ij} are the material parameters to be defined either by an experimental test data, or the calculation from a curve fitting programme.

With the uniaxial data for rubber material DC001 (Dunlop Aircraft Tyres Limited 2010), the 2nd order of Mooney-Rivlin model requires C10, C01 and D; the pre-process curve fitting can be seen in Figure-4.28(1), the calculated parameters from curve fitting program are listed in the table. 3rd order of Mooney-Rivlin requires C10, C11, C01 and D, which provides a more accurate fitting. The curve fitting program is able to process up to 9 parameters for Mooney-Rivlin model, the fitting curve is also shown in Figure-4.28(3).

The Mooney-Rivlin model is one of the most favourite constitutive models, but with a disadvantage that the material parameters must be obtained by experiments. Another disadvantage in Ls-Dyna is that the material card of Mooney-Rivlin model only provides 2 parameters' option. Unfortunately, with only uniaxial data, Mooney-Rivlin model with 2 parameters can't provide an accurate fitting for this H41 model.

Mooney-Rivlin	2 parameters	3 parameters	9 parameters
C10	1.032	0.237	-28.670
C01	-0.678	0.753	32.538
D	0	0	0
C11		0.035	-414.114
C20			183.223
C02			253.613
C21			-0.012
C12			-45.698
C03			34.397

Table-3.1 Mooney-Rivlin Parameters for DC001

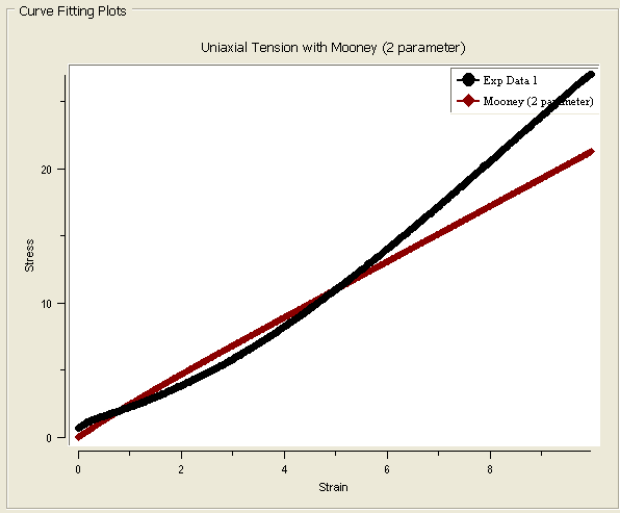

Figure-3.1 (1) DC001 Mooney-Rivlin 2 parameters

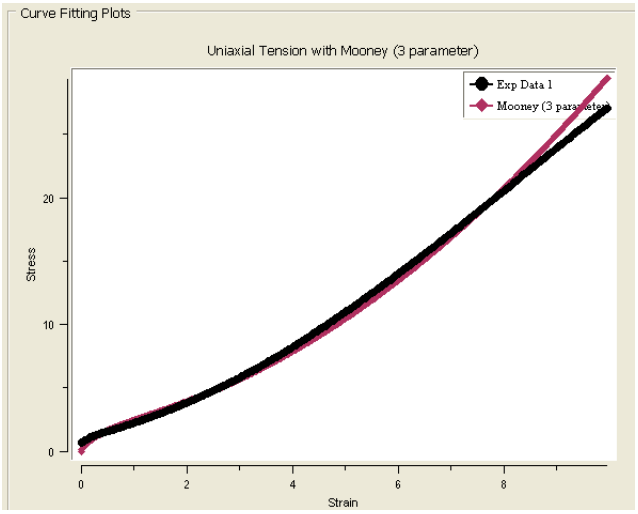

Figure-3.1 (2) DC001 Mooney-Rivlin 3 parameters

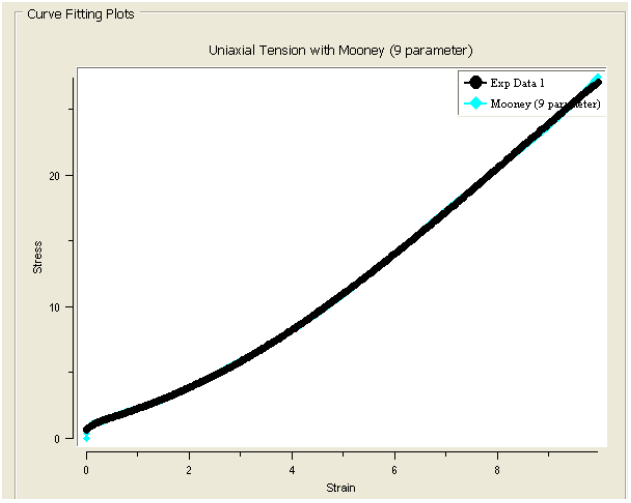

Figure-3.1 (3) DC001 Mooney-Rivlin 9 parameters

Figure-3.1 Mooney-Rivlin curve fittings (Stress: N/mm^2)

Regarding the fact that the actual material properties data provided by Dunlop has the results of load curve giving force versus actual change in the gauge length only from a uniaxial tensile test, from a sample gauge length 25mm, width 4mm and thickness 2mm (Dunlop Aircraft Tyres Limited 2010), the Yeoh model, which is represented as *Mat_77 hyperelastic rubber in Ls-Dyna has been chosen.

For Yeoh model, strain energy function is as follow, when N = 3 is the Reduced Polynomial model.

$$U = \sum_{i=1}^{3} C_{i0}\left(\overline{I_1} - 3\right)^{i} + \sum_{i=1}^{3} \frac{1}{D_i}(J_{e1} - 1)^{2i} \qquad \text{Equation 14}$$

The initial shear modulus and bulk modulus are given by:

$$\mu_0 = 2C_{10}\ ,\ K_0 = \frac{2}{D_1} \qquad \text{Equation 15}$$

The Yeoh model has been chosen to describe the hyperelastic properties of rubber compounds for the reasons as follow (Ghosh, Saha and Mukhopadhyay 2003):

- Yeoh model is applicable for a much wider range of deformation
- Yeoh model is able to predict the stress-strain behaviour in different deformation modes from data gained in one simple deformation mode like uniaxial extension

With uniaxial force vs. extension data, the 1st order of Yeoh model calculates C10 and D1, the fitting curve can be seen below along with the coefficients. The 2nd order calculates C10, C20, D1 and D2, 3rd order C10, C20, C30, D1, D2 and D3, which provides an accurate and expected fitting curve as shown in figure below.

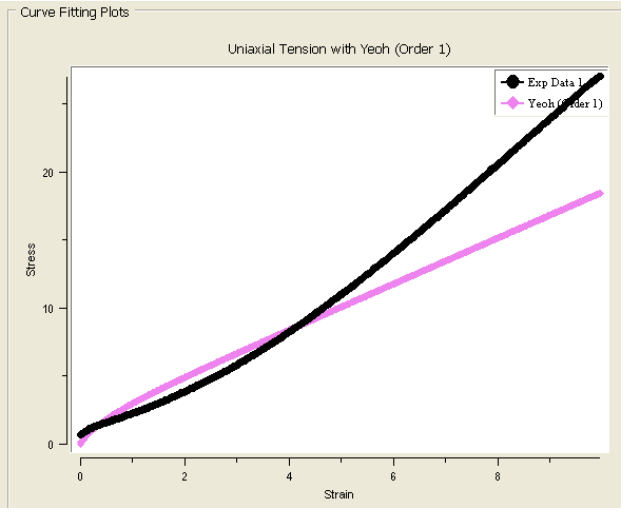

Figure-3.2 (1) DC001 Yeoh 1st order

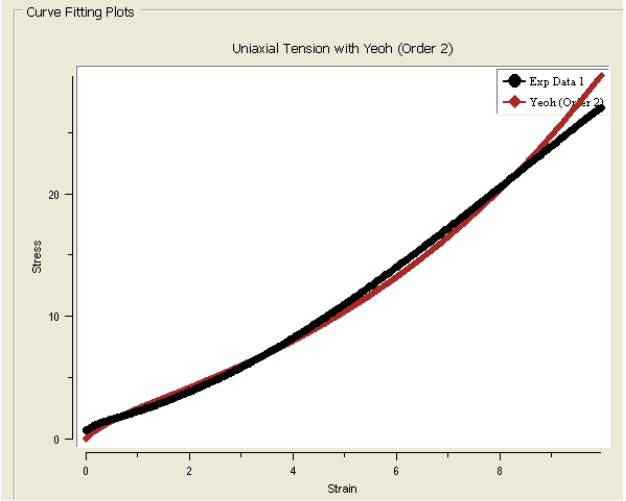

Figure-3.2 (2) DC001 Yeoh 2nd order

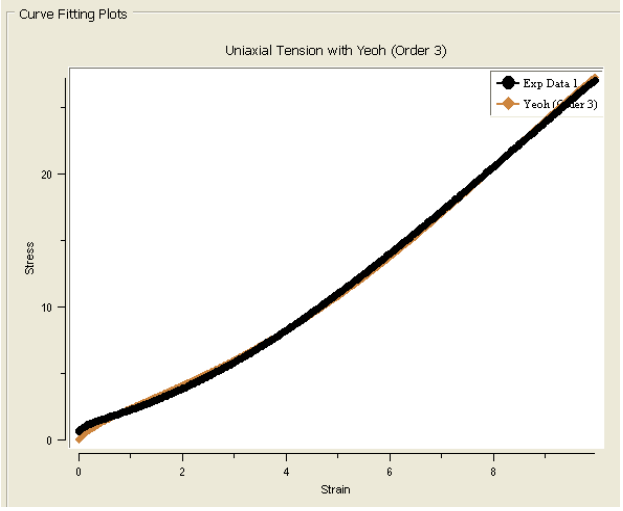

Figure-3.2 (3) DC001 Yeoh 3rd order

Figure-3.2 Yeoh model curve fittings (Stress: N/mm^2)

Therefore, in detail, the material card in Ls-Dyna for rubber DC001 is defined as *Mat_77, hyperelastic rubber, with the 3rd order of curve fitting using uniaxial force vs. displacement experimental data.

The simulations for material characterization correlation have been processed using *Mat_77 for each individual rubber material involved in this finite element H41 model.

The FE sample model, with regard to the actual sample size for experimental tensile test in DATL has been built (25mm in length, 4mm in width and 2mm in thickness). The boundary conditions and loads on the finite element model are the same as the experimental test: constrains of Y direction translation at one end of the sample and a prescribed motion of 250mm displacement on Y direction at the other end.

A cross-section has been set in the middle of the sample to collect the force vs. time curve from the simulation, along with a *HISTORY_NODE setting which is located at the edge of the sample with prescribed displacement to collect sample extension vs. time data. With the displacement vs. time output, force vs. displacement curve can be calculated, and then compared with the actual experimental load vs. deflection data.

The finite element model, experimental test and curves from simulation and experiment for DC001 can be seen in Figure-4.30

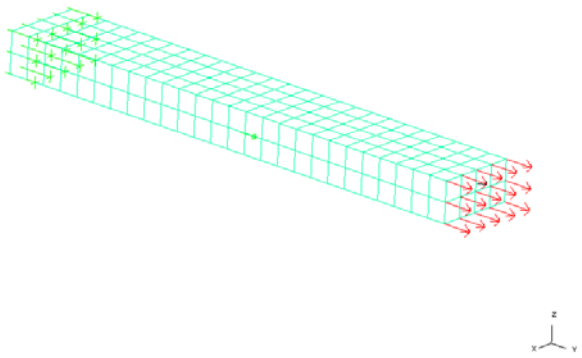

Figure-3.3(1) LS-Dyna Material Sample model for Rubber

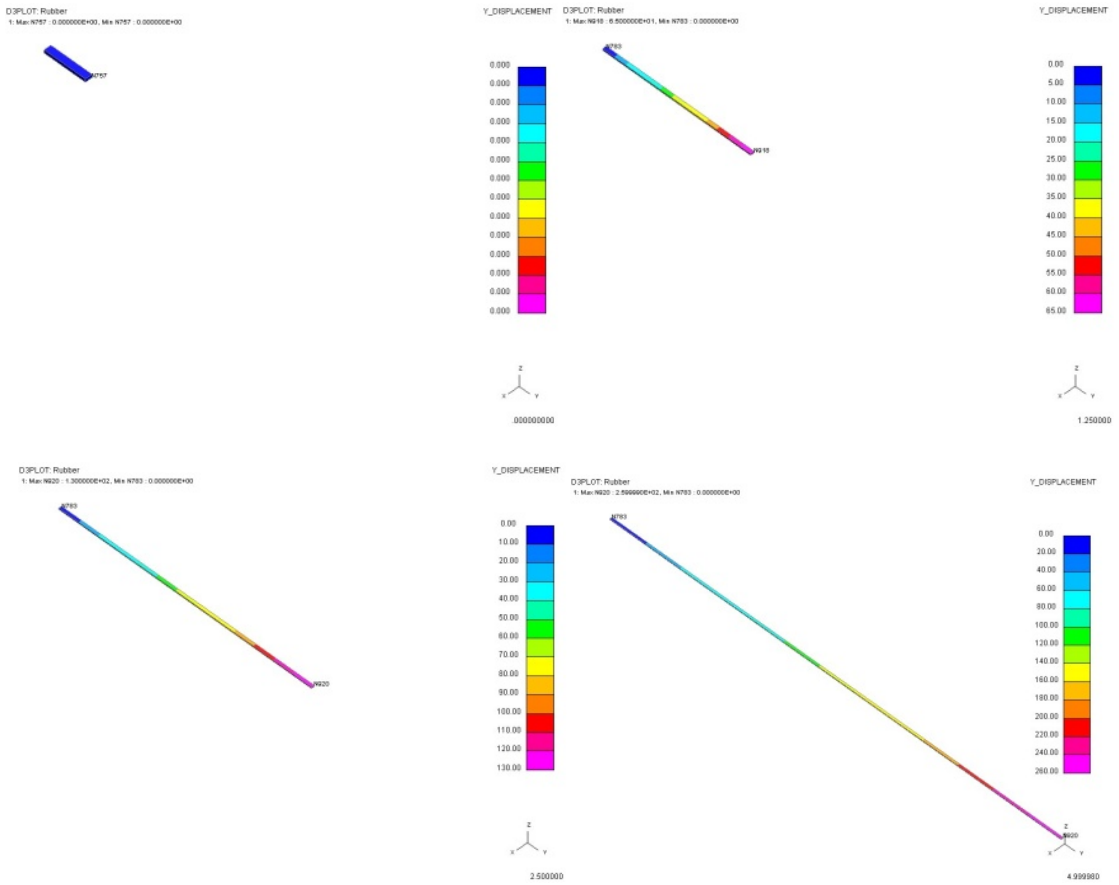

Figure-3.3 (2) Dyna simulation result (displacement)

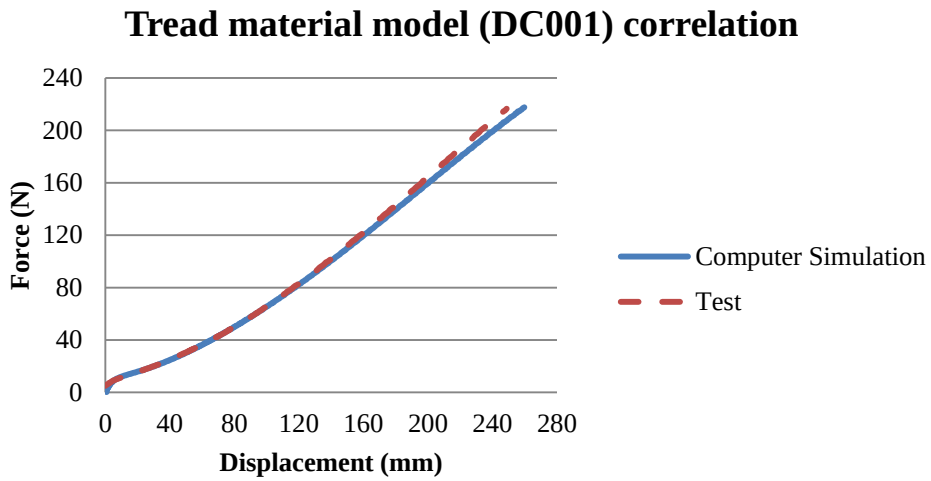

Figure-3.3 (3) Dunlop load vs. displacement / LS-Dyna load vs. time DC001

Figure-3.3 Tread rubber material correlation

From Figure-3.3, it can be concluded that the tread material model has been correlated to the test.

Fabric, Mat_71

The properties of fabric materials in H41 tyre have also been provided by DATL. The data are the force vs. displacement relationships from uniaxial tensile test as well, using samples of 250mm in length, various diameters.

The reason of choosing *Mat_67, nonlinear elastic discrete beam is because the fabric cords encased by the rubbers are considered as elastic cables (do not take bending) merged with rubber compounds in this finite element model. The data of each individual fabric provided by DATL contains a force vs. displacement curve from uniaxial tensile test that specifies its property, regarding its non-linear elastic behaviour. And for *Mat_67, this force vs. displacement curve can be used to define the elastic behaviour of the material in a certain axis, which permits the cables to be realistically modelled. (LSTC 2007)

As mentioned above, the belt and inner tread fabrics are considered as the contributor of longitudinal reinforcement of the tire, the axis of elastic behaviours for them are only activated along the longitudinal direction. On the other hand, the body ply fabrics, although do have an angle of +/-88 deg (1st to the 3rd plies), but initially they are considered as the reinforcement contributor in radial direction, the axis of elastic behaviours for them are only activated along radial direction. Although other material models are available for this kind of orthotropic elastic material, but at this moment, they are beyond the scope of this research.

LS-Dyna sample models for fabric material correlation have been built and simulations have been processed using fabric material DF014 for inner tread fabric. The corresponding model consists of a beam of 250mm length, 0.54mm diameter has been loaded with a prescribed motion of 100mm displacement in Y direction, and the other end of the beam has been constrained. Cross-section has been used to collect the force vs. displacement data to compare with experimental results. The curves can be seen below.

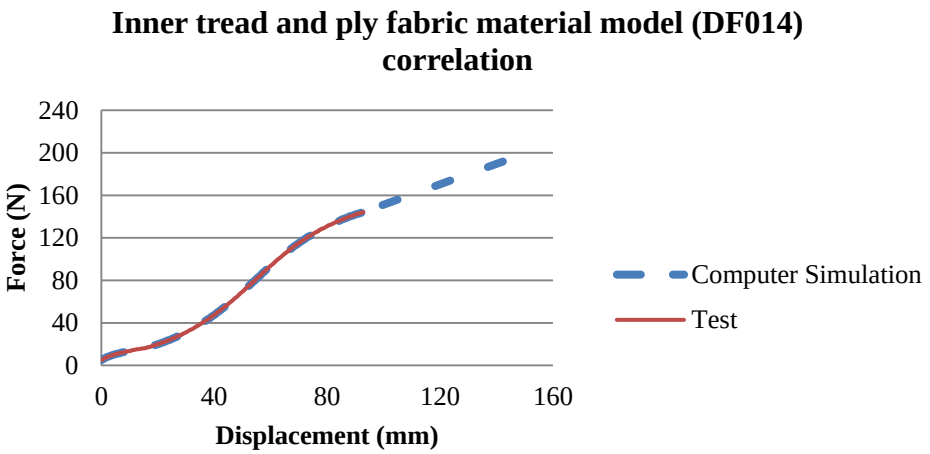

Figure-3.4 Dunlop load vs. displacement / LS-Dyna load vs. time DF014

The results show that the fabric material has been correlated to test.

Following the same process, the correlations of other rubber and fabric materials used in the H41 tyre model have been achieved. All material models have been validated through comparing LS-Dyna simulation to DATL test data. (Shown in Figure-3.5)

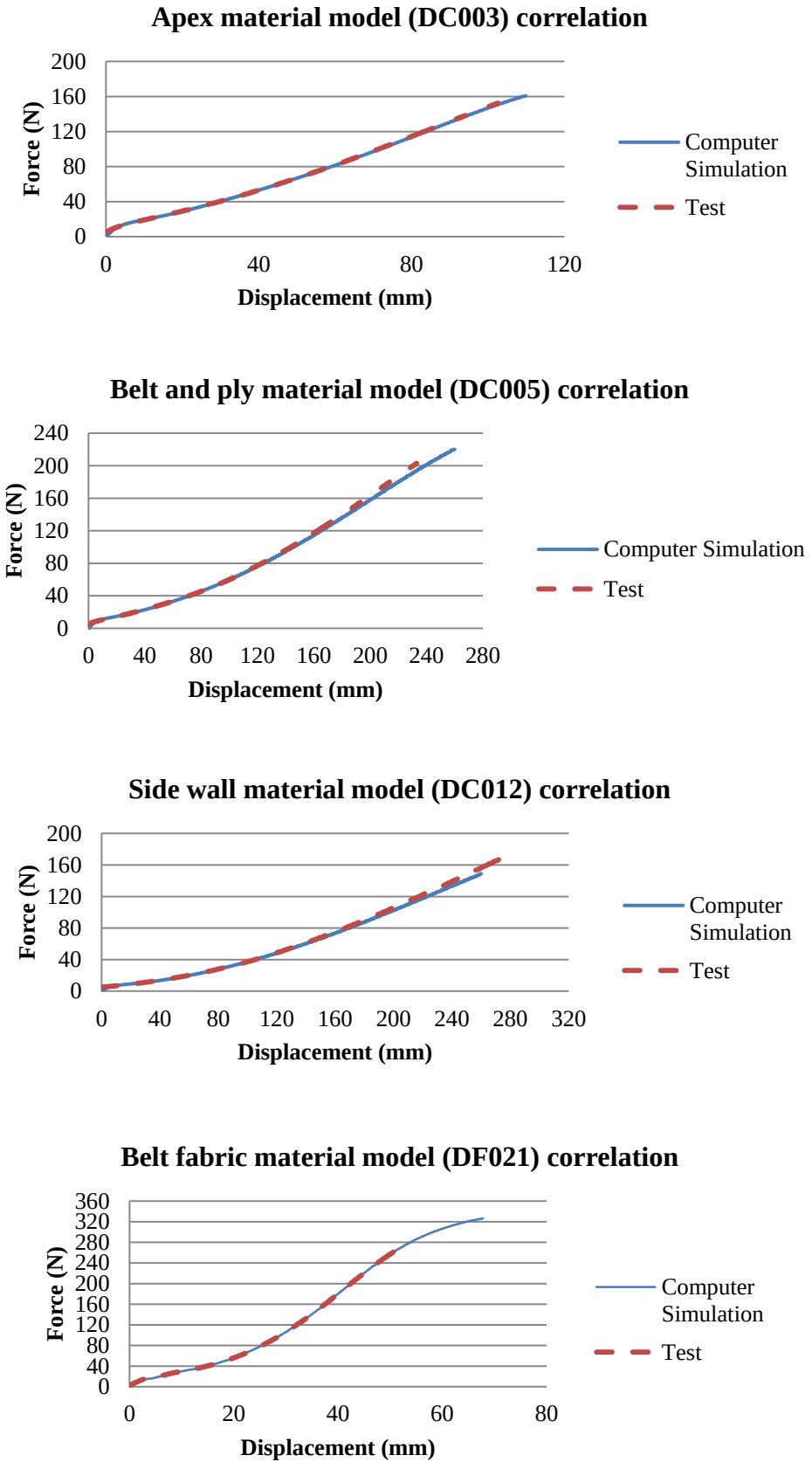

Figures-3.5 Material correlations for DC003, DC005, DC012 and DF021

As a conclusion, Table-3.2 shows all the details of the element types (section card in LS-Dyna), finite element formulation and material model (material card in LS-Dyna) that were used for the tyre finite element model respectively.

Part	Material Code	Poisson's Ratio	Density kg/mm^3	Young's modulus GPa	Element	Mat_Card
Tread	DC001	0.495	1.10e-6	N/A	Solid	Mat_77
Belt	DC005	0.495	1.10e-6	N/A	Solid	Mat_77
Sidewall	DC012	0.495	1.10e-6	N/A	Solid	Mat_77
Apex	DC003	0.495	1.10e-6	N/A	Solid	Mat_77
Plies	DC005	0.495	1.10e-6	N/A	Solid	Mat_77
Belt Fabric	DF021	0.28	7.86e-6	200	Beam	Mat_67
IT Fabric	DF014	0.28	1.39e-6	5	Beam	Mat_67
Ply Fabric	DF014	0.28	1.39e-6	5	Beam	Mat_67
Bead	N/A	0.28	7.86E-6	200	Solid	Mat_1

Table-3.2 H41 tyre model details

Mat_77: Hyperelastic rubber
Mat_67: nonlinear elastic discrete beam
Mat_1: elastic

4. Finite element models for tyre and wheel

The following chapter will introduce the development steps of the tyre and wheel finite element model. Parts of the wheel and the tyre, finite element meshing process, modelling details of meshing size and time steps chosen, rubber and fabric material properties are explained. The material characteristic correlation in Ls-Dyna and the validation of the finite element model through inflation test scenario have also been introduced in details.

4.1 Finite element aircraft wheel model

The finite element wheel model is developed to simulate a stress analysis for the Dunlop aircraft 13x4.25-6 tyre test wheel. The simulation then is validated by comparing results with existing data provided by Dunlop. The finite element methodology and strategy are used to model the tyre/wheel interaction finite element model.

Solid 3D model building

The Solid 3D (Geometry) models of the test wheel, including female and male hub, were built in CATIA. The wheel geometry was provided in the form of 2-D DXF data from Dunlop. The bolts and nuts, as well as the washers and covers are made from steel. Both the male and female hubs are made from Aluminium. The materials and their properties are listed in Table-4.1 below:

	E (MPa)	G (MPa)	NU	RHO (t/mm^3)
Steel	2.1E+5	8.1E+4	0.3	7.8E-9
Aluminium	7.2E+4	2.6E+4	0.33	2.8E-9

Table-4.1

E: Elastic modulus

G: Shear modulus

NU: Poisson’s ratio

RHO: Density

CATIA solid modelling

The X- view in 2-D DXF file provided detailed geometry of the wheel hubs. Draw a Profile in YZ-plane Sketch and constraint it by the data from DXF file. Then using Shaft command, rotating the Profile around Horizontal axi by 360 degree, the solid model of female hub is shown below.

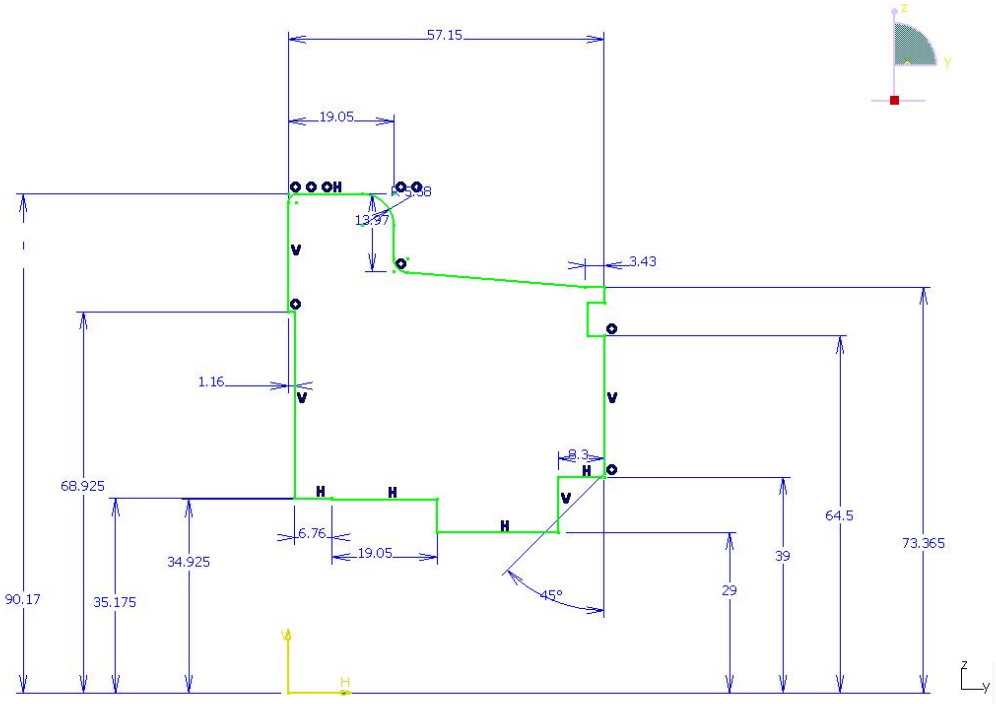

Figure-4.1 Profile of Female hub

Choose the contact surface of the hub, draw the circle of D=16.5in at the certain place for the holes. Use Pocket to drill the hole, then use circular pattern to do the group of 6 thru holes for M16 bolts.

Final shape of the female hub can be seen in Figure-4.2

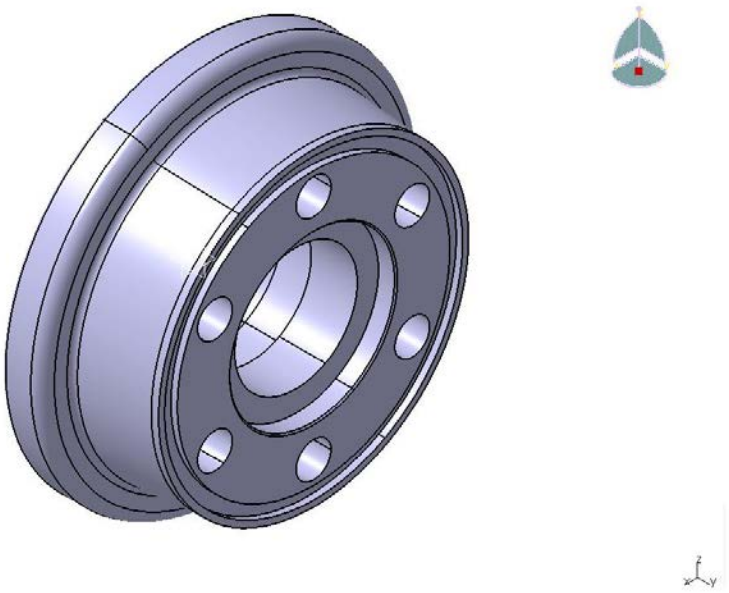

Figure-4.2 Female Hub

Same process was taken to build the other half of the test wheel as shown above. The male hub of the test wheel has been built as shown in Figure-4.3 and 4.4.

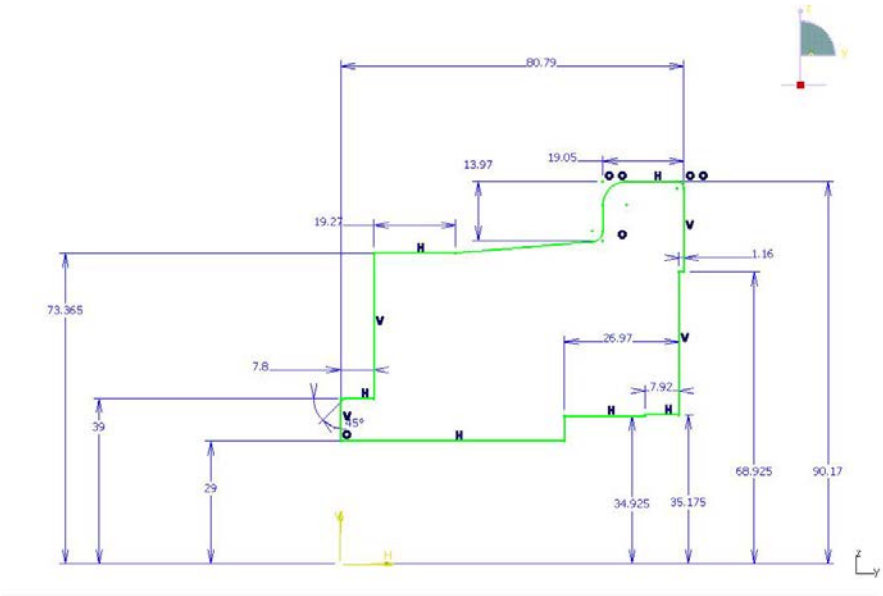

Figure-4.3 Profile of Male hub before shaft

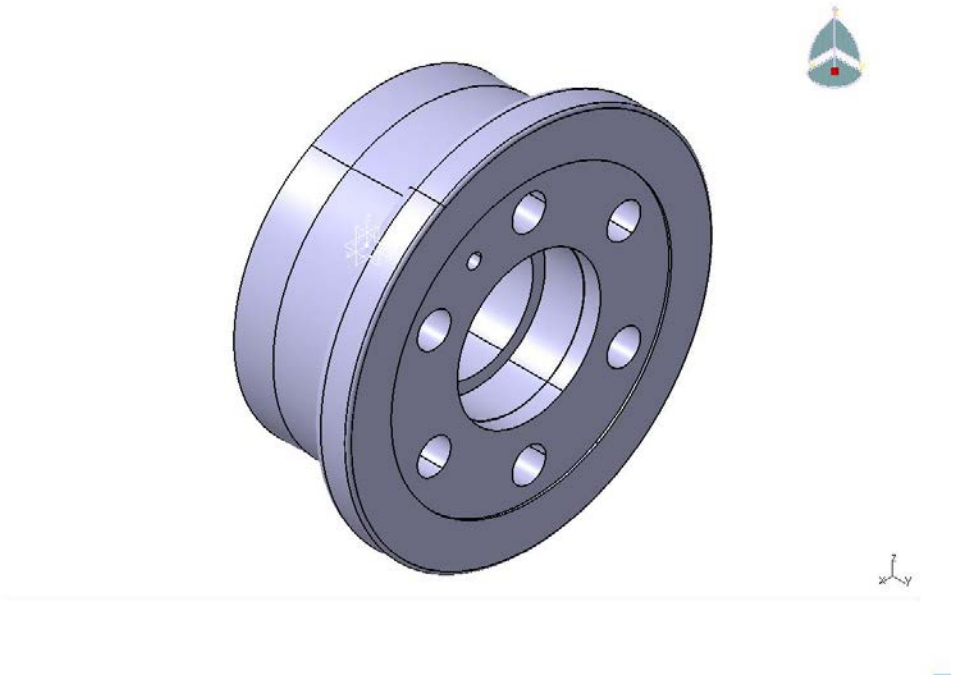

Figure-4.4 Male hub

It has to be mentioned that the valve-hole part of the male hub was not completed in the first 3D model. The vertical hole was not displayed. For sure it could be represented as a drilled hole, and this structure change has been accomplished in the following updated models. Another simplified assumption is that the tapping drill area of the valve hole was set to be a smooth surface.

Also from the DXF file, it could be seen that two excluder rings, an ‘O’ ring, 6 x M16 bolts as long as their accessories and the bearings should be on the assembled test wheel as well. As mentioned before, bearings are ignored. The covers, bolts, washers, and nuts have been built separately in CATIA, following the same approach as the female and male hubs 3D model building.

A simple way to join the two hubs was to fix the female part, and then set up a CATIA surface contact between those two hubs to join them together. The assembled hubs can be seen in Figure-4.5. By fixing the contact surfaces between the washers, nuts, covers and bolts, rest of the components have been assembled as well. Then the 3D assembled model has been transferred into IGS file for further use.

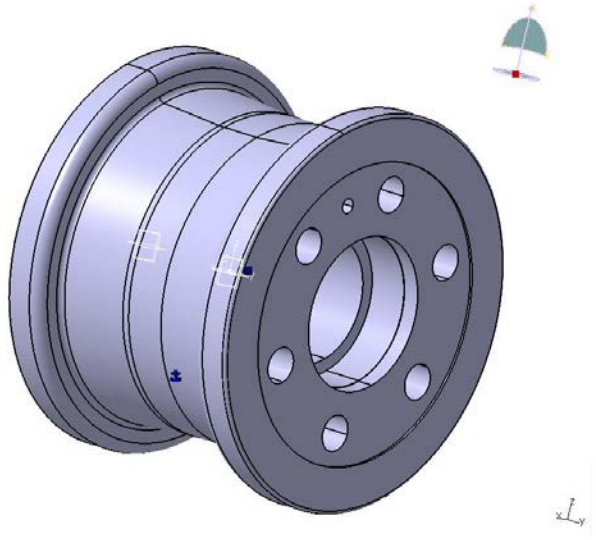

Figure-4.5 Assembled model

Model Meshing and Pre-process

The geometry file in IGS is generated by CATIA, as shown in Figure-4.6:

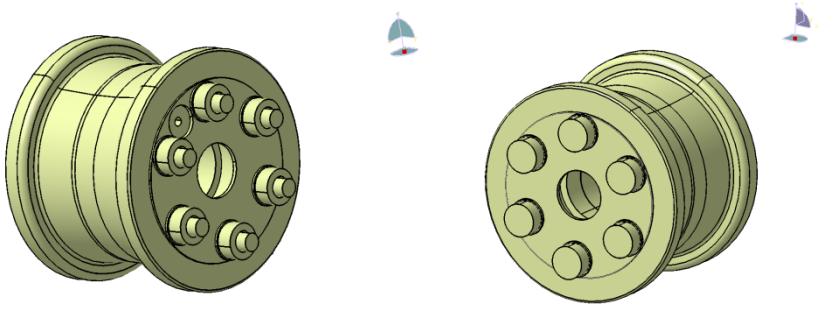

Figure-4.6 Test wheel IGS

Several assumptions have been made to simplify the model

a. The hexagonal chamfers of the nut and the bolt head have been removed
b. The screw areas have been defined as smooth surfaces.

Wheel hub Meshing strategy

The female and male hubs were meshed by using Trias elements on the surfaces. Figure-4.7 shows the well meshed areas of male hub.

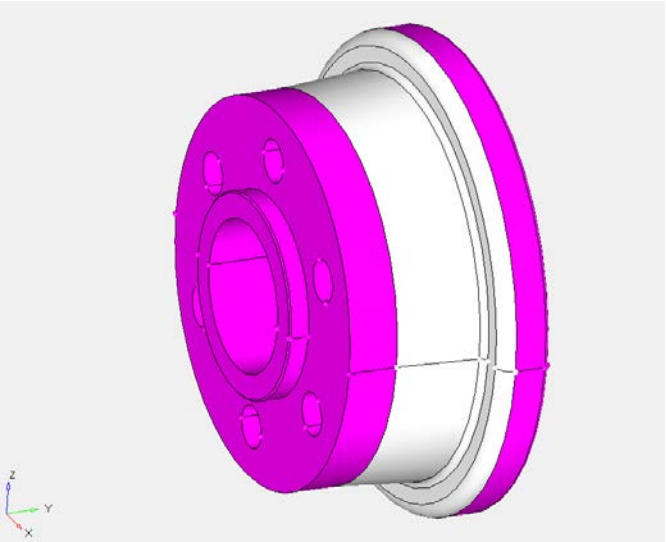

Figure-4.7 Well-Meshed surfaces

Since the target model contains slightly complicated structure such as bolt holes, it is easier to generate 3D meshing with tetrahedral rather than hexahedral elements. It is also known that the solver technology developments in most commercial FEA codes in last decade have led to the similar results in accuracy for hex and tetra mesh for most engineering problems. Although tetra mesh needs more computing resources during solving stage, it can be offset by the time saved in mesh generation.

Therefore, Tetramesh function in HyperMesh was employed to build the 3D meshing. The meshed male hub can be seen in Figure-4.8.

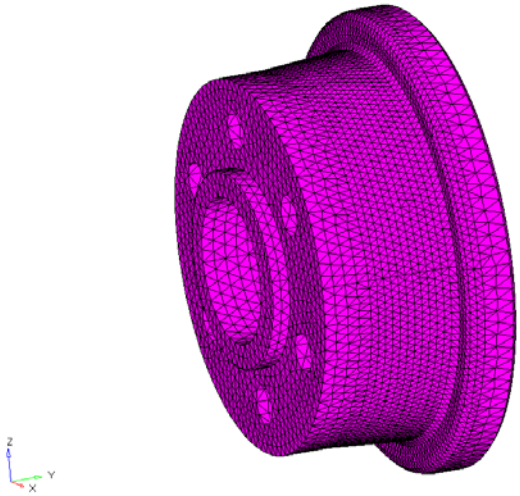

Figure-4.8 Meshed male hub

Bolt-preload solution

Regarding the importance of bolt-preload in this finite element wheel model for stress analysis, the review of bolt-preload solutions in finite element environment has been processed.

Referring to Ken-An Lou, an approach of applying bolt-preload in LS-DYNA has been published (Lou and Perciballi 2008).

To simulate the bolt-preload, tension load was applied to the two cut bolt faces in opposite direction. The bolt was pretensioned and analyzed to create the initial strain.

In Lou's LS-DYNA simulation, an initial 0.008 in. gap has been applied to create a clearance between two cut surfaces. The gap would close when preload applied. The two faces became tied by using LS-DYNA's

*CONTACT_TIED_SURFACE_TO_SURFACE feature.

Figure-4.9 below shows Lou's LS-DYNA bolt model.

Figure-4.9 Bolt with middle section cut (Lou and Perciballi 2008)

Another detailed approach of representing bolt-preload has been demonstrated by Jonathan Bowen of Jaguar Land Rover (Bowen 2008).

In this model, the bolt assembly has been cut into 4 parts, the nut, head, middle and body, with a shell using *MAT_NULL contacted to the bolt body to improve lateral contacts as shown in Figure-4.10.

Figure-4.10 Bolt in LS-DYNA (Bowen 2008)

The null elements with material represented as *MAT_NULL in LS-Dyna allows equations of state to be considered without computing deviatoric stress. Sometimes it is advantageous to model contact surfaces via shell elements which are not part of the structure, but necessary to define areas of contact including solid element types. In Bowen's model, the shells that cover the divided bolts have been modelled with *MAT_NULL. The Null shells connected the surfaces between each part of the bolts, thus ensured the contact feature in simulation, and also kept the integrity of the bolt structure. The mass of the null shell elements is computed and added to the nodal points which define the connectivity. The Young's modulus and Poisson's ratio are used only for setting the contact interface stiffness, and it is recommended that reasonable values be input. (LSTC 2007)

The key point of Bowen's model was the application of *INITIAL_STRESS_SECTION feature in LS-DYNA. The purpose of using *INITIAL_STRESS_SECTION is to initialize the stress in solid elements that are part of a section definition to create a preload. The stress component in the direction normal to the cross-section plane is initialized. This option works with a subset of materials that are incrementally updated including the elastic, viscoelastic and elastoplastic materials.

A load curve is defined to represent the preload value. A ramp starting at the origin should be used to increase the stress to the desired value. The time duration of the ramp should produce a quasi-static response. When the end of the load curve is reached, or when the value of the load decreases from the maximum value, the initialization stops. (LSTC 2007)

Figure-4.11 below shows the initial stress section applied in the middle part of the bolt assembly in Bowen's model. The *SURFACE_TO_SURFACE and other contacts listed below have been employed for the bolt preload FE model. The stress vs. time curve is also shown, in which stress is calculated by:

$$\delta = \frac{F}{A} \qquad \text{Equation 21}$$

Where:

δ : Stress

F : Force

A : Area

Figure-4.11 *INITIAL_STRESS_SECTION (Bowen 2008)

DATL 13x4.25-6 Tyre Test wheel bolt-preload approach

Learning from the successful applications of FE bolt pre-load representation, the methodology used in this DATL 13x4.25-6 Tyre Test wheel FE modelling has been decided, which was to apply solid bolt simulation method and also use *INITIAL_STRESS_SECTION function in LS-DYNA. Therefore, several refinements and adjustments have been made to improve the previous FE model.

Bolt meshing refinement

Referring to Bowen's model, the bolt of the target wheel assembly has been divided into 5 parts, head, nut, bolt body first half, bolt body second half and the middle part on which *INITIAL_STRESS_SECTION applied.

The *NULL_SHELL element has been used to keep the integrity of the bolt body and to build contact between the bolt parts. To simplify the model, bolt nuts, heads and the associated washers were modelled as conjunct rigid bodies.

Also finite element meshing improvement has been made. The tetra mesh in LS-DYNA, which was using triangular solid element to represent the bolts in previous DATL 13x4.25-6 Tyre test wheel finite element model, was determined to be not recommended meshing method in this case, not only because of the increased element number but also the more complex equilibrium calculation for tetra element. Therefore, the bolt was finally meshed using solid layer element, leading to a significant reduction of element number and calculation time.

Figure-4.12 shows the refined bolt (left). The assembly of bolts and covers have also been shown (right).

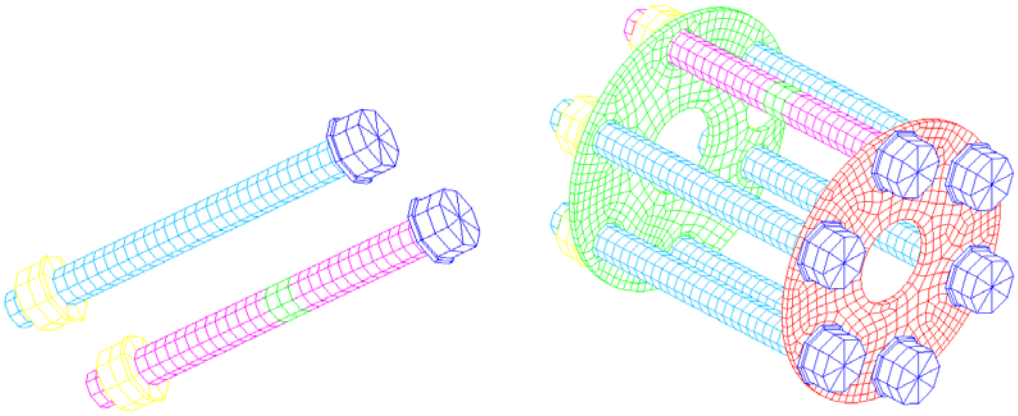

Figure-4.12 Meshing of the bolt and assembly

Null_Shell application and merge

The *NULL_SHELL in LS-DYNA, which allows equations of state to be considered without computing deviatoric stress, has also been used in the updated test wheel finite element model. The shells were defined as not part of the structure, but necessarily to define areas of contact within nodal rigid bodies or between nodal rigid bodies. The mass of the null shell elements was computed and added to the nodal points which define the connectivity. The Young's modulus and Poisson's ratio of the component were used to set the contact interface. (LSTC 2007)

In the updated test wheel finite element model, *NULL_SHELLS have been applied on bolt assembly as mentioned above. Also considering the significance of the contact between hubs,*NULL_SHELLS have been built for hubs as well.

Another thing worth mentioning, the contact between the bolts and null shells in this case were not exactly rigid bodies, hence the merging of the shells and bolts has to be processed.

Figure-4.13 shows the finite element model of the wheel assembly. The null shells: left for the male hub, right for the female hub.

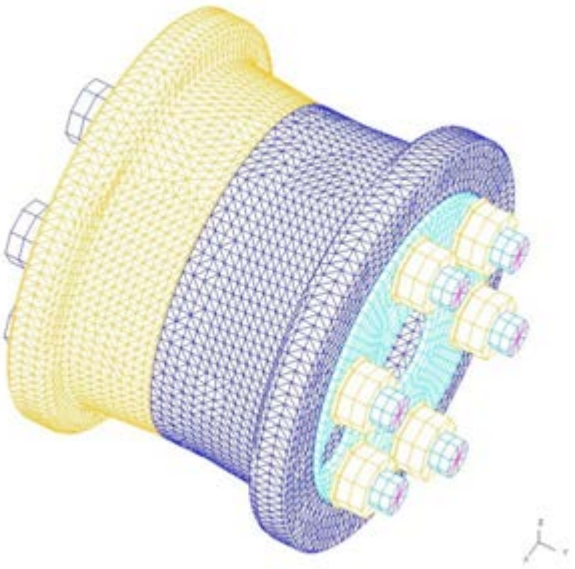

Figure-4.13 FE wheel model

Other key functions in LS-DYNA

*INITIAL_STRESS_SECTION and RBE3 element for load application

Several other key functions in LS-DYNA have been utilized to improve the finite element model as well.

First key function was the *INITIAL_STRESS_SECTION. The set up of this function includes direction setting and load curve settings. The maximum value of the stress load curve is defined by the calculation:

$$\delta = \frac{F}{\pi\left(\frac{D}{2}\right)^2} \qquad \text{Equation 22}$$

The magnitude of preload force (F) and the dimension of the bolts (D) are defined by DATL.

Figure-4.14 shows the locations of all the 6 *INITIAL_STRESS_SECTIONS.

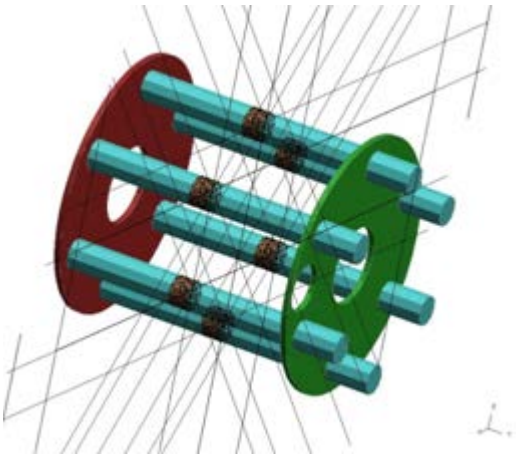

Figure-4.14 *INITIAL_STRESS_SECTIONS

The external vertical load at the bottom of the assembly was represented using RBE3 element and *LOAD_ON_NODE card in DYNA. Load curve was defined by the magnitude of force from DATL. Figure-4.15 shows the surfaces where pressure loads were applied (left) and the RBE3 element with vertical load (right).

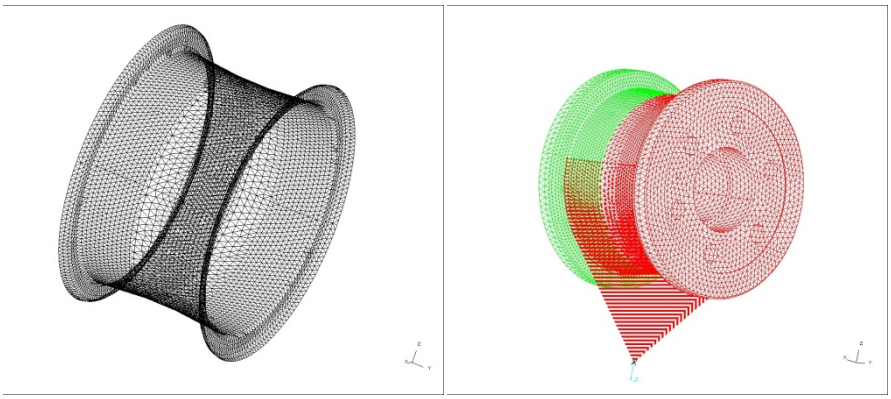

Figure-4.15 Pressure load on surfaces and Vertical load with RBE3 element

Adjustment to solve equilibrium problem

An equilibrium run was processed to clear all gaps. The results indicated this attempt to be successful. Therefore, an update was made which was to introduce a gap between the contact surfaces of 0.1 mm. The contact surfaces include: nuts to cover, cover to hub, hub to hub and heads to cover.

Figure-4.16 shows the gaps between nuts to cover (top left), heads to cover (top right) and hubs (bottom) in the new model.

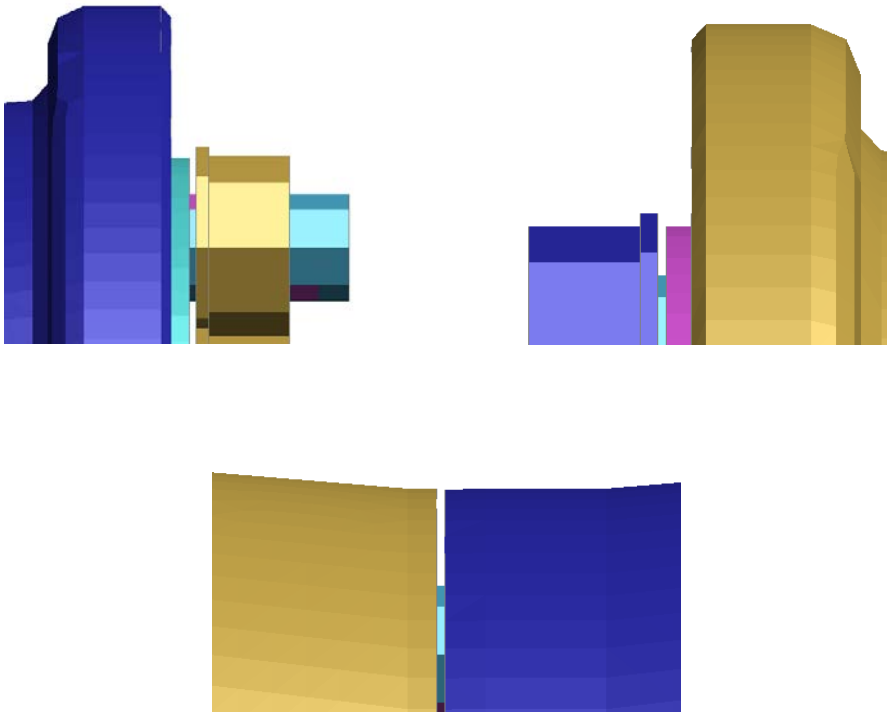

Figure-4.16 Gaps in LS-Dyna model

Results and discussion

The stress analysis simulation of FEA Dunlop test wheel model was finally carried out on High Performance Computer (HPC) in Coventry University. The loading cases of the simulation included: internal air pressure applied on the wheel surfaces that in contact with tyre volume; external vertical load at the bottom of the wheel assembly and the bolt-preload on the bolts. With a time step 0.1 second and total run time 1s, the simulation is divided into 10 steps. The results have indicated the success of the methodology using *INITIAL_STRESS_SECTION to represent bolt preload and the model improvement.

The model deformation and the movement of the components were reasonable. The movement velocities of the components pointed to the centre of the model. Deformation of the hubs reflected the bolt preload force as the hubs were pushed towards to each other.

The results of displacement and stress from LS-Dyna simulation provided a similar trend with the Dunlop documents. Looking into the magnitude, it can be found that the Maximum Von Mises Stress and Maximum Principal Stress are very close to each other. (267MPa to 233MPa, Von Mises; 92MPa to 110MPa, Max Principal)

The magnitudes of max displacement of the male hub have an over 0.1mm difference, (0.049mm to 0.179mm) but it can be explained.

The gaps between the components have been built in order to sort equilibrium problem, which was 0.1mm between the male and female hub. The Constrains in LS-DYNA have been set on the female hub bearing area, when the simulation started, the male hub was pushed towards the female hub first, the gap would close up before structure interaction, after then, simulation moved on. Therefore, that 0.1mm pre-set gap would still be counted as in the displacement result, meaning that the actual maximum displacement (male hub) of Dyna model was 0.179-0.1mm= 0.079, which was an acceptable difference for Dunlop.

Detailed magnitudes and plots can be seen as follow. The plots on the left side are from Dunlop analysis, and on the right side are Ls-Dyna simulation results.

Table-4.2 below shows the detail output comparison of Dunlop model and Dyna model.

Output	Dunlop results	Dyna simulation results
Max Displacement	0.049 mm	0.179 mm (0.079mm)
Max Von Mises Stress	267 MPa	233MPa
Max Principal Stress(Peak value)	93MPa	110MPa
Max Principal Stress(Bottom value)	-45MPa	-38MPa

Table-4.2 Comparison between Dunlop results and Ls-Dyna simulation

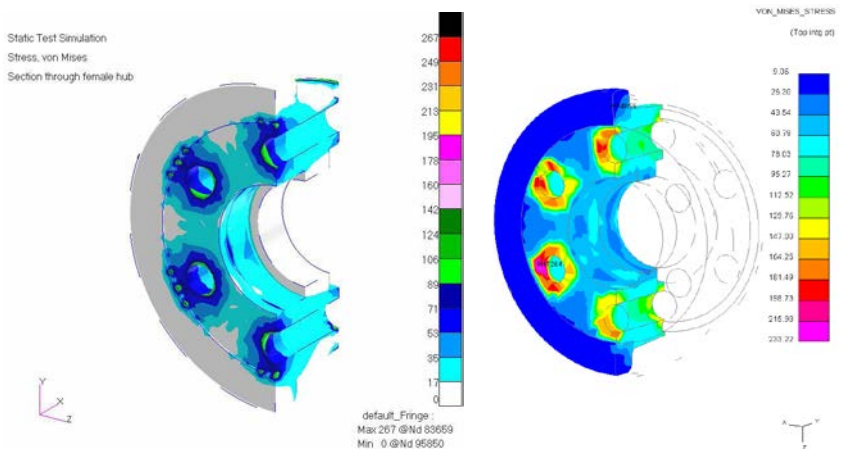

Figure-4.17 Von Mises Stress of female hub

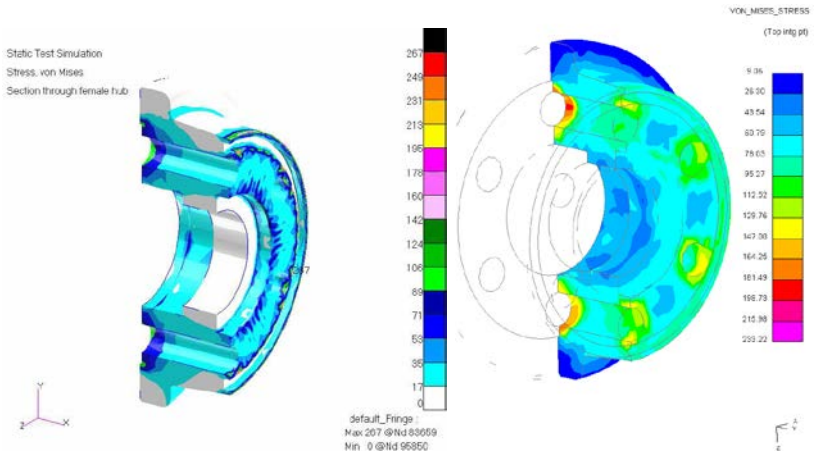

Figure-4.18 Von Mises Stress of male hub

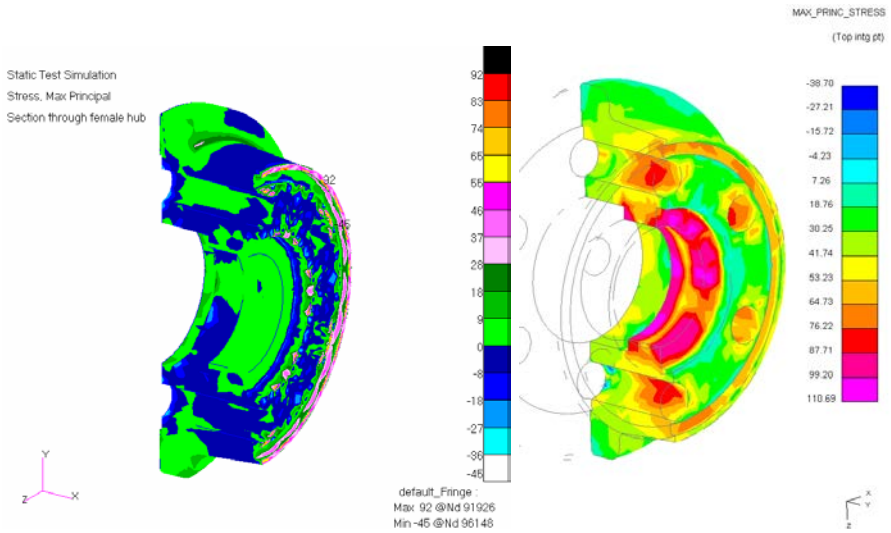

Figure-4.19 Max Principal Stress of female hub

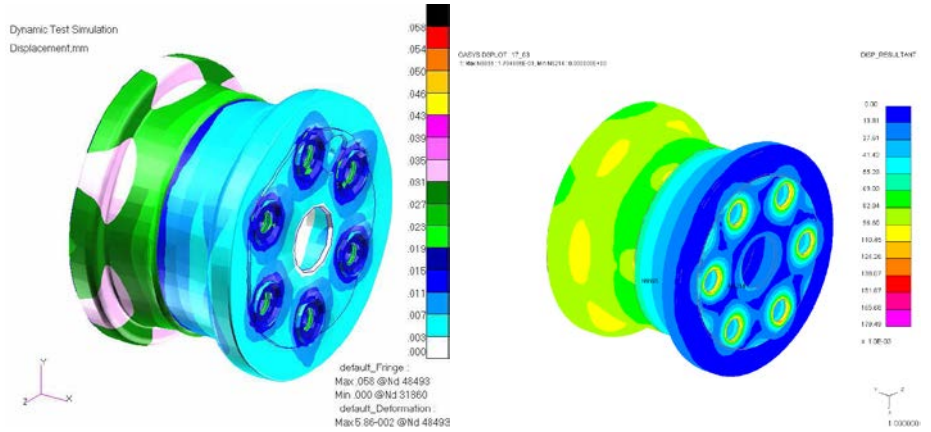

Figure-4.20 Displacement of the wheel (female hub view)

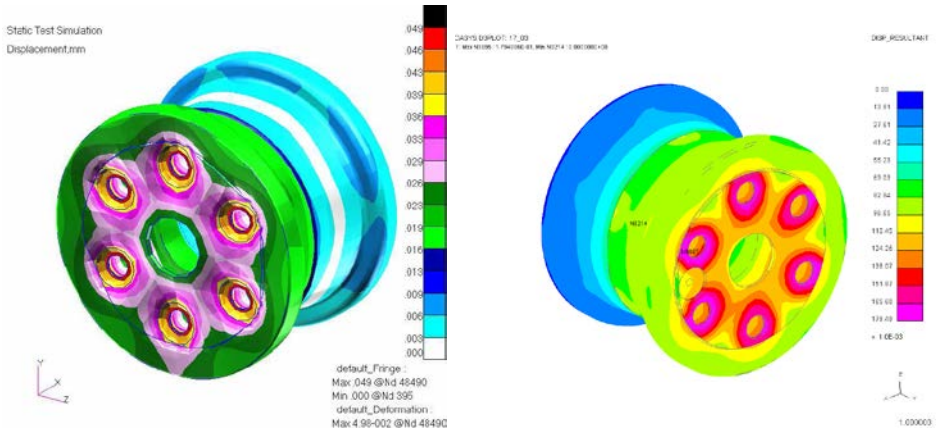

Figure-4.21 Displacement of the wheel (male hub view)

The modelling of the finite element test wheel has achieved positive progress. It is also noticed that the bolt pre-preload mainly affects the stress distribution around bolt-hole areas. The interaction area where tyre and wheel are in contact is not significantly influenced. Therefore, the tyre and wheel interaction model in this project has used a more simplified model to replace this full-scaled detail wheel model. Nevertheless, this finite element wheel modelling is considered as an important milestone in this project, and the model may be used in a complex tyre and wheel assembly model for more detailed purpose.

4.2 Finite element aircraft tyre model

The particular target tyre for the finite element model development is the Dual bead H41x16.0R20 testing tyre from Dunlop. The main reason of choosing this specific tyre was the industrial test result availability in Dunlop. Also, from the industrial point of view, Dunlop would like to look into the interaction between tyre and wheel, especially the interaction on the wheel rim edges.

Structure

Typical aircraft radial tyres contains one bead cord (Figure-4.22), hence a small bead chafer area is in contact with the wheel rim. Under a certain load condition, a small area will experience large contact pressure. However, the chosen H41x16.0R20 test tyre has a double bead cord design (Figure-4.24), which enlarged the chafer area compared to the single bead cord design.

The finite element modelling of this specific tyre/wheel interaction is expected to provide detail result around the contact area which could be utilized in further industrial product development.

Figure-4.22 Radial-ply aircraft tyre construction (Tanner and Daugherty 2005)

The geometries of the H41x16.0R20 test wheel and the cross-section details were given by Dr. Wei Ding, Dunlop. Figure-4.23 shows the target test wheel and tyre.

Figure-4.23 H41x16.0R20 test wheel and tyre (Dunlop Aircraft Tyres Limited 2010)

The structure definition for the target tyre, which includes:

Cable bead: Bead Code, Wrapping

Fabric: Chafer, 1st to 4th Plies, Bias Breakers, 0 Deg Belts, Inner Tread Fabric

Rubber Compound: Chafer, Inner Liner, Apex, Clinch, Insulations, Sidewall, Breakers Cushion and Strips, Sub Tread, Tread

Figure-4.24 H41x16.0R20 tyre cross-section (Dunlop Aircraft Tyres Limited 2010)

Several simplifications in finite element model have been made: clinch and sidewall are considered as the same part; Chafer and Apex are categorised as the same part although they are separated in the model.

The major construction sections used in tyre finite element model includes:

a. Tread

Tread is the component of the tyre that is in contact with the ground. It generally has some form of pattern because differing patterns can create different traction properties. More types of tread pattern design occur in automotive area, to eject water from the contact interface, to provide better traction in mud or snow, etc. But in this particular test tyre case, the pattern is for just all around performance.

Solid elements are used to model the tread with three element layers across the cross-section in order to effectively model bending stresses. A selective reduced fully integrated 8 nodes brick solid element is specified.

The tread material is *Mat_77 in Ls-Dyna, a hyperelastic rubber, with a density of 1.10e-6kg/mm^3 and a Poisson's ratio of 0.495. The reason of chosing *Mat_77, hyperelastic rubber will be explained in the following chapter. Other material properties required for hyperelastic rubber are obtained from DATL's laboratory testing and then adjusted to Ls-Dyna material card requirements during simulation of Material Characterization Correlation.

b. Belts

Belts play an important role in the function of a tyre. They provide puncture resistance as well as help the tyre to stay flat so that it makes the best contact with the road. Located under the tread, belts are composed of fabrics that are encased in rubber. Each fabric consists of individual wires similar to the steel bead.

In order to model the belts, two separate parts are used. 'Belts' part in the finite element model are represented using solid element, *Mat_77 hyperelastic rubber with the same density and Poisson's ratio as the tread, but different other properties. And the belt

fabrics are modelled using beam element, resultant warped beam. The material is *Mat_71, cable discrete beam, with a density of 7.86E-6 kg/mm^3, Young's modulus of 200GPa and posion's ratio of 0.28, and other properties provided by DATL. The reason of chosing *Mat_71 will be explained afterwards.

c. Sidewall and Apex

The sidewall and Apex are the portion of rubber that runs from the rim of the wheel and the bead up to the tread. They provide lateral stability to the tyre and also provide resistance to the vertical compression of the tyre. Higher sidewall stiffness will provide better driver control as it increases cornering siffness, however, it also increases tyre compressive stiffness, which requires a harder suspension system.Solid elements are used to model the sidewall and Apex, the selective reduced fully integrated solid element with 8 nodes, and both use the material *Mat_77 with same density of 1.10e-6kg/mm^3 and Poisson's ratio of 0.495, but different other properties respectively.

d. Bead

Tyre beads carry forces exerted on the sidewall that would otherwise cause the sidewall to separate from the rim and therefore lose air pressure. They effectively lock the tyre onto the wheel rim. The beads are constructed with a high strength cable encased in Apex rubber. The reinforcement layers in the plies warp around the steel beads.Solid elements 8 nodes, fully intergrated selectived reduced, are used to model the steel beads, using an elastic material, *Mat_1 with a density of 7.86E-6kg/mm^3, Young's modulus of 200GPa and posion's ratio of 0.28 (Steel). Nodes are merged between the Bead and Apex/Sidewall so they are essentially glued together.

e. Plies

The carcass plies increase the lateral load capacity of the tyre and add sidewall stiffness. They are made of a polyester material that runs perpendicular to the direction of the tread and belts. The plies serve as the main reinforcement materials. Different types of

tyres contain different layers of plies, 4 layers in this H41 tyre, which are encased in rubber to aid adhesion to other components. The method for modelling the plies is using solid elements, *Mat_77 with a density of 1.10e-6kg/mm^3 and a Poisson's ratio of 0.495 to represent the plies rubber and using beam elements that run perpendicular to the tread going from one bead to the other side to represent the fabrics. A node located in center of the tyre is used for the beam orientation. Those fabrics are *Mat_71 as well but with a density of 1.39e-06 kg/mm^3, a young's modulus of 5GPa, Poisson's ratio of 0.28.

Modelling the ply with beams and solid elements allows the different materials to behave independently, which affects the vertical compressive strength of the tyre. However, this method still allows the tyre to get lateral stability from the beams, which are only tied together in the radial direction by the sidewall rubber (Reid, Boesch and Bielenberg 2006).

The average tyre element mesh size in the model was set to be 5mm, that is finer than the work already published (Behroozi, Olatunbosun and Ding 2012), which used a size of 10mm to represent a detailed configuration. The study on mesh size from Behroozi's work indicated small element size is required for accurate prediction of stresses in the rubber componets. Compared with Behroozi's model mesh size, the proposed mesh size configuration in this H41 tyre model will be fine enough for an accurate rubber componets stress prediction.

Additionally, the mesh size of 5mm is also set so that the timesteps allows acceptable mass-scaling.

Mass-scaling refers to a technique whereby nonphysical mass is added to a structure in order to achieve adjust timestep in explicit simulations. In such simulations, the timestep usually is very small to maintain numerical stablity. However, small timesteps often require more CPU cost. To reduce the cost and improve performance, mass-scalling is used to increase the timestep in each cycle. In LS-Dyna, one of the methods is to specify a desired minimum time step size in *Control_Timestep.

The timesteps value is between 0.5 microsecond and 1 microsecond, for standarded industrial impact simulations . The simulatons of this H41 model run with a timestep of 0.5microseconds, therefore a mass scaling of 1% can be achieved.

The actual 2D finite element H41 dual bead tyre model and its computer model are shown in Figure-4.25

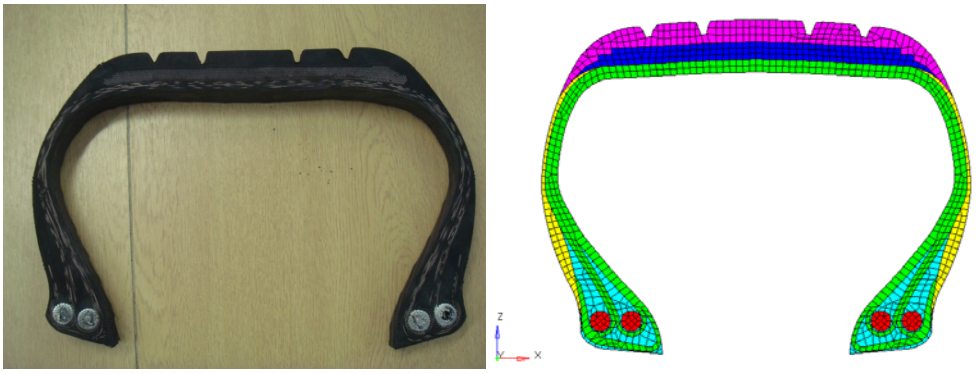

Figure-4.25 2D H41 Dual bead tyre

The approach of developing 3D tyre model is to rotate 2D cross-section model 360 degrees by 10 degrees per step. 3D solid elements are therefore generated by rotating the shell elements. The components of the tyre are individually signed with different material properties, which have been discussed in Chapter 3.

The beam elements are then generated through extracting lines on solid elements' boundaries. It is worth mentioning that the plies' fabric run perpendicular to the direction of the belts' fabrics as shown in Figure-4.26.

The total element numbers for the tyre model are: 40140 solid elements and 18972 beam elements.

Initially, the simulation time step was set to be 4.43154e-7s in LS-Dyna, which resulted in a 0% added mass at time step 0s. Referring to the simulation result, the 100 smallest time steps were controlled by solid elements in the Apex part. Those elements are located around the contact area between the tyre and the wheel rim, and needed to be small to duplicate the actual geometry.

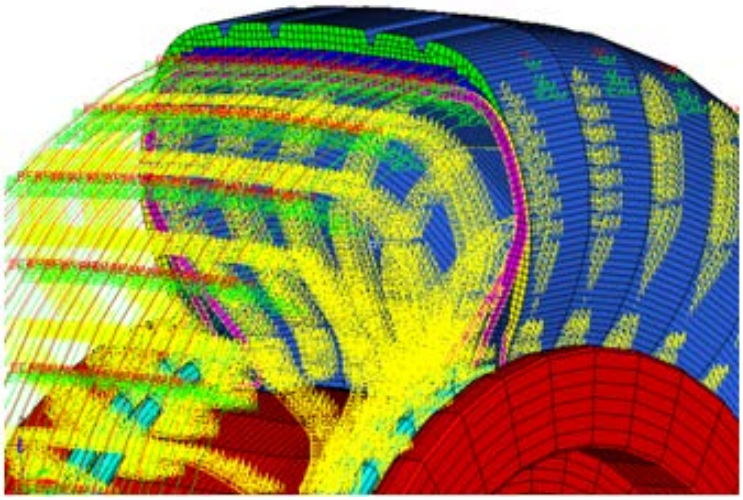

Figure-4.26 3D H41 meshed tyre

The relationship between time step and percentage added mass is shown in Figure-4.27. It is worth mentioning that a 2% age added mass has been recognized as an industry standard criterion, beyond which LS-Dyna finite element models are considered as not reliable because of added inertial effects (Bastien 2013). Therefore, the finite element models with 2 different simulation time steps (0% and 2% added mass) have been processed. The results and comparison between them will be discussed in the following section.

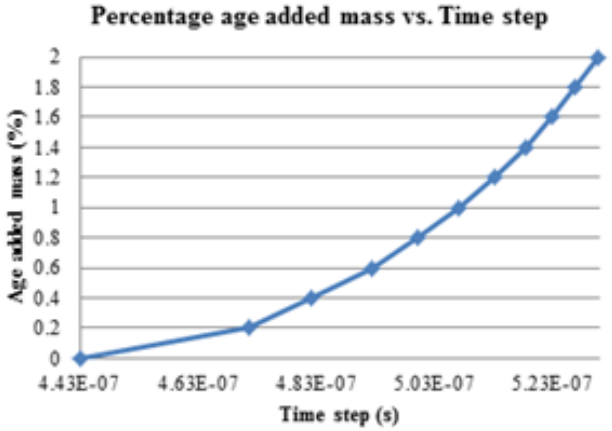

Figure-4.27 Percentage age added mass vs. time step

Time Step (s)	Age added mass (%)
4.43E-07	0
5.07E-07	1
5.31E-07	2

Table-4.3 Time Steps for specific percentage mass scaling

4.3 Material models used in H41 tyre model

As discussed in Chapter-3.11, the Yeoh model, represented as *Mat_77 hyperelastic rubber in LS-Dyna has been chosen to model the rubber. *Mat_67 nonlinear elastic discrete beam in LS-Dyna has been used to model the fabrics. The correlation progresses have been introduced in Chapter-3.11, and the results have shown positive agreement with Dunlop's experimental data.

Table-4.4 shows all the details of the element types (section card in LS-Dyna), finite element formulation and material model (material card in LS-Dyna) that were used for the H41 tyre finite element model respectively.

Part	Material Code	Poisson's Ratio	Density kg/mm^3	Young's modulus GPa	Element	Mat_Card
Tread	DC001	0.495	1.10e-6	N/A	Solid	Mat_77
Belt	DC005	0.495	1.10e-6	N/A	Solid	Mat_77
Sidewall	DC012	0.495	1.10e-6	N/A	Solid	Mat_77
Apex	DC003	0.495	1.10e-6	N/A	Solid	Mat_77
Plies	DC005	0.495	1.10e-6	N/A	Solid	Mat_77
Belt Fabric	DF021	0.28	7.86e-6	200	Beam	Mat_67
IT Fabric	DF014	0.28	1.39e-6	5	Beam	Mat_67
Ply Fabric	DF014	0.28	1.39e-6	5	Beam	Mat_67
Bead	N/A	0.28	7.86E-6	200	Solid	Mat_1

Table-4.4 H41 tyre model details

Mat_77: Hyperelastic rubber
Mat_67: nonlinear elastic discrete beam
Mat_1: elastic

4.4 Single bead H41 dummy tyre model

To compare with H41 dual-bead tyre, a 3D single bead tyre finite element model has also been developed. This 'Dummy' single bead tyre model has been estimated and generated based on the actual dual bead tyre structure.

As shown in Figure-4.28, single bead tyre has only one bead cord on each side and the number of the layers in body plies rubber and fabric compound has been reduced. The tyre/wheel rim contact area has also decreased, which leads to the structure change of the Apex part as well.

Apart from the parts mentioned above, the structures of Tread, Belt and side wall (including rubber and fabric) remain the same as the dual bead tyre. The materials used in single bead model are the same as the ones correlated and used in dual bead tyre model.

Although the actual geometry of H41 single bead tyre has several changes in detail, such as enlarge bead diameter to enhance the load capability and a thinner but stronger ply fabric to ensure the stability; this estimated single bead model is still considered as reasonable after confirming with the senior engineers from Dunlop aircraft tyres.

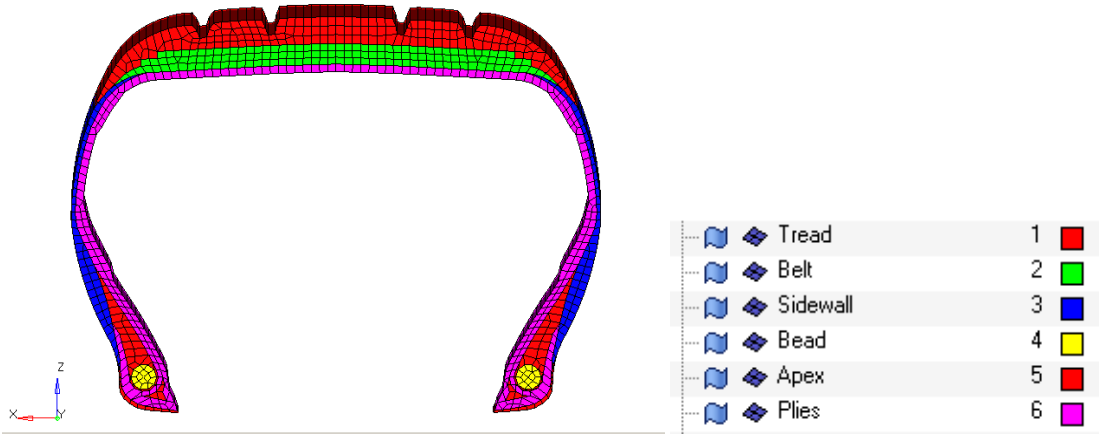

Figure-4.28 'Dummy' single bead H41 tyre cross-section

4.5 Tyre/wheel assembly finite element model

The tyre/wheel assembly model has been developed for the tyre/wheel interaction simulations. As mentioned above, the bolt pre-load will mainly affect the stress distribution change around the bolt holes area. On the tyre/wheel interaction area, there's no significant stress contribution from the bolt pre-loads. Therefore, initially, the structure of the assembled wheel hub has been simplified: the wheel hubs are considered as the same part without bolt-hole structures as shown in Figure-4.29

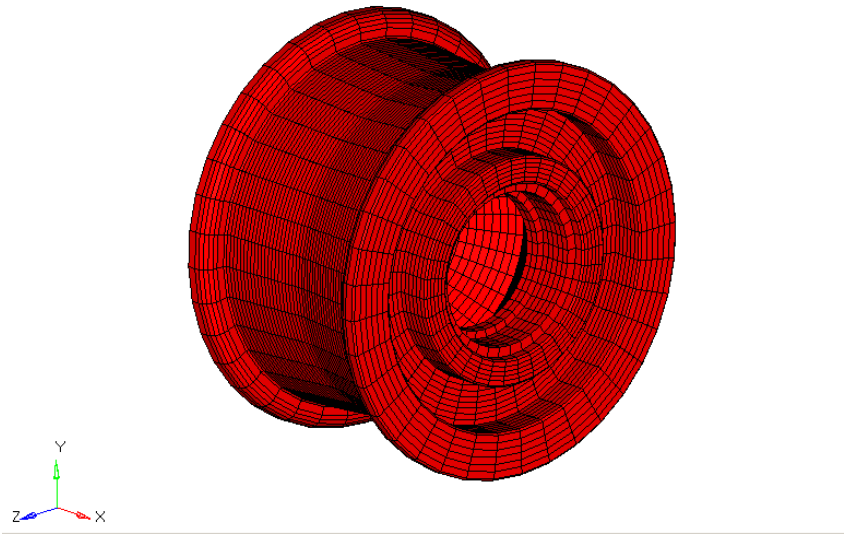

Figure-4.29 3D simplified H41 test wheel hub finite element model

Both the dual bead and single bead 3D H41 finite element tyre models have been mounted on the wheel hub. The dual bead mounted tyre on wheel is shown in Figure-4.30.

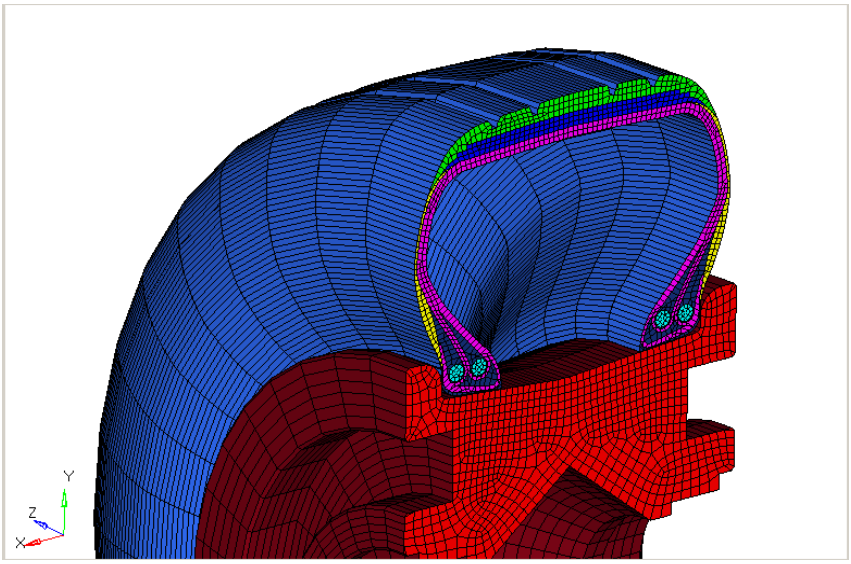

Figure-4.30 3D H41 dual bead tyre/wheel assembly

To extract the load (force) value on the beads, cross-sections have been set in both dual and single bead models as shown in Figure-4.31.

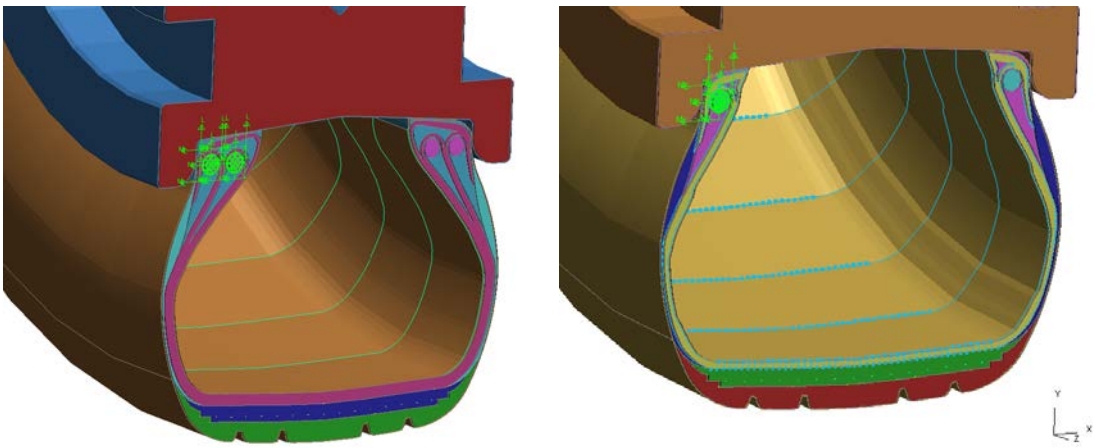

Figure-4.31 Dual/Single bead assembly cross-section

4.6 Summary of aircraft wheel and tyre modelling

With a certain geometry detail of any wheel and tyre types, the finite element models can be built up by following the modelling and meshing strategy mentioned above.

The stress analysis and distribution comparison between LS-Dyna simulation and Dunlop simulation results has confirmed the reliability of the finite element wheel hub model.

The advantage of the test wheel assembly model was that the model building and meshing processes were simple and easy. With the profile geometries (which is in industry standard) provided, using CATIA and HyperMesh could get the modelling done quickly.

Disadvantages include: the implicit simulation would take a fairly long time to run; hardware, such as memory and CPU requirements were correspondingly high as well.

Although for a further research, this detailed model can certainly be employed to develop a complex tyre/wheel model, but in the current situation, a simplified model is a more reasonable choice.

For the finite element aircraft tyre model, it can be noticed that 2D cross-section has been spanned by 360 degree with 36 steps on spin as shown in Figure-4.26. Because the elements of in this H41 3D model are elongated or ‘skinny’, the aspect ratio, the ratio between the element’s largest and smallest dimension, has been considered carefully. In the final version shown in Figure-4.26, the maximum aspect ratio (the elements in Tread part with the largest diameter from the centre) is 5 (25:5, element length: size), which is still within safe range (Aspect ratio over 10 is considered as not safe).

In an actual tyre construction, bead and fabrics provide the reinforcement in the rubber composite materials. Bead has been modelled as an individual part merged with Apex and Plies. Considering the significance of the fabrics and the incompressible nature of rubber compounds, the finite element model has been developed using solid elements for rubber and beam elements for fabric, with their own material characteristics applied respectively. Then the fabric and rubber are merged together to represent the composites, which ensures the reinforcement at both vertical and horizontal directions.

5. Simulations in different scenarios

In order to validate the finite element tyre model, simulations duplicating aircraft tyre testing scenarios have been designed and tested. The following chapter will also introduce several LS-Dyna simulations duplicating aircraft tyre operational dynamic scenarios. The purpose of the dynamic simulations is to assess tyre safety upon various landing speeds. The simulation results and comparison with Dunlop actual test data will also be discussed.

5.1 Simulation and validation under static load scenarios

The simulation and results of dual bead H41 FE tyre model were compared with experimental test to achieve finite element model validation. The testing scenarios included inflation and static load and deflection test.

Setup of the Inflation scenario

In this scenario, the 3D FE tyre model was mounted on the corresponding wheel finite element model, which is fully constrained at the bearing. The cavity of the tyre was inflated from 0 to a 187psi (1.289MPa) pressure recommended by the tyre manufacturer. The tyre pressure can be modelled in different ways (Danielson 1996, Hall, Jones and Mottram 2005). In LS-Dyna, one of the approaches is to use a simple airbag model, which allows the user to define the airbag using thermodynamic and other properties. Since thermo effects are not in consideration, this approach is not suitable.

The method used in this project has used *LOAD_CURVE function in LS-Dyna, which requires the input of time at which pressure is applied, and load curve defining pressure versus time. Within this model, the control volume is inflated with a pressure defined as a function of time. The pressure is uniform throughout the control volume.

The deformations of the tyre cross-section and the airbag pressure from simulation have been compared with the experimental data in order to validate the finite element model, as will be explained in this section.

Setup of the Static load scenario

This scenario involves squashing the tyre against a rigid plane. To achieve this, the wheel is clamped, with the inflated tyre mounted on it. The vertical load is achieved by placing a rigid moving wall below the tyre and then prescribing an upward displacement towards the tyre. The actual simulation process is: first inflating the tyre, then pushing the rigid wall against the inflated tyre.

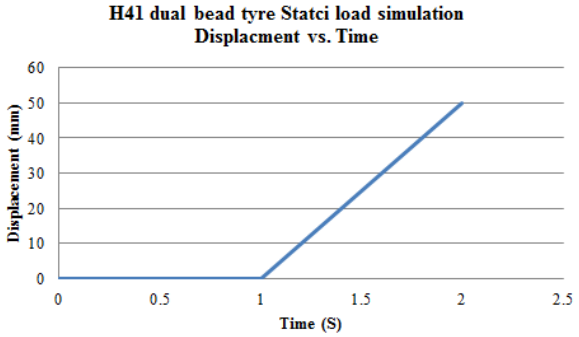

Figure-5.1 Static load displacement vs. time input

Forces on the wall, as well as the tyre deformation on the tyre/road contact interfaces are recorded in order to compare with the experimental test results from DATL. The static load scenario in LS-Dyna is shown in Figure-5.2

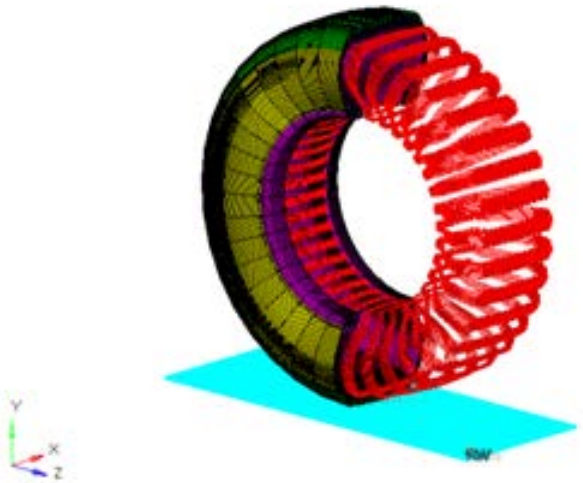

Figure-5.2 Static load scenario in LS-Dyna

Results and comparison of both scenarios

Inflation

The deformations of the tyre cross-section have been selected to examine the reliability of the tyre finite element model.

The expected tyre cross-section widths, X deformation, outside diameter and Z/Y deformation have been listed in Table-5.1 below. The relevant results provided by the LS-Dyna inflation simulation have also been listed.

Neglectable differences are between the experimental inflation test and the LS-Dyna simulation. Compare 0% age added mass simulation with the test data, the X deformation has an only 0.3mm difference at section width measure point. And the Y/Z deformation only has a 3.44% difference.

Outlay of the inflated tyre model in LS-Dyna can be seen in Figure-5.3 below (points of measurements and deformations in x and y directions).

The plots are showing that the pressure is applied as expected to the tyre as the tyre diameter is increasing due to the inflation loading (Figure-5.4). For Y deformation, inflation simulation have resulted in just a slight difference as shown in Table-5.1.

		Section Width (mm)	X deform (mm)	Out diameter (mm)	Y/Z deform (mm)
Dual Bead DATL test		330.00	2.5	1034.00	20.35
LS-Dyna Simulation 0% added mass	Magnitude	329.4	2.2	1032.60	19.65
	Difference (%)	1.08%	12%	0.14%	3.44%
LS-Dyna Simulation 2% added mass	Magnitude	328.5	1.75	1032.70	19.70
	Difference (%)	1.35%	30%	0.13%	3.19%

Table-5.1 Inflation test and simulation results

It is noticed that there is a 30% difference in X deformation from 2% added mass time step simulation. However, the actual magnitude difference is only 0.75mm out of 2.5mm. Regarding the small difference in actual section width (1.08% and 1.35%), that 30% difference is not considered as a fault. To prove this point, both 0% and 2% added mass simulations have been processed in static load scenario, and the outputs are compared in the following section to validate the reliability of the 2% added mass time step simulation.

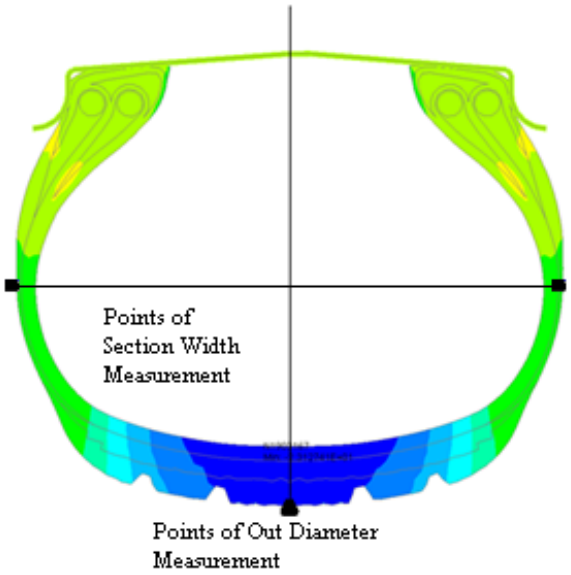

Figure-5.3 Tyre cross-section after inflation, points of measurements

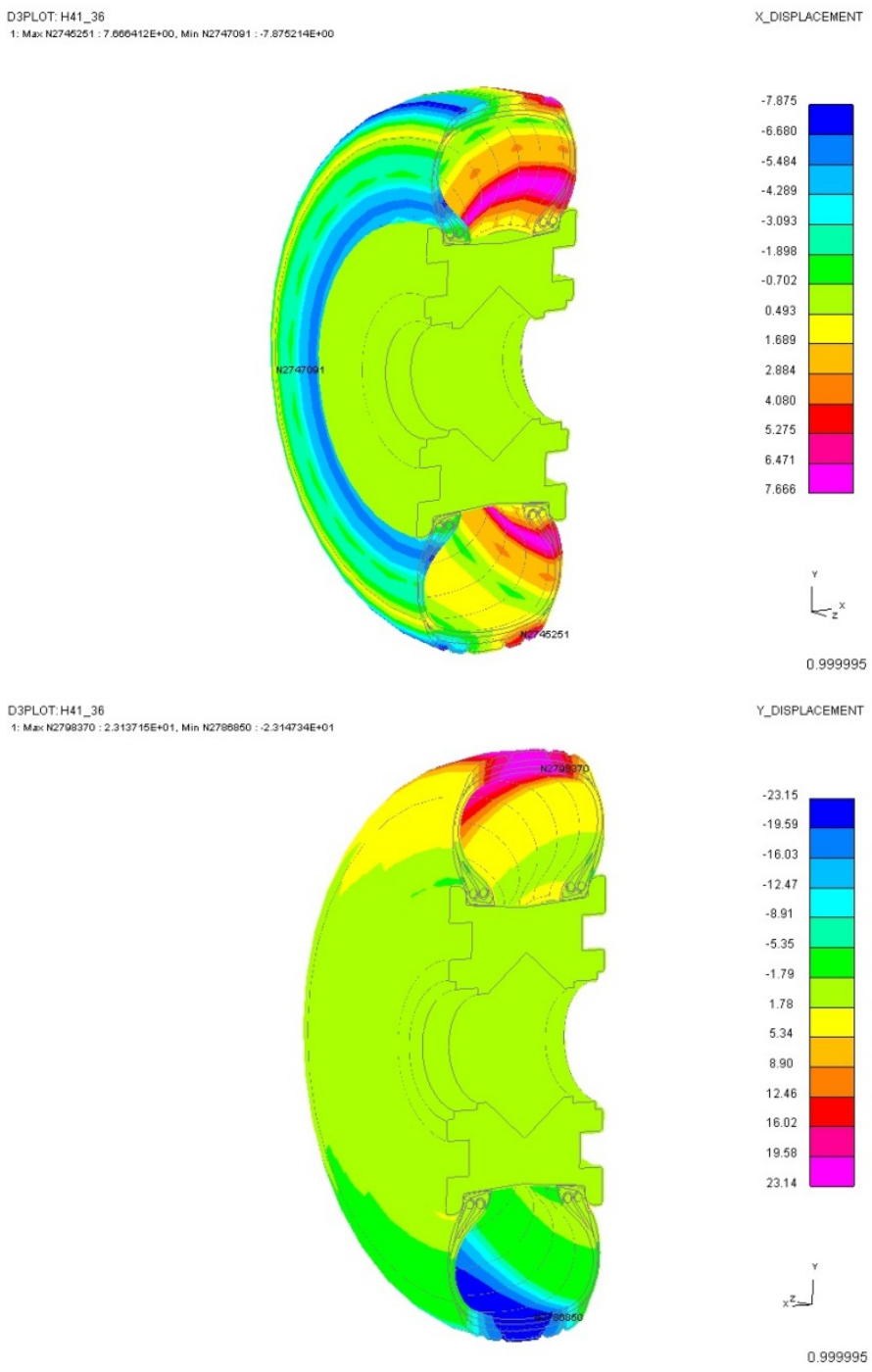

Figure-5.4 X and Y deformation after inflation

Static load

The deformation and displacement at the end of static load simulation for Dual bead tyre are shown in the Figures-5.5 below. The tyre cross-section before and after load are displayed in Figure-5.6 and 5.7.

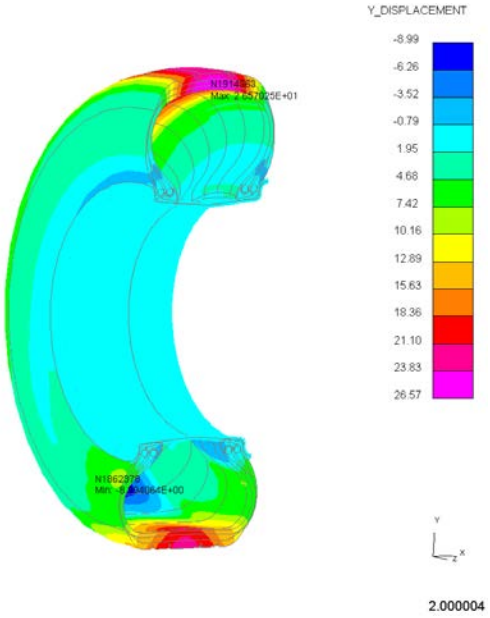

Figure-5.5 LS-Dyna static load simulation output (0% added mass)

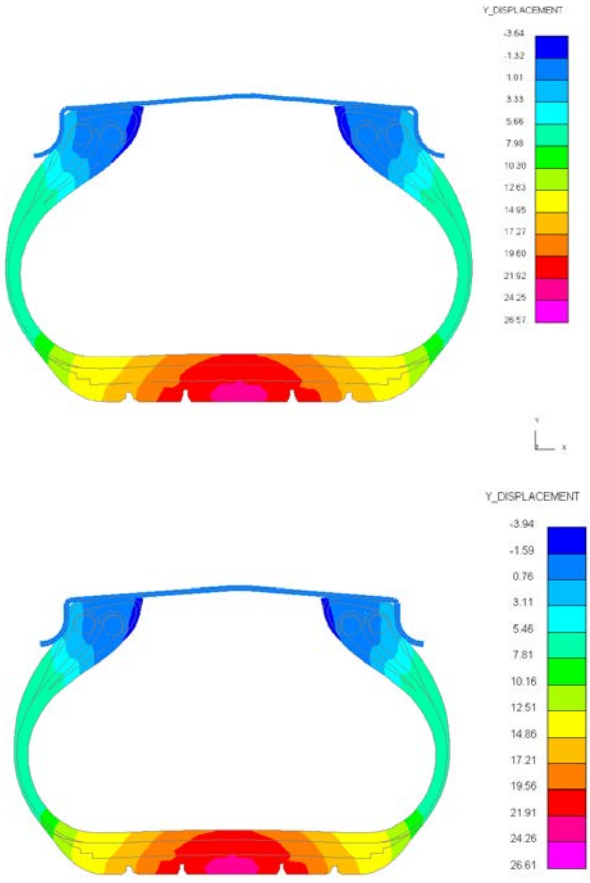

Figure-5.6 Tyre cross-sections after static load

(Y deform top: 0% added mass, bottom: 2% added mass)

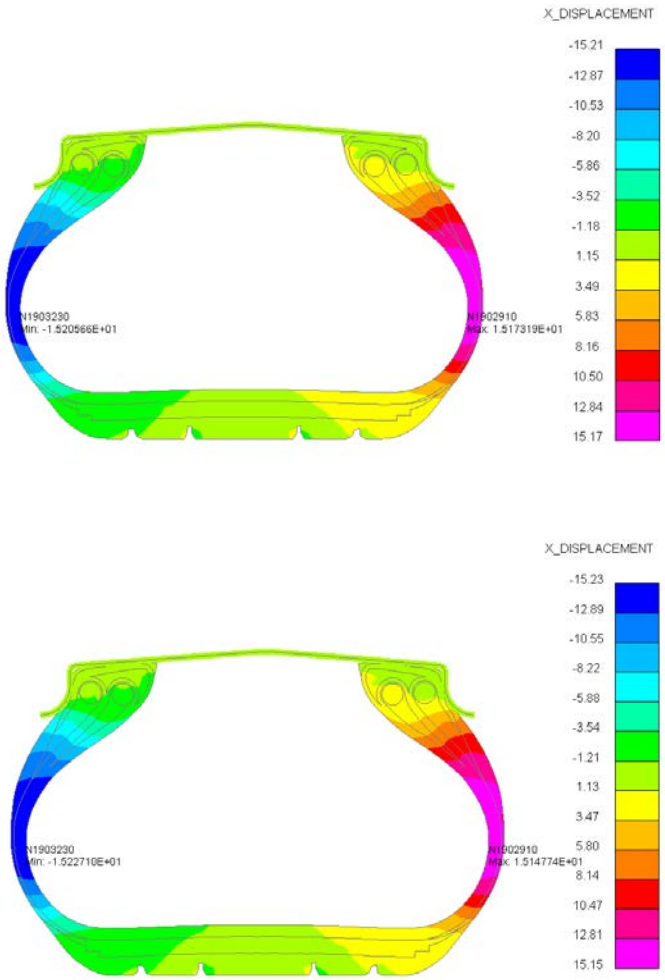

Figure-5.7 Tyre cross-sections after static load

(X deform top: 0% added mass, bottom: 2% added mass)

It is worth mentioning that in static load scenario, the deformation of the tyre under both 0% and 2% added mass time steps are following the same trend as expected. The recorded Y deformations and X deformations are listed in Table-5.2. The differences are negligible, which indicates the reliability of the 2% added mass time step simulation.

Time Step (s)	Mass scaling	X deformation (mm)	Y deformation (mm)
4.43E-07	0% added mass	15.17	26.57
5.31E-07	2% added mass	15.15	26.61
Difference (%)		0.13%	0.15%

Table-5.2 Static load scenario results

The load vs. force curve from the static load simulation has also been compared with DATL load vs. deflection result, which can be seen in Figure-5.8. The results from DATL test and LS-Dyna simulation are very close, and the trends of two curves were similar as expected.

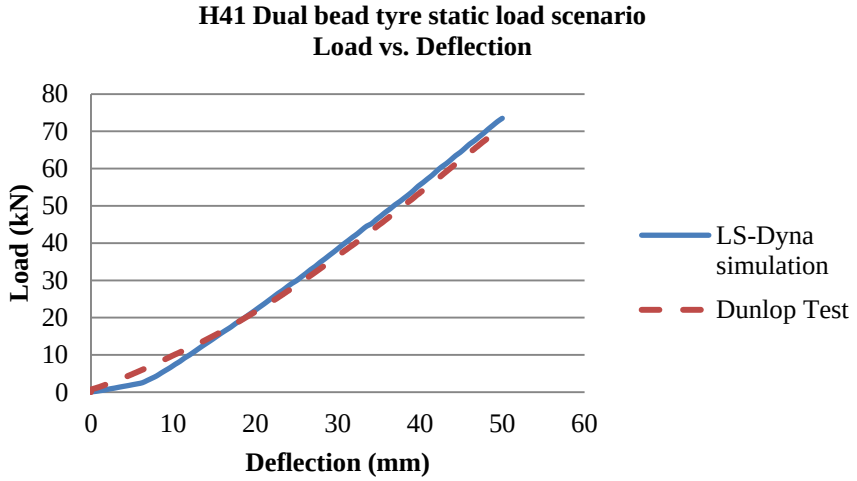

Figure-5.8 Load vs. Deflection Dual Bead H41 tyre/wheel assembly under static load

5.2 Analysis and comparison between single and dual bead tyres

Both the dual bead and single bead 3D H41 finite element tyre models have been mounted on the simplified wheel hub; with the same simulation scenarios including inflation and static load as described above.

Inflation on tyre/wheel assembly model

For the tyre/wheel assembly model, the outputs from inflation simulation are as shown in the Figures below. The results for dual bead tyre/wheel are listed on the left side, and the single bead on the right.

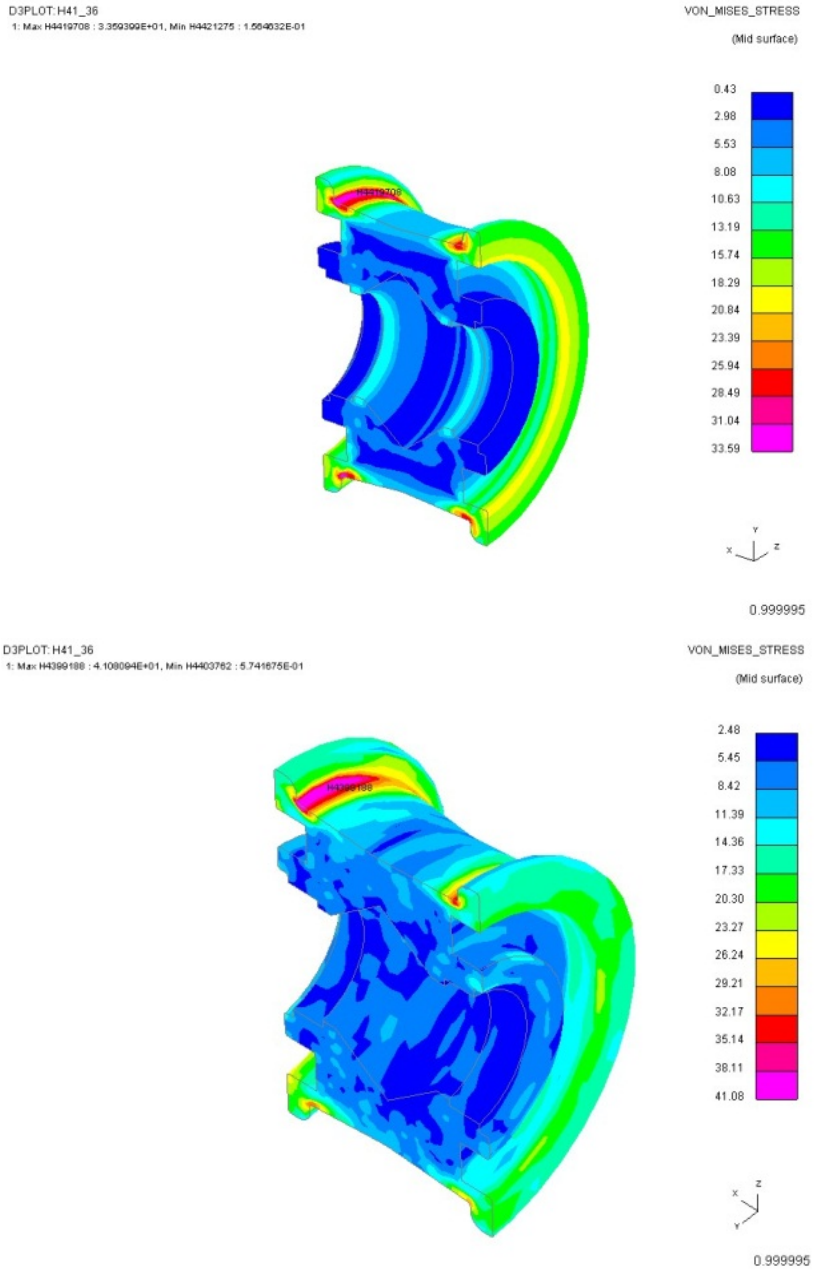

Figure-5.9 Assembly Inflation, Von Mises Stress distribution on Hub

Top: Dual Bead Maximum value 33.59 MPa

Bottom: Single Bead Maximum value 41.08 Mpa

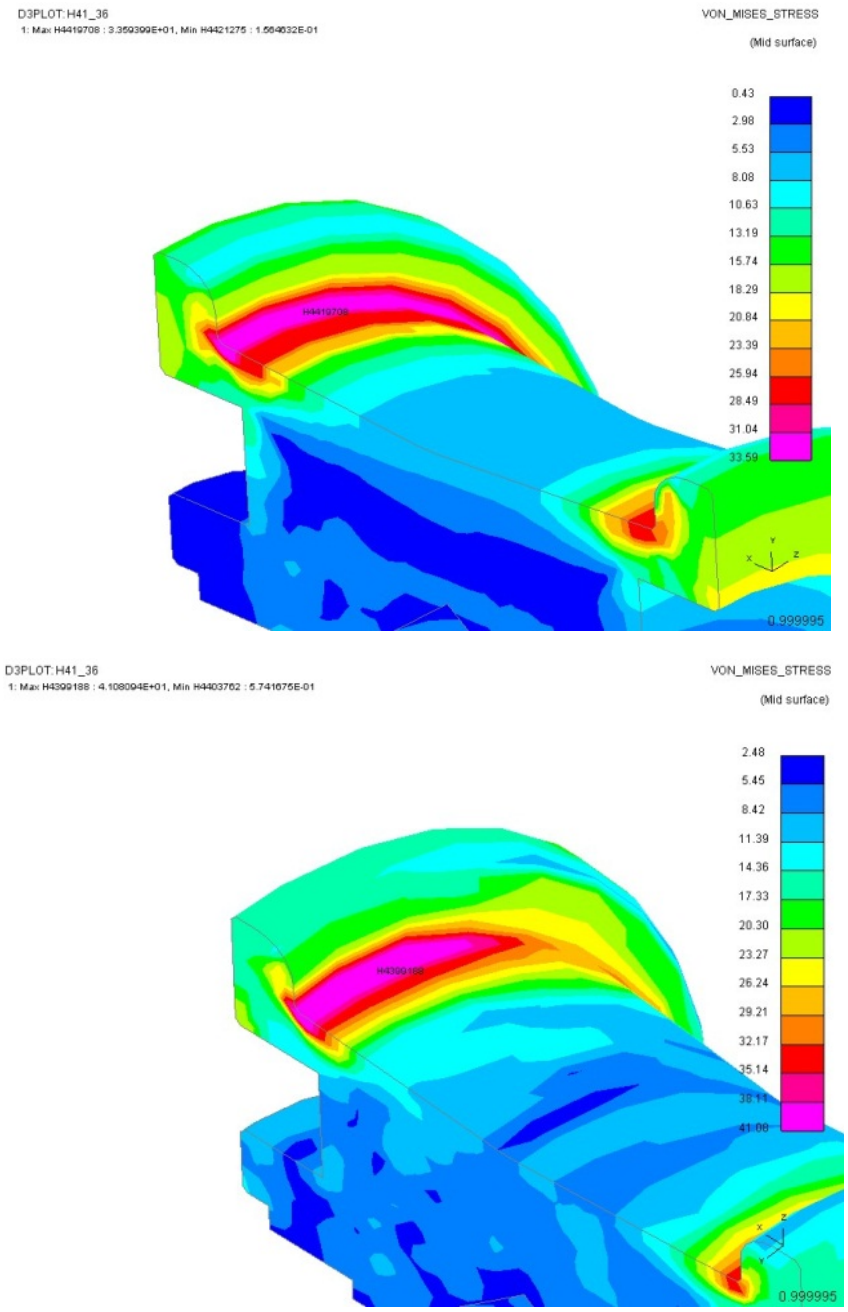

Figure-5.10 Assembly Inflation, Von Mises Stress Detailed Rim area

Top: Dual Bead 33.58MPa, Bottom: Single Bead 41.08MPa

It can be noticed that due to the tyre strucutre change, the interaction between tyre/wheel has been significantly affected. The magnitude of the Von Mises Stress value on the wheel hub with single bead tyre mounted, is 22% more than the dual bead tyre. The difference between single bead and dual bead model is intuitive: single bead tyre has a smaller sized bead and apex geometry, hence the contact area, and the decrease of

contact area will result in increased stress. It also has been reflected by the stress distribution outlay on the detailed rim, the area with high stress loaded in dual bead model is larger than the single bead model as shown in Figure-5.10.

Static load on tyre/wheel assembly model

For the tyre/wheel assembly model, the deformations and stress distribution are shown in the Figure-5.11 and 5.12.

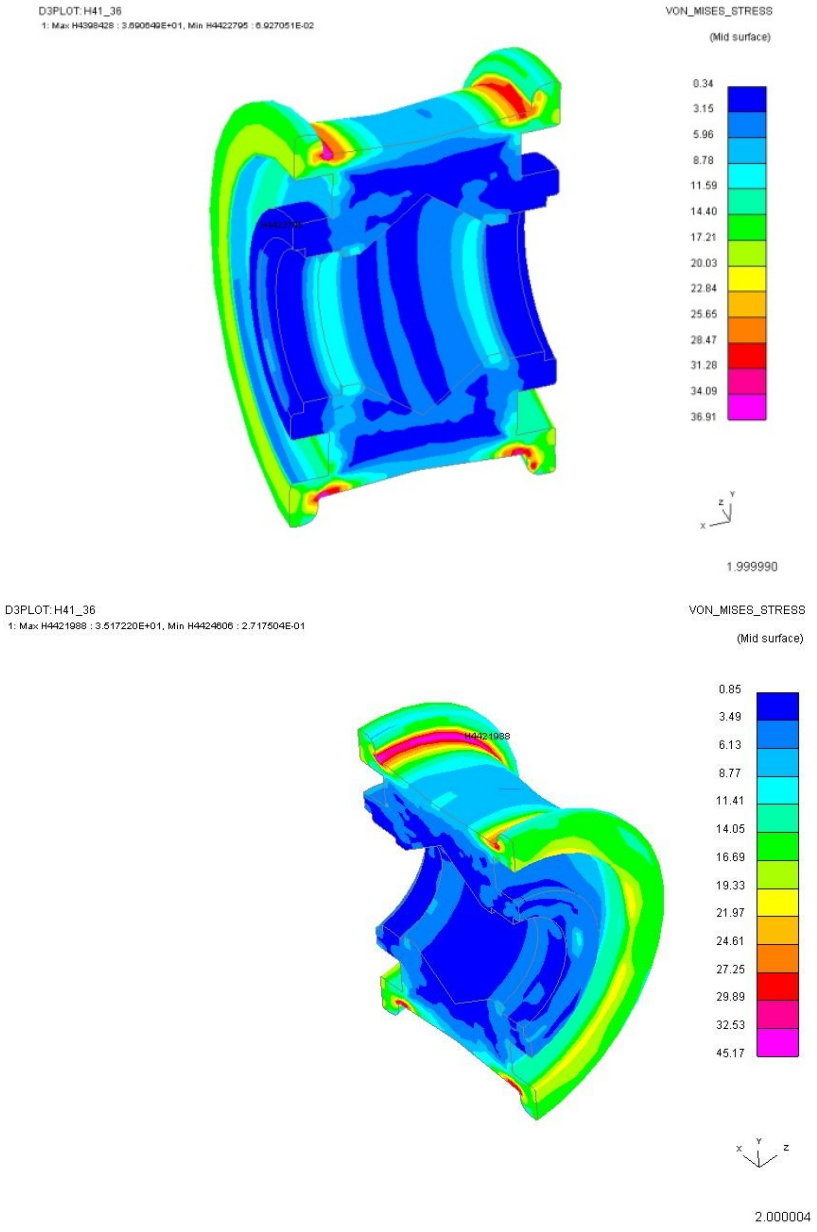

Figure-5.11 Static load Von Mises Stress distribution

Top: Dual bead Max 36.91 MPa, Bottom: Single bead model Max 45.17 MPa

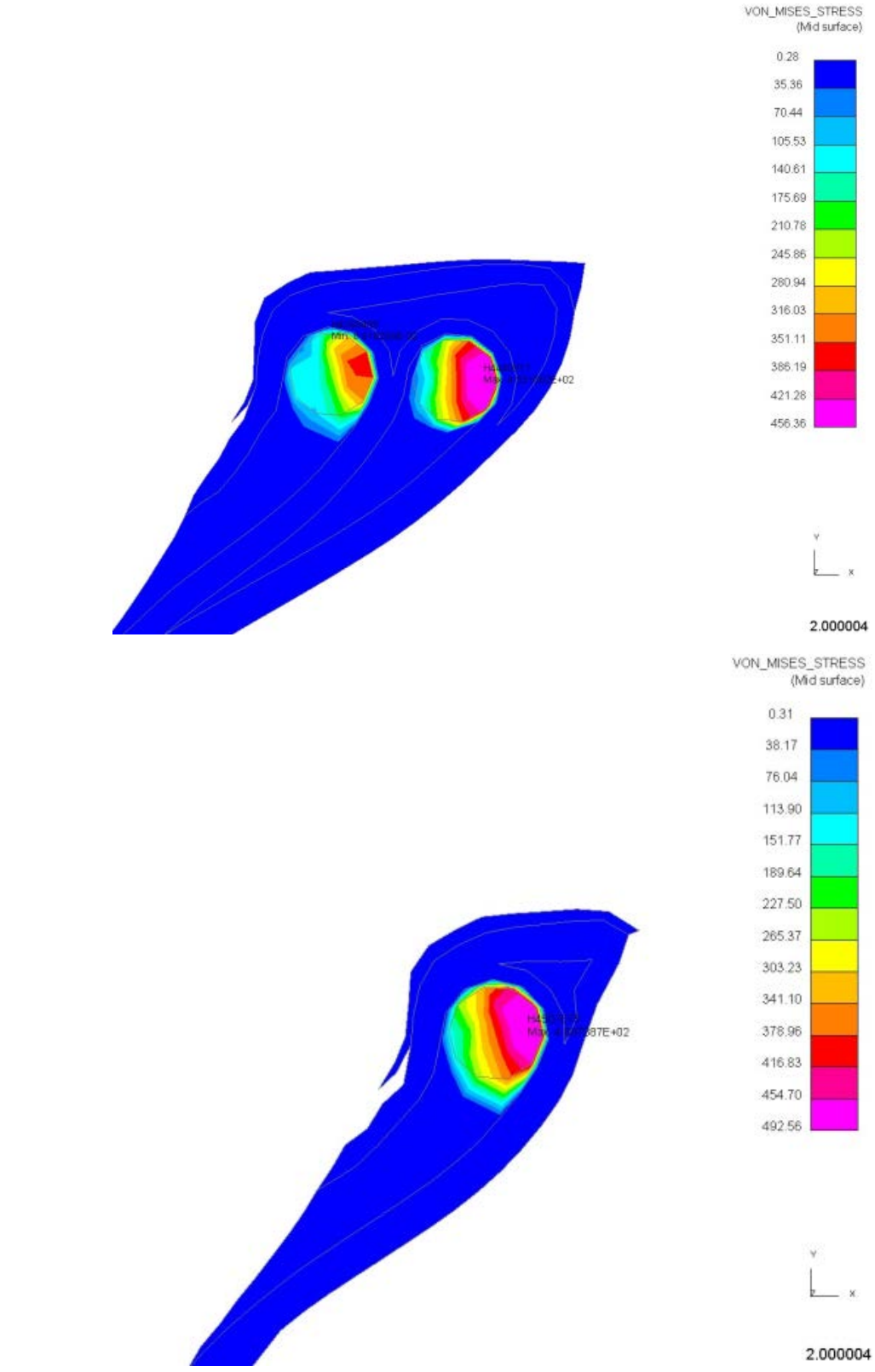

Figure-5.12 Static load Von Mises Stress in Bead

(Cross-section on the tyre/road contact side)

Top: Dual bead Max 456.36 MPa, Bottom: Single Bead model Max 492.56 MPa

The results from static load on assembly model follow the same trend as the inflation scenario. The deformations have a slight difference between dual and single bead structure. The maximum stress value around the tyre/wheel rim contact area differed as well: single bead model has a larger magnitude than dual bead model. It is also shown in Figure-5.12, the stress distribution on component boundary differed due to tyre structure change. The bead and the part of apex that are in contact with bead cord suffered 7% more stress in single bead model.

5.3 Dynamic simulations for landing safety assessment

The dynamic simulations are designed to duplicate scenarios that the finite element aircraft tyre falls and hits a rigid ground, carrying certain aircraft weights with various vertical landing speeds.

Set up of vertical impact scenario

As shown in Figure-5.13, the simulation duplicates a tyre drop on a rigid ground vertically from a certain height. The additional aircraft weight is achieved by assigning *ELEMENT_MASS on the node at the centre of the tyre. *RBE3 rigid body elements are used to constrain wheel rim to the node. Landing speed is achieved by applying *INITIAL_VELOCITY_GENERATION on the model.

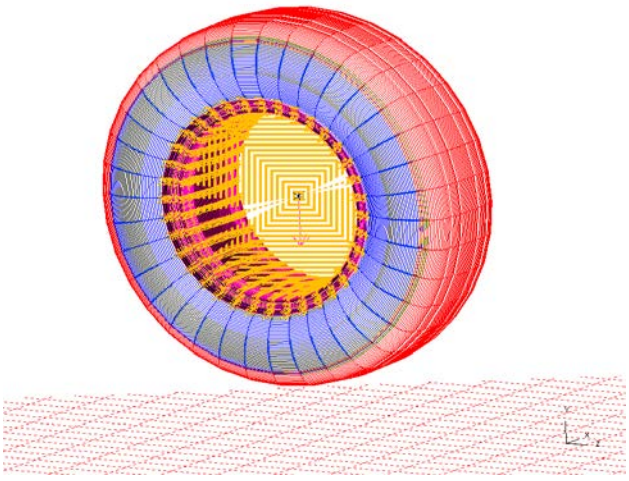

Figure-5.13: Tyre and Rim constrains in LS-Dyna

The wheel weight is defined as 128.6kg from LS-Dyna calculation. Two different aircraft weight load cases are assumed and applied on tyre: empty weight 7400kg and Max landing weight approximate 11675kg. The assumption is that the actual size of the H41 testing wheel is close to the commercial aircraft tyres that are used on Boeing 737-200. As shown in Table-5.3, (Michelin) the H41 radial tyres are actually used on ERJ-190 aircraft, however, the aircraft data for Boeing 737-200 are easier to obtain from public sources. The confirmation has been made with DATL that the sizes of ERJ-190 and Boeing 737-200 are comparable, therefore, the assumption has been considered as reasonable.

Boeing 737-200 has 6 tyres (2 nose tyres, 4 main tyres) and its empty weight: 29600kg; max landing weight: 46700kg (Boeing Commercial Airplanes July 2004). Assuming 4 tyres equally carry the aircraft weight upon landing, the mass on each tyre will be: 7400kg in empty weight and 11675kg in max landing weight. In this study, the damping efforts from suspension and landing gear system have been considered as invalid. This is due to the fact that extreme landing scenarios have been designed to assess the tyre's failure criteria, therefore the worst landing cases have been set up, which is that the wheels directly carry the aircraft weight without any suspension operating.

	Aircraft Type	Main Tyre Code/Size	Rated Load(lbs)
General Aviation/ Business Aircraft	Cessna 172, Skyhawk	6.00-6	2350
	Cessna 172 RG, Cutlass RG	15x6.00-6	3200
	Dassault 10, Falcon	22x5.75-12	5700
Commercial Aircraft	Douglas DC-4	15.50-20	20500
	Boeing 737-200	H40x14.5-19	36800
	ERJ-190	H41x16.0-20	32825
Military Aircraft	Helio U10A, Courier	6.50-8	3150
	Lockheed F-16 Fighting Falcon	25.5x8.0-14	16200
	Boeing B52, Stratofortess	56x15	76000

Table-5.3: Aircraft tyre application and data (Michelin)

Downward vertical velocity (vertical landing speed) is defined:

- 2 to 4 m/s normal landing
- 6 to 8 m/s hard landing
- Over 8m/s crash landing (The Goodyear Tyre & Rubber Company April 2010)

Considering the significance of landing speed change in crashworthiness certifications and analysis, the simulations have been processed with 0 m/s (free fall), 3m/s, 5m/s, 7m/s, 8m/s and 10m/s landing speed, separately.

Tyre safety criteria and threshold upon landing

Initially, three criteria have been chosen to analyse the tyre safety upon landing (vertical impact):

a. Tyre Deflection rate:

$$\%deflection = \frac{Free\ height - Loaded\ free\ height}{Free\ height} \qquad \text{Equation 23}$$

(The Goodyear Tyre & Rubber Company April 2010)

For safety assessment, aircraft tyres are designed to operate at 32% deflection, some at 35%, if deflection rate constantly goes above 35%, the function of tyre will be compromised.

b. Rated load, also known as the maximum static rated load capability of the tyre as listed in Table-5.3

c. The maximum stress in the steel bead.

The thresholds of the criteria have been defined as:

a. Tyre deflection rate upon touchdown should not go above 70%.

Previous NASA research (Davis 1997) and DATL industrial experiences have indicated that an aircraft tyre must be able to carry significant load and impact upon landing. NASA research (Davis 1997) has investigated a yield radial-belted tyre at 52% deflection rate under a quasi-static test. The DATL industrial experiences has confirmed that upon hard landing or even more extreme load cases, the threshold is raised up to 70% deflection, above which the tyre will completely lose its function, therefore the wheel rim directly come into contact with the ground and causes damage. For this study, the threshold is defined as 70% to simulate an extreme landing case.

b. The tyre load upon landing should not exceed its bottoming load, which is approximately 2.8 times its rated load.

As indicated, the rated load is the maximum static load capacity of the tyre, which is 14,889 kg (32825 lbs). The load on a tyre upon aircraft landing will significantly

increase due to the landing impact. The threshold is defined as the tyre bottoming load, above which the tyre will lose its function. The magnitude is provided by DATL, which is approximate 2.8 times the tyre's rated load. Therefore the value of the bottoming load is 14,889 x 9.80665 x 2.8 = 408.031 kN.

c. The stress and load on the tyre bead and the area around should not exceed the material's yield or tensile strength.

   The material of the bead is defined as high-speed steel in this LS-Dyna tyre model. The threshold is set to be the same as the material's yield and tensile strength value, which are obtained from material property data base. (Granta Design Limited 2013)

Simulation results and conclusion

The free height and loaded free height are calculated from Equation 24 and 25.

$$Free\ height = \frac{Outside\ Diameter - Flange\ Diameter}{2} \qquad \text{Equation 24}$$

$$Loaded\ free\ height = Loaded\ Radius - \frac{Flange\ Diameter}{2} \qquad \text{Equation 25}$$

Loaded free height can also be considered as the minimum Y-axis (Vertical) distance between the node at the tyre / road contact and the node on the bottom side of wheel rim. (The Goodyear Tyre & Rubber Company April 2010)

The simulation results from inflation scenario shows the free height is 227.15mm.

From the 'landing' simulation, the time history of distances between tyre / road contact node and the bottom side of rim has been recorded and displayed in Figure-5.14. Simulation started before tyre inflation, and then distance reaches its maximum value after inflation finished. When tyre hit and bounced on the rigid ground, distance between two nodes decreased first then increased again. At 4.5s, it reached minimum value where maximum deformation occurred. The value was 154.46mm as recorded.

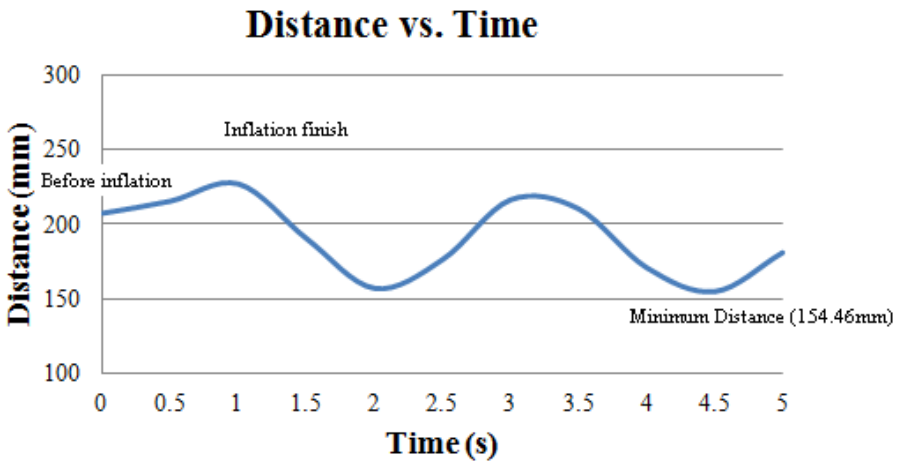

Figure-5.14 Distance (Loaded Free Height) vs. Time, 0 m/s (Free Fall)

Hence, the deflection rate of each simulation can be calculated through Equation 23.

For 0m/s (Free fall), deflection rate = 32% as:

$$\text{Deflection rate} = \frac{227.15 - 154.46}{227.15} = 0.32$$

From simulations with various landing speed, deflection rates have been calculated.

As displayed in Figure-5.15 and 5.16, the deflection rate and tyre load vs. different landing speed (Dual bead model) are shown separately.

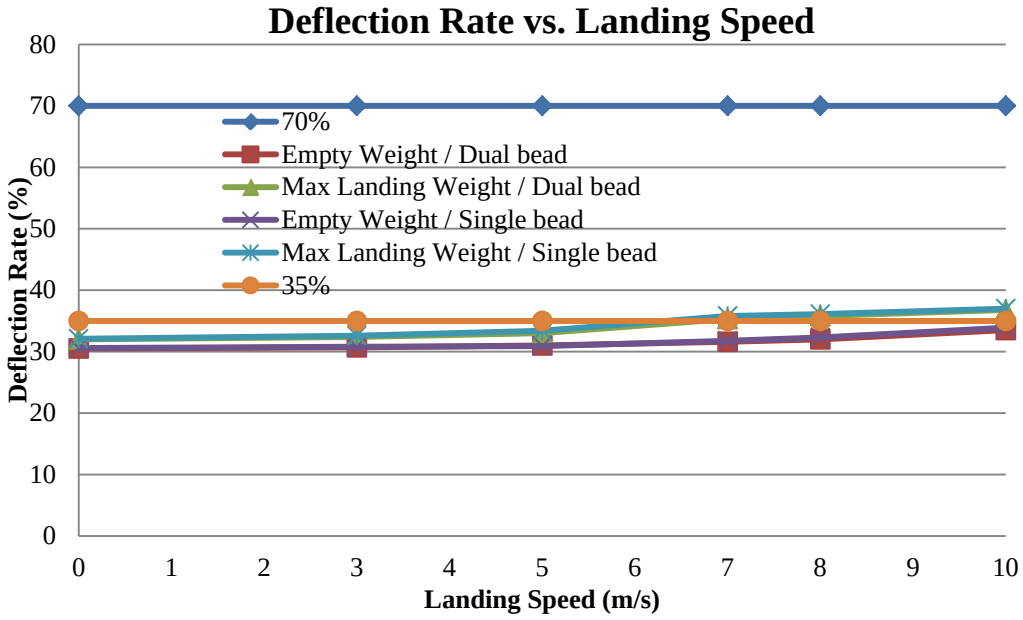

Figure-5.15 Deflection Rate under different weight& speed

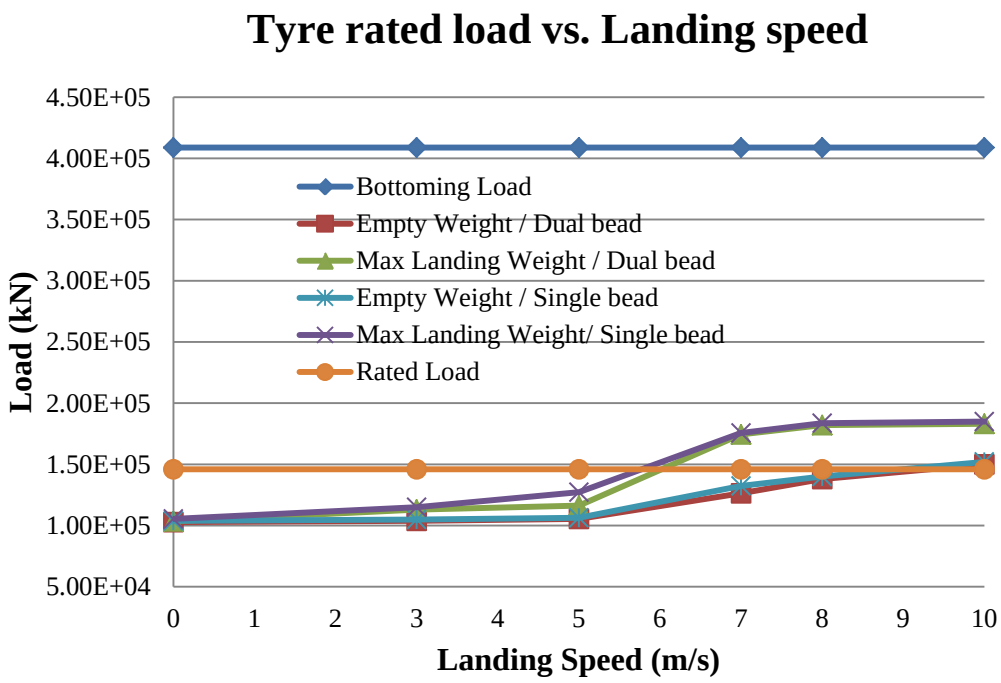

Figure-5.16 Tyre load under different weight & speed

The simulations have shown that with an empty aircraft weight, the tyre is safe at all landing speed range, the deflection rate and tyre load are all under the thresholds of 70% and rated bottoming load 408.831kN. Even comparing with the operational criteria, deflection rate of 35%, the tyres are within the range.

With the maximum landing weight, when tyre hits the ground at a higher landing speed (10m/s which is over 8 m/s crash landing speed), both the tyre deflection rate and load went over 35%, however, they are still in the safe range of under 70%.

At a lower speed (7 m/s, in range of a hard landing), the deflection rate was in the range of 35.3%, the load on tyre was over the rated load (174.5kN over 146.0kN), but still in the safe range of the bottoming load.

The simulation results show that upon hard landing, the target tyre is possibly to suffer a deformation and load over its normal operational range with maximum landing weight; however, since the transient magnitudes do not exceed the thresholds, the tyres will still be safe upon such an impact.

Table-5.4 shows the comparison of maximum force and stress in bead between dual bead and single bead model under different vertical touchdown speed.

In Figure-5.16, a comparison of the maximum stresses on beads with the yield strength (620MPa) and tensile strength (700MPa) of high-tensile steel (Granta Design Limited 2013) can be seen. The simulations are processed on both dual and single bead tyre models under various touchdown speeds with maximum landing weight.

	Dual Bead Model				
Speed (m/s)	0	3	5	8	10
Max Bead Force (kN)	40.51	42.43	45.42	67.76	73.57
Max Stress (MPa)	456.36	487.53	492.27	529.34	554.68
	Single Bead Model				
Speed (m/s)	0	3	5	8	10
Max Bead Force (kN)	46.76	48.97	57.67	74.34	85.46
Max Stress (MPa)	492.56	507.39	510.45	553.10	590.43

Table-5.4 Maximum Force/Stress value comparison

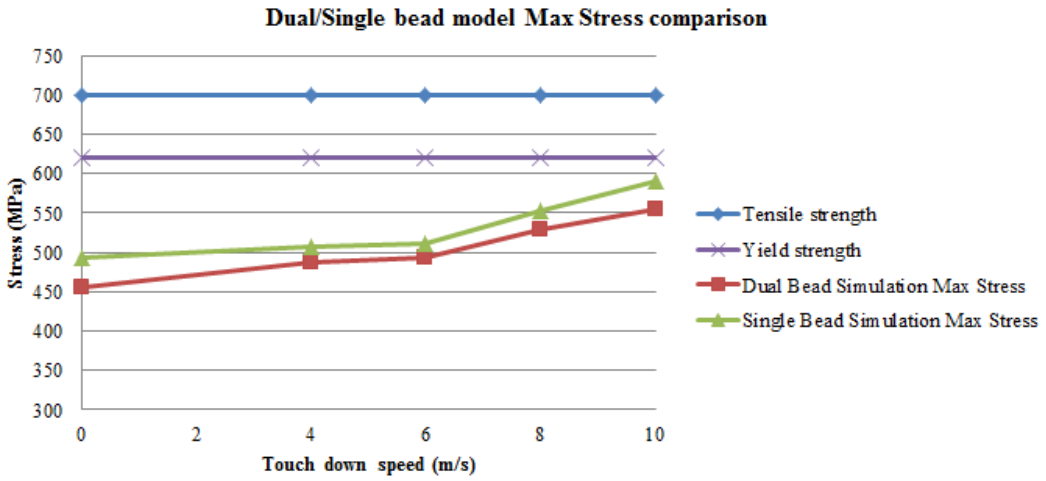

Figure-5.17 Max Stress comparison between dual bead and single bead model

The stresses in belt, carcass plies and other rubber parts, along with the stress on the wheel hub have also been recorded for each simulation. However, since they are well below the relevant failure stresses, only the results from 10m/s touchdown simulation (the most extreme simulation) have been listed in Table-5.5. (Aluminum material for aircraft wheel, yield strength 440 MPa, tensile strength 490MPa; Rubber material for tyres, yield strength 17.3MPa, tensile strength 17.3MPa) (Granta Design Limited 2013)

	Dual Bead Model					
Speed (10m/s)	Tread	Belt	Apex	Sidewall	Plies	Wheel
Max Von Mises Stress (MPa)	2.59	2.22	11.64	11.34	11.64	46.53
	Single Bead Model					
Speed (10m/s)	Tread	Belt	Apex	Sidewall	Plies	Wheel
Max Von Mises Stress (MPa)	3.81	4.02	12.32	12.11	12.73	54.87

Table-5.5 Maximum Stress value in rubber and wheel

Comparing the dynamic simulation results between the dual and single bead models, it can be found that both the force and stress maximum value from a single bead model are higher than a dual bead model. It is consistent with the conclusion from inflation and static load scenarios. It is also noticed that the values increase with the increasing touchdown speeds, which follows the trend as expected.

From Fig-5.16, it can also be seen that for both models, the maximum stresses are within the range of the bead material's yield and tensile strength. The stresses in other rubber components and the wheel hub (as listed in Table-5.5) are well below the relevant failure stresses. The dynamic simulations have indicated that the materials are in safe range for both the dual and single bead designs even under a high touchdown speed. (10m/s, crash landing) Although other parameters have exceeded the tyre operational criteria with maximum landing weight at a higher touchdown speed (from

7m/s, hard landing range), the safety thresholds have not yet been reached. The tyre is still considered as reliable at the speed/weight range from the dynamic simulation.

Therefore, the conclusion is that even the materials themselves do not exceed failure; the tyre structure may go over the operational criteria; however, as long as the safety thresholds not been exceeded, the tyre will still survive the transient impact and load under extreme load case.

Although the current research and simulation have indicated the reliability of the target test tyre through comparing simulation output and safety thresholds, there are more industrial criteria for the tyre safety and reliability assessment. A full-scaled certification of tyre safety should put all the aspects into consideration.

5.4 Summary and comments

The outcome of deformation trends provided by inflation simulation and static load simulation did match with the experimental result from Dunlop. Load vs. deflection relationship from Ls-Dyna static load simulation also matched with actual industry test.

The tyre/wheel interaction models have provided acceptable deformation results compared with DATL test. The comparison of the stress distribution between dual and single bead tyres has proved the significance of tyre structure change in this tyre/wheel interaction study.

The research has introduced a detailed approach of developing finite element model for aircraft tyre and wheel assembly. Comparing with experimental test data, the results have indicated a successful progress in aircraft tyre/wheel interaction finite element modelling, which also has demonstrated the effective use of finite element models as predictive engineering tool.

The model is suitable to run with a time step up to 5.31E-07s, giving a mass scaling of 2% at the beginning of the simulation, which is compatible to industry standards.

The current investigations have covered tyre inflation and static load scenarios, and also considered the effect of the aircraft landing phase on the tyre, by modelling and predicting a single tyre hitting the ground.

The results have shown that the target test tyre can survive even at a hard landing speed. The response is in agreement with the manufacturer and aviation guidelines.

On-going research will investigate a combined 'free-falling' tyre with a rotation motion against a rigid road, duplicating the actual aircraft working condition. In that circumstance, rotational motion, frictions and thermal effects will be put into consideration. The simulation will aim to replicate tyre deformations, motions, and rebound energy in order to validate this finite element model in more complex dynamic events.

6. Conclusions and future studies

The finite element modelling and analysis technologies have been applied to research the pneumatic tyres since just after the maturity of the finite element method as a general tool of analysis. This project has also used this finite element method to develop 3-dimensional model to study the interaction between aircraft tyre and the wheel hub. The results have indicated a positive progress in this aircraft tyre/wheel interaction finite element modelling.

The achieved outcomes include:

a) The research has introduced a detailed approach of developing finite element model for aircraft tyre and wheel assembly. Comparing with experimental test data, the results have indicated a positive improvement in aircraft tyre/wheel interaction finite element modelling, which also has demonstrated the effective use of finite element models as predictive engineering tool.

b) The model is suitable to run with a time step up to 5.31E-07s, giving a mass scaling of 2% at the beginning of the simulation, which is compatible to industry standards.

c) The current investigations have covered tyre inflation and static load scenarios, also considered the effect of the aircraft landing phase on the tyre, by modelling and predicting a single tyre hitting the ground.

d) The results have shown that the target test tyre is reliable even at a hard landing speed. The response is in agreement with manufacturer and aviation guidelines.

The current work has demonstrated the effective use of finite element models as a predictive engineering tool. In the current case, the model can help the tyre manufacturers to refine their design, therefore prevent tyre failure at higher landing speeds.

The conclusion of this PhD project includes the uniqueness of the study, the speciality of the finite element model, the limitation of current study and recommended potential future studies

6.1 Uniqueness of the study

There appeared a large number of publications regarding the subject of finite element tyre modelling as listed in Chapter 2 – literature review. The finite element theories and some modelling techniques that have been used are in common. In this project, research concentration and analysis details are in differ with previews researches.

a) Tyre/wheel contact analysis

Although there are a large number of publications that have studied the finite element tyre modelling and simulation, however, most of them focused on tyre/road contact under static or dynamic conditions to achieve footprint, pressure and stress distribution etc. The tyre/wheel interaction and contact effect, on the other hand, have not received as much attention as the other. This project focuses on the tyre/wheel interaction finite element modelling, and has generated models that provided detailed stress distribution on the concerned areas (tyre/wheel contact rim) as expected.

b) Material characteristics, simulation results validation

The materials, especially the rubber and fabric materials have been selected and correlated through procedures that match with industrial test data. As mentioned in Chapter – 3 and 4, the selection of finite element rubber material models are of great significance. And the correlation simulations have indicated the proper use of the *Mat_77 Hyperelastic (Yeoh) model in Ls-Dyna for this project.

The inflation and static load simulation for the actual dual bead H41 tyre/wheel assembly have been validated through the comparison with DATL industrial test data. Tyre deformation and Load vs. Deflection data have both been compared.

c) Tyre safety predictive assessment

The study has also considered the effect of the aircraft landing phase on the tyre, by modelling and simulating a single tyre hitting the ground. An initial safety assessment, focusing on tyre operational criteria (tyre deflection rate and rated load) and material

properties (yield and tensile strength) of the test tyre has been achieved. The result is in agreement with manufacturer and aviation guidelines. The current work has demonstrated the effective use of finite element models as a predictive engineering tool.

6.2 Speciality of the finite element model

a) Straightforward modelling process

It is noticed that the finite element modelling methodology employed in this project is a straightforward way to process the development of a complex full-scaled 3D tyre/wheel finite element model. With data from DATL, actual geometry was reflected in finite element model. Correlating with uniaxial tensile material test, proper and reliable finite element material models have been chosen and used for rubber and fabric in FE model. It is also worth mentioning that single bead tyre model has been developed based on the dual bead structure, which also means various types of aircraft or even automotive tyre/wheel assembly can be generated with essential data.

b) Flexible simulation scenarios

The existing simulation scenarios that have been developed for this project include inflation, static load and falling (single tyre hitting rigid ground).

Furthermore, other simulation including: static load with camber, cornering force, slipping angle and bumping (tyre/wheel assembly hits a block) etc., are also accessible.

Various models generated through the methodology will allow the tyre manufactures to check that new tyre designs do not load wheels in a manner that will exceed limit failure stresses. As mentioned in Chapter 1, the development of such models also adds to the general drive towards the use of more virtual prototypes in an area traditionally reliant on experimental testing

6.3 Limitations of current study

As mentioned in the previous chapters, several limitations of the current study are listed here:

a) The landing gear, especially suspension has been considered as neglected in this study as to simulate extreme (worst) landing case. However, in actual aircraft operational scenario, the damping effect from suspension will significantly reduce the load on the tyres.

b) The current study only simulates a single tyre hitting the rigid ground to achieve an initial tyre assessment. The actual scenario is more complex, involving tyre rotation, friction between tyre and road and the thermal effects from the heat generated by impact and friction.

c) Rubber material aging effects have not been considered in this study. As a matter of fact, a large number of aircraft tyres serve for quite a long time, within which rubber aging will influence material properties. However, it is recognized that researches regarding this issue can't be processed without sufficient experimental data.

6.4 Recommendations for future studies

a) The methodology used in this project can be applied on different types of aircraft tyre/wheel assembly. The finite element simulation scenarios can also be designed to duplicate various actual operational scenarios, for instance: simulation with tyre camber and cornering. Those proposed scenarios will be valuable for aircraft on-road dynamic analysis.

b) As mentioned in Chapter 4- Finite element modelling, the bolt-preload has a minor effect on the stress distribution on wheel rim compared with the loads from internal pressure and tyre structure. However, it is also achievable to put bolt-preload effect into consideration in the finite element tyre/wheel assembly model to duplicate the actual assembly under certain load condition.

c) Suspension (damping) effect can be put into consideration to simulate actual load transferred to the tyre. Based on this more accurate assumption, the performance, safety and failure assessment of tyre and wheel assembly under more realistic operational scenarios can be achieved.

d) A more complex dynamic scenario, involving tyre/wheel assembly falling and hitting rigid ground with a rotational motion has also been considered to duplicate the actual aircraft tyre landing phase. The tyre rotation, friction between tyre and road will be of significant influence. Thermal effect on tyre materials will also be considered.

e) Rubber aging effect will influence material properties. With more detailed experimental data, this effect can also be investigated.

References

3DS SIMULIA (2009) *Abaqus Benchmark Manual*.

3DS SIMULIA (2009) *Tyre Modelling and Analysis in Abaqus*

3DS SIMULIA (2007) *Abaqus Users' Manual*.

Achenbach, M. and Duarte, J. (2003) 'A Finite Element Methodology to Predict Age-Related Mechanical Properties and Performance Changes in Rubber Components'. in *Constitutive Models for rubber III*. ed. by AnonBusfield, UK: Balkema ublishers

Adams, V. and Askenazi, A. (eds.) (1999) *Building Better Products with Finite Element Analysis.* 1st printing edn. New Mexico: OnWord Press

Al, R. (7 Dec 2008) *JetBlue Not Responsible for Landing Accident* [online] available from <http://www.canyon-news.com/artman2/publish/losangelesnewscategory/JetBlue_not_responsible_for_the_landing_accident_in_2005_printer.php> [May 2012]

Ali, A., Hosseini, M., and Sahari, B. B. (2010) 'A Review of Constitutive Models for Rubber-Like Materials'. *American J. of Engineering and Applied Sciences 3 (1):* 232-239

Bastien, C. (2013) 'M23MAE Vehicle Crashworthiness'. MSc Lecture notes, Coventry University

Behroozi, M., Olatunbosun, O. A., and Ding, W. (2012) 'Finite Element Analysis of Aircraft Tyre - Effect of Model Complexity on Tyre Performance Characteristics'. *Journal of Materials & Design* 25, pp. 810-9

Berry, P. (1999) 'Landing Gear Design in the Conceptual Design Phase'. *SAE International*, 1999-01-5523

Boeing Commercial Airplanes (2004) *Boeing 737 Airplane Characteristics for Airport Planning*

Bol, M. and Reese, S. (2003) 'Finite Element Modelling of Polymer Networks Based on Chain Statistics'. in *Constitutive Models for Rubber III*. ed. by AnonBusfied, UK: Balkema Publishers

Bolarinwa, E. O. and Olatunbosun, O. A. (2004) 'Finite Element Simulation of the Tyre Burst Test'. *IMECHE, Part D Journal of Automobile Engineering* No. D11 (Vol. 218), pp. 1251-1258

Bowen, J. (2008) *Bolt Preload Case Study in LS-Dyna*: Jaguar Land Rover

Boyce, M. C. and Arruda, E. M. (2000) 'Constitutive Models of Rubber Elasticity: A Review,'. *Rubber Chemistry and Technology* Vol. 73 (No. 3), pp. 504-523

Chagnon, G., Markmann, G., and Verron, E. (2004) 'A Comparison of the Hart-Simith Model with Arruda-Boyce and Gent Formulations for Rubber Elasticity'. *Rubber Chemistry and Technology* 77, pp. 724-735

Chang, T. Y. P., Saleeb, A. F., and Li, G. (1991) 'Large Strain Analysis of Rubber-Like Materials Based on a Perturbed Lagrangian Variational Principle'. *Comput. Mech.* 8, pp. 221-233

Danielson, K. T. (1996) 'Computational Strategies for Tyre Modelling and Analysis'. *Computers & Structures*, Volume 61, Issue 4, Nov. 1996, pp. 673-693

Davis, P. A. (1997) *Quasi-Static and Dynamic Response Characteristics of F-4 Bias-Ply and Radial-Belted Main Gear Tires*: NASA Technical Paper 3586

Du Bois, P. A. (2010) *Oasys LS-DYNA UK Users' Meeting*. 'Crashworthiness and Impact Engineering with LS-DYNA', Solihull, UK, 2010

Du Bois, P. A. (2003) *4Th European Ls-Dyna Users' Conference*. 'A Simplified Approach to the Simulation of Rubber-Like Materials Under Dynamic Loading', Ulm, Germany, 2003

Dunlop Aircraft Tyres Limited (2010) *H41x16.0R20 Tyre Documents*

Dunlop Aircraft Tyres Limited *Dunlop's Markets* [online] available from <http://www.dunlopaircrafttyres.com/about/aircraft-tyre-markets.aspx> [Jan. 2012]

Ersahin, M. A. (2003) *Finite Element Analysis of Cornering Characteristics of Rotating Tires*, PhD thesis, The Middle East Technical University

Fish, B. E., Pajot, J. J., and Patterson, D. K. (2002) *World Aviation Congress & Display*. 'FEA Cyclic Symmetric Fatigue Analysis of Aircraft Wheels', Phoenix, USA, Nov. 2002: *SAE International*, 2002-01-3001

Fleming, W. B. (2010) *The History of Tyre*. Columbia University: BiblioBazaar

Forni, M., Martelli, A., and Dusi, A. (1999) 'Implementation and Validation of Hyperelastic Finite Element Models of High Damping Rubber Bearings'. in *Constitutive Models for Rubber*. ed. by UK: Balkema Publishers

Gent, A. N. *Elasticity in Engineering with Rubber*. 1992. New York: Hanser Publishers

Ghosh, P., Saha, A., and Mukhopadhyay, R. (2003) 'Prediction of Tyre Rolling Resistance using FEA'. in *Constitutive Models for Rubber*. ed. by Busfiled, UK: Balkema Publishers

Goodyear *Goodyear Aircraft Tyre Data Book* [online] available from <http://www.goodyearaviation.com/resources/pdf/db_airdatabook.pdf> [Sep. 2012]

Gough, V. E. (1981) 'Structures of the Pneumatic Tire'. in *Mechanics of Pneumatic Tires* . ed. by Washington D.C.: US Department of Transportation, pp. 203-248

Granta Design Limited (2013) *CES EduPack Software, Coventry University* [online]

Guan, Y., Zhao, G. and Cheng, G. (2006) 'Influence of Belt Cord Angle on Radial Tire under Different Rolling Stats', *Journal of Reinforced Plastics and Composites*, 25(10), pp. 1059-1077

Guo, Z. and Sluys, L. J. (2006) 'Application of a New Constitutive Model for the Description of Rubber-Like Materials Under Monotonic Loading'. *Int. J. Solids Struct.* 43, pp. 2799-2819

Hall, W., Jones, P. R., and Mottram, J. T. (2005) *3rd European LS-Dyna Conference* 'Modelling of an Automobile Tyre using Ls-Dyna 3D', Paris, France, 2001

Hall, W., Mottram, J. T., and Jones, R. P. (2004) 'Finite Element Simulation of a Rolling Automotive Tyre to Understand its Transient Macroscopic Behaviour', *Proceedings of the Institution of Mechanical Engineers Part D*, 218 1393 – 1408 (0954 - 4070)

Horton, W. (11 April 2010) *Wheel and Tyre Damage to Qantas A380* [online] available from <http://www.flightglobal.com/blogs/wings-down-under/2010/04/photos-of-wheel-and-tyre-damage-to-qantas-a380.html> [June 2012]

Impact Engineering Solutions Inc. (2005) *Analysis Hyperelastic Materials: Some Practical Considerations*

Kaliske, M. (2010) 2010 *9th Ls-Dyna Forum*. 'Numerical Modelling in Tyre Mechanics', Bamberg, Germany, 2010

Kelliher, D. S. (1999) *1999 Abaqus Users' Conference*. 'Temperature Prediction Analysis in an Off-Road Tyre using Abaqus/Standard', Chester, UK, 1999

Kennedy, R. H. (2003) *2003 Abaqus Users' Conference*. 'Experiences with Cylindrical Elements in Tyre Modelling', Munich, Germany, 2003

Koishi, M. and Kabe, K. (1998) *1998 Abaqus Users' Conference*. 'Simulation of Rolling Tyre with Abaqus', Newport, RI, 1998

Korochkina, T. V., Claypole, T. C., and Gethin, D. T. (2005) 'Choosing Constitutive Models for Elastomers used in Printing Processes'. in *Constitutive Models for Rubber*. ed. by UK: Balkema Publishers

Lemaitre, J. (2001) 'Background on Modelling'. in *Handbook of Materials Behaviour Models*. ed. by USA: Academic Press

Lou, K. and Perciballi, W. (2008) *10Th international LS-Dyna Users Conference*. 'Finite Element Modelling of Preload Bolt Under Static Three-Point Bending Load', Dearborn, USA, 2008

LSTC (2007) *LS-Dyna Keyword Users' Manual*. version 971

Marco, S. and Antonio, P. (2003) *2003 Abaqus Users' Conference*. 'Numerical Simulation of Full Vehicle Dynamic Behaviour Based on the Interaction between Abaqus/Standard and Explicit Codes ', Munich, Germany, 2003

Markmann, G. and Verron, E. (2006) 'Comparison of Hyperelastic Models for Rubber-Like Materials'. *Rubber Chem. Technol.* Vol. 79, No. 5, pp 835-858

Marlow, R. S. (2003) 'A General First-Invariant Hyperelastic Constitutive Model'. in *Constitutive Models for Rubber*. ed. by Busfield, UK: Balkema Publishers

Mars, W. V. and Fatemi, A. (2004) 'Observations of the Constitutive Response and Characterization of Filled Natural Rubber Under Monotonic and Cyclic Multiaxial Stress States'. *J. Eng. Mater. Technol.* 126, pp. 19-28

Mayer, L. S. (2000) 'Simulation of Aircraft Landing Gear Dynamics using CATIA, CATDADS, DADS and NASTRAN at Cessna Aircraft'. *SAE International*, 2000-01-1699

Mayersohn, N. (3 January 2005) *Reinventing the Wheel (and the Tire, Too)* [online] available from <http://www.nytimes.com/2005/01/03/automobiles/03cars.html> [January 2012]

Michelin *Michelin Aircraft Tyre Engineering Data* [online] available from <http://www.airmichelin.com/uploadedFiles/MichelinAirDev/StandardContent/Resource/databook.pdf> [Sep. 2012]

Nakajima, Y. and Padovan, J. (1987) 'Finite Element Analysis of Steady and Transiently moving/rolling Nonlinear Viscoelastic Structure III '. *Impact/contact Simulations, Computers and Structures* 27(2), pp. 275-286

Ogden, R. W., Saccomandi, G., and Sgura, I. (2004) 'Fitting Hyperelastic Models to Experimental Data'. *Comput. Mech.* 34, pp. 484-502

Ogden, R. W. (1972) 'Large Deformation Isotropic Elasticity on the Correlation of Theory and Experiment for Incompressible Rubber-Like Solids'. *Proc. R. Soc. Lond.* 326, pp. 565-584

Ojala, J. K. (2005) *2005 Abaqus Users' Conference*. 'Using Abaqus in Tyre Development Process', Stockholm, Sweden, 2005

Orengo, F., Ray, M. H., and Plaxico, C. A. (2003) *ASME International Mechanical Engineering Congress and Exposition*. 'Modelling Tyre Blow-Out in Roadside Hardware Simulations using Ls-Dyna', Washington, D. C, USA, 2003.

Pacejka, H. B. (2005) *Tyre and Vehicle Dynamics*. Burlington: Elsevier

Peeters, F. and Kussner, M. (1999) 'Material Law Selection in the Finite Element Simulation for Rubber-Like Materials and its Practical Application in the Industrial Design Process'. in *Constitutive Models for Rubber*. ed. by UK: Balkema publishers

Pucci, E. and Saccomandi, G. (2002) 'A Note on the Gent Model for Rubber-Like Materials, '. *Rubber Chem. Technol.* 75, pp. 839-851

Raoult, I., Stolz, C., and Bourgeois, M. (2005) 'A Constitutive Model for the Fatigue Life Prediction of Rubber'. in *Constitutive Models for Rubber*. ed. by UK: Balkema publishers

Reid, J. D., Boesch, D. A., and Bielenberg, R. W. (2006) *Icrash 2006*. 'Detailed Tyre Modelling for Crash Applications', Athens, Greece, 2006

Reza Ghoreishy, M. H. (2008) 'A State of the Art Review of the Finite Element Modelling for Rolling Tyres '. *Iranian Polymer Journal* 17(8), pp. 571-597

Ridha, R. A. (1980) 'Computation of Stresses, Strains and Deformations of Tires'. *Rubber Chemistry and Technology* 53(4), pp. 849-902

Robert Bosch GmbH (2007) *BOSCH Automotive Handbook*. 7th edition

Sasso, M., Palmieri, G., Chiappini, G., and Amodio, D. (2008) 'Characterization of Hyperelastic Rubber-Like Materials by Biaxial and Uniaxial Stretching Tests Based on Optical Methods'. *Polymer Test* 27, pp. 995-1004

Seibert, D. J. and Schoche, N. (2000) 'Direct Comparison of some Recent Rubber Elasticity Models'. *Rubber Chem. Technol.* 73, pp. 366-384

Sharma, S. (2003) 'Critical Comparison of Popular Hyperelastic Material Models in Design of Anti-Vibration Mounts for Automotive Industry through FEA'. in *Constitutive Models for Rubber*. ed. by Busfield, UK: Balkema publishers

Shiraishi, M., Iwasaki, N., Saruwatari, T., and Hayashi, K. (2009) *7Th European Ls-Dyna Users' Conference*. 'Developing FE-Tyre Model Library for Durability and Crash Simulations', Salzburg, Austria, 2009

Shiraishi, M., Yoshinaga, H., Iwasaki, N., and Hayashi, K. (2000) *6Th International LS-DYNA User's Conference*. 'Making FEM Tire Model and Applying it for Durability Simulation', Detroit, USA, 2000

Shiraishi, M., Yoshinaga, H., Miyori, A., and Takahashi, E. (2000) 'Simulation of Dynamically Rolling Tire'. *Tire Science and Technology* 28(4), pp. 264-276

Singh, M. G. (28 November 2011) *Landing Gear Mechanism of Aircraft, a Study* [online] available from <http://www.exposeknowledge.com/kb/6803-landing-gear--mechanism-aircraft-study.aspx> [June 2012]

Smiley, R. F. (1960) *Mechanical Properties of Pneumatic Tyres with Special Reference to Modern Aircraft Tyres*: NASA Technical Report, R-64

Smith, L. P. (1993) *The Language of Rubber: An Introduction to the Specification and Testing of Elastomers*. London, England: Butterworth-Heinemann Ltd

Tanner, J. A. and Daugherty, R. H. (2005) 'Mechanical Properties of Radial- Ply Aircraft Tyres'. *SAE International*, 2005-01-3438

Teo, A., Rajashekara, K., Hill, J., and Simmers, B. (2008) 'Examination of Aircraft Electric Wheel Drive Taxiing Concept'. *SAE International*, 2008-01-2860

The Goodyear Tyre & Rubber Company (April 2010) *Goodyear Aircraft Tyre Care and Maintenance*

Timbrell, C., Wiehahn, M., Cook, G., and Muhr, A. H. (2003) 'Simulations of Crack Propagation in Rubber'. in *Constitutive Models for Rubber*. ed. by Busfield, UK: Balkema publishers

Tokura, S. (2007) *6Th European Ls-Dyna Users' Conference*. 'Contact and Sliding Simulation of Rubber Disk on Rigid Surface with Microscopic Roughness', Gothenburg, Sweden, 2007

Tompkins, E. (1981) *The History of the Pneumatic Tyre*.: Eastland Press

Toth, B. K., Faffai, G., and Bojtar, I. (2005) 'Analysis of the Mechanical Parameters of Human Brain Aneurysm'. *Acta Bioeng. Biomech.* 7, pp. 3-23

Wang, P. and Dacko, L. (2009) 'Aircraft Level Steering Runaway Failure Analysis'. *SAE International*, 2009-01-3136

Woehrle, W. J. and Carlson, D. (2012) 'An Analysis and Evaluation of the Damage and Durability Performance of Steel Belted Radial Ply Passenger Tyres that have Experienced Severe Impact '. *SAE International*, 2012-01-0795

Yang, X. and Olatunbosun, O. A. (2010) 'Materials Testing for Finite Element Tyre Model'. *SAE International*, 2010-01-0418

Yang, X. (2009) 'Generation of Tyre Cross-Sectional Geometry for FE Tyre Model using Image Processing Techniques'. *International Journal of Engineering Simulation*, 10, 1: 3-10, ISSN: 1468-1137

Yeoh, O. H. and Fleming, P. D. (1997) 'A New Attempt to Reconcile the Statistical and Phenomenological Theories of Rubber Elasticity'. *J. Polymer Sci.Part B* 35, pp. 1919-1931

Zamzamzadeh, M. and Negarestani, M. (2006) *Tire Society Conference*. 'A 3D Tire/Road Interaction Simulation by a Developed Model'. Akron, USA, 2006

Zhang, X., Tamini, N., and Palmer, T. (2004) 'Finite Element Tire Model Parameters for Road Load Predictions'. *SAE Paper*, No. 05M-242

Appendix: Publication

Journal

Guo, H., Bastien, C., Blundell, M., and Wood, G. (2014) 'Development of a Detailed Aircraft Tyre Finite Element Model for Safety Assessment'. *Journal of Materials & Design* 53, pp. 902-909

Conference

Guo, H., Bastien, C., Blundell, M., and Wood, G. (2013) *9Th European LS-Dyna Conference*. 'A Detailed Aircraft Tyre Finite Element Model for Hand Landing Safety Assessment', Manchester, UK, 2013